Engineering

U. S.

Journal of Research

of the National Bureau of Standards

OCTOBER 1934

VOL

U. S. DEPARTMENT OF COMMERCE
Sinclair Weeks, Secretary
NATIONAL BUREAU OF STANDARDS
A. V. Astin, Director

OCTOBER . 1954
VOLUME . 53
NUMBER . 4

JOURNAL OF RESEARCH

of the

NATIONAL BUREAU OF STANDARDS

PERIODICALS OF THE NATIONAL BUREAU OF STANDARDS

The National Bureau of Standards is engaged in fundamental and applied research in physics, chemistry, mathematics, and engineering. Projects are conducted in seven fields: chemistry and chemical engineering, optics and metrology, heat and power, atomic and radiation physics, electronics, organic and fibrous materials, metallurgy, mineral products, building technology, applied mathematics, data processing systems, aeronautical engineering, radio propagation, and radio standards. The Bureau has custody of the national standards of measurement and conducts research leading to the improvement of scientific and engineering standards and of techniques and methods of measurement. Methods and instruments are developed; physical constants and properties of materials are determined; and technical processes are investigated.

JOURNAL OF RESEARCH

[illegible] publishes papers by authors [illegible] engineering, mathematics, chemistry, and engineering. Complete details of the [illegible] experimental data, experimental procedure, and theoretical and mathematical analysis. Annual subscription: Domestic, $6.00; foreign, $7.00.

TECHNICAL NEWS BULLETIN

Publication of [illegible] research at the National Bureau of Standards is announced each month in the Technical News Bulletin. The articles are brief [illegible] of research, digests of the technologic [illegible] Research Papers [illegible] Applied [illegible] Materials [illegible] Miscellaneous Publications [illegible] Publications, as issued, are two-page; [illegible]. Annual subscription: [illegible]

BASIC RADIO [illegible]

[illegible] information [illegible] communication [illegible] the world at [illegible] are important to all [illegible] to inventions [illegible] and three [illegible] Annual [illegible]

[illegible] been [illegible]

Research of the National Bureau of Standards Vol. 53, No. 4, October 1954 Research Paper 2533

Application of Infrared Spectroscopy to the Determination of Impurities in Titanium Tetrachloride[1]

Rolf B. Johannesen, Charles L. Gordon, James E. Stewart, and Raleigh Gilchrist

The infrared spectrum of pure titanium tetrachloride was measured in the range of 2 to 15 microns, and, by adding known amounts of certain substances, it was possible to identify the common impurities likely to be found in refined titanium tetrachloride and to establish their limits of detection. The application of infrared spectroscopy made possible a sensitive method of following the process of purification of the tetrachloride.

1. Introduction

In preparing titanium tetrachloride of high purity for fundamental research, it is necessary to be able to determine the over-all purity of the final product and to identify as well as to determine, the remaining impurities.

As the total amount of impurities will be small, one must use methods that are far more sensitive than ordinary chemical tests. To this end a number of physical methods may be employed, namely, the freezing and melting behavior of the substance, from which the over-all purity can be computed; emission spectroscopy and absorption spectroscopy in ultraviolet, visible, and infrared.

This paper describes the infrared absorption spectrum of titanium tetrachloride, the effect of certain impurities on the spectrum, and some techniques found useful in handling titanium tetrachloride.

2. Spectrophotometer Cell

The high reactivity of titanium tetrachloride with moisture and with many organic compounds presented special problems in the design and use of a suitable cell for holding the liquid during measurement. The most desirable cell would have been one constructed entirely of glass transparent to infrared light, capable of being evacuated, and filled by transfer in a high-vacuum system. Practically, it was necessary to use the customary rock-salt windows on a body of glass. Because the beam of radiation of the spectrophotometer (Perkin-Elmer, model 21) converges in passing through the sample, the cell was made in the shape of a truncated cone. Two types of cell were constructed, one with a long optical path, useful in the range of 2μ to 9.4μ, and one with a short optical path, useful in the range of 9.4μ to 15μ.

2.1. Cell With Long Optical Path

This cell, depicted in figure 1, was made from a 125-ml Erlenmeyer flask by cutting off the bottom and a part of the neck. The first cut was made perpendicular to the axis of the flask at a point where the diameter was slightly less than 2 in. The second cut was made parallel to the first at a distance of 50 mm. The cut edges were ground flat so that the distance between them was from 47 to 49 mm, and were within 1 degree of being parallel.

Attempts to fasten the rock-salt windows to the glass cell by pressure, using polyethylene or polytetrafluoroethylene gaskets, were unsuccessful. These gasketing materials were so hard that the windows could not be pressed tightly enough to prevent leaks without cracking the rock salt. Polychlorotrifluoroethylene wax proved workable, but it was soluble in the tetrachloride. The problem was solved very simply by sealing the rock-salt windows to the cell by means of a plasticized cellulose nitrate cement (Duco). This was done by coating the ends of the cell with the cement and pressing the windows against them. After a short setting period, the outside of each seal was coated with the cement, and later again coated. After allowing the cement to dry thoroughly, for a period of 48 hr, the cement was found to be inert to the titanium tetrachloride and could be left in contact with it for many days without causing any visible change, or adding any absorption bands to the spectrum. The only precaution necessary, other than to allow ample time for drying, was to keep the cement out of the path of the infrared beam.

A distinct advantage of this method of assembly was that the cell could be taken apart for cleaning and for repolishing of the windows, and then reassembled without altering the length of the optical path. This was accomplished by soaking the cell in acetone.

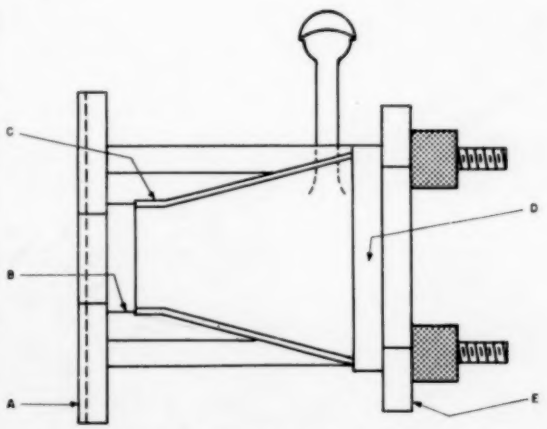

FIGURE 1. *Cross section of 50-mm cell.*

A, Cell holder frame; B, sodium chloride window; C, glass cell; D, sodium chloride window; E, clamp ring.

[1] Financial support of this work was furnished by the Metallurgy Branch of the Office of Naval Research, Department of the Navy, Washington 25, D. C.

314715—54——1

Diametrically opposite sidearms were sealed close to the large end of the conical cell. The sidearms ended in standard spherical joints to which were fitted filling tubes and stopcocks.

The support and holder for the cell was composed entirely of brass and consisted of a ¼-in.-thick plate, 2 by 3 in., with edges milled to fit the Perkin-Elmer spectrophotometer cell clamp, at the center of which a hole, 13/16 in. in diameter, was cut. Four ¼-in.-posts, 3½ in. long, and threaded at the upper ends, permitted a ¼-in.-thick ring, 1⅝ in. in inside diameter and 2¾ in. in outside diameter, to be pressed against the cell by four nuts with springs under them, when the cell was in position with the small window against the hole in the base plate.

2.2. Cell With Short Optical Path

The thin cell was constructed and assembled as shown in figure 2. The spacer, C, was made from polytetrafluoroethylene sheet of 0.25-mm thickness. This was cemented between the two rock-salt windows. Two holes were drilled in window D, over which were cemented two filling tubes, F. Each filling tube had a slightly expanded diameter just inside a blind stem, which was inserted in one of the alining holes in the clamp ring, G. These filling tubes must have flat ends in the same plane. This was accomplished by inserting four filling tubes in the four inner holes shown in the ring at G, and lapping them on a plate with fine emery. The two extra tubes were necessary to prevent rounding of the ends of the two to be used. By sealing a spherical joint on the end of each of tubes F, the thin cell could be mounted and filled in a manner identical with that for the large cell.

3. Method of Filling the Cell

Procedure A. To fill the cell with freshly distilled titanium tetrachloride, the arrangement depicted in figure 3 was devised. With tube B closed with a rubber stopper, the system was evacuated a pressure of 5 mm of mercury through a 2 ay stopcock attached to joint L. Dry nitrogen was ien admitted through L to a pressure of 1 atm. The system was evacuated and filled with nitrogen or 5 times, after which dry nitrogen was admitted o a pressure of 1 or 2 mm above atmospheric. A this stage the rubber stopper at B was removed. and the nitrogen allowed to flush through the sy em. While the flow of nitrogen continued, about 75 ml of titanium tetrachloride was poured in through the sidearm, B, which was subsequently sealed with a flame, the flow of nitrogen being stopped as the sealing operation was completed. The system was then evacuated to a pressure of 120 mm and this pressure maintained by means of an adjustable leak at the pump.

The titanium tetrachloride in flask A was warmed gently to boil out dissolved gases. After the tetrachloride refluxed for a short time in section C, it was distilled slowly. It was important that the distillate be kept cold at all times to prevent its condensation on the walls of the bell jar. The liquid distillate, caught in funnel E, quietly ran into the cell. When the cell was full, the distillation was stopped, and flask A was cooled with tap water. Finally, dry nitrogen was admitted to the bell jar, the bell jar removed, and the stopcocks of the cell closed.

Procedure B. In determining the effect of impurities, the cell was filled by suction. To accomplish this, the portion of the apparatus in figure 3

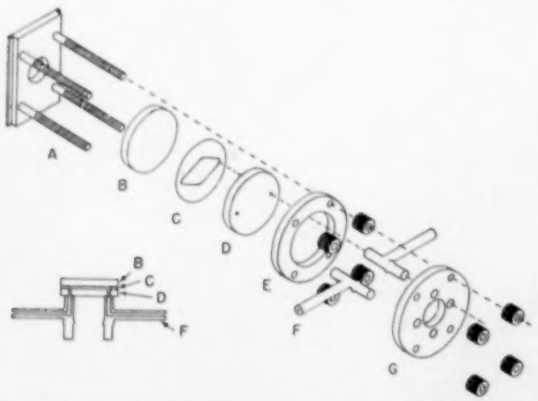

FIGURE 2. *Thin cell (chamber thickness equal to thickness of spacer C).*

A, Frame; B, window; C, spacer; D, window with filling holes; E, cell clamping ring; F, filling tubes; G, filling tube clamping ring (also fitting tube grinding jig).

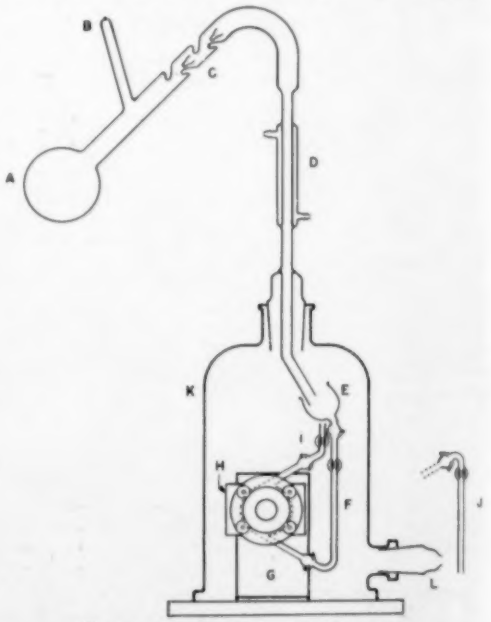

FIGURE 3. *Apparatus for filling cell.*

A, Distilling flask; B, filling tube; C, reflux condenser; D, delivery condenser; E, receiving funnel; F, filling side-arm; G, stand; H, cell holder with cell; I, venting side-arm; J, rinsing side-arm; K, bell jar; L, connection to vacuum and nitrogen.

labeled F, G, H, and I was used. A two-way stopcock attached to vent tube I permitted air and moisture to be displaced from the cell by a current of helium. Reversing the stopcock allowed a sample of titanium tetrachloride to be drawn by vacuum into the cell through a glass tube attached to filling tube F. When the cell was filled, the stopcocks were closed, and the spectrum could be measured at once. After the measurement was completed, the titanium tetrachloride was blown into a waste flask by pressure of dry helium, and the cell was rinsed with three portions of dry carbon tetrachloride. The last drop of carbon tetrachloride rinse was evaporated in a stream of helium. The cell could then be refilled as described above. Bands of carbon tetrachloride were never found in the spectrum.

4. Infrared Spectrum

The absorption of infrared radiation was measured in the range from 2 to 15 μ by means of a Perkin-Elmer model 21 double-beam recording spectrophotometer.

The titanium tetrachloride here involved was first chemically refined by W. Stanley Clabaugh, and then further purified by distillation in a highly efficient column by Robert T. Leslie of the Bureau. Description of the methods used will be given in a separate paper. The best titanium tetrachloride used in this work had an overall purity of 99.9991 mole percent, as measured by George T. Furukawa, of the Thermodynamics Section of the Bureau, by analysis of the melting curve. The spectrum of pure titanium tetrachloride appeared to be quite simple, showing only six broad absorption bands in the region from 2 to 15 μ. Table 1 shows the location of these absorption maxima and their absorbance indices.

The infrared spectrum is given in figure 4.

The weak absorption at about 3 μ arises from titanium dioxide deposited on the cell windows, and the weak sharp lines near 6 μ are produced by uncompensated atmospheric water vapor. The weak sharp doublet near 3.5 μ is due to hydrogen chloride (about 12 ppm), which was not entirely eliminated in filling the cell.

Infrared absorption spectra were measured for commercial samples of titanium tetrachloride as received and at successive steps in the purification process. Certain absorption peaks, present in the crudest material, disappeared from the spectrum after a simple distillation. No attempt to identify these peaks was made. Certain other peaks persisted, the wavelengths of which could be associated with specific molecular groupings (e. g., $\diagdown C{=}O$, $H{-}Cl$). The nature of the likely contaminants could be inferred from these peaks. Table 2 lists the absorption peaks and limits of detection of substances found to be persistent contaminants, or so reported in the literature.

TABLE 1. *Infrared spectrum of titanium tetrachloride*

Absorption bands		Absorbance index, a
	[a]	
μ	cm^{-1}	cm^{-1}
6.76	1,479	0.058
7.35	1,361	.125
7.94	1,259	.033
9.00	1,111	.056
10.20	980	19.0
11.16	897	Shoulder
11.44	874	19.8

$$a=\frac{1}{b}\log\frac{I_0}{I}$$

[a] The symbols used are defined in "Spectrophotometry," NBS Circular 484, Sept. 15, 1949.

TABLE 2. *Characteristic infrared absorption peaks and limits of detection of common impurities in titanium tetrachloride*

Impurity	Wavelength of peak	Limit of detection
	μ	*ppm*
Hydrogen chloride, HCl	3.53	2
Carbon dioxide, CO_2	4.30	?
Vanadium oxytrichloride, $VOCl_3$	4.84	40
Phosgene, $COCl_2$	5.51	about 2
Chloroacetyl chloride, $ClCH_2COCl$	5.55	0.5
Dichloroacetyl chloride, $Cl_2CHCOCl$	5.55	1
Trichloroacetyl chloride, Cl_3CCOCl	5.55	0.5
Silicon tetrachloride, $SiCl_4$	8.14	200
Hydrolysis product	8.45	?

No effort was made to ascertain the limits of detection for carbon dioxide or hydrolysis product, because both of these substances could be eliminated by a single careful distillation in an inert atmosphere or in a high vacuum. Qualitatively, the sensitivity was high as shown by the rapid increase in absorption at these wavelengths when the sample was exposed even briefly to ordinary air.

The limit of sensitivity is not good for either vanadium oxytrichloride or silicon tetrachloride by this method. Spectrophotometry in the visible region

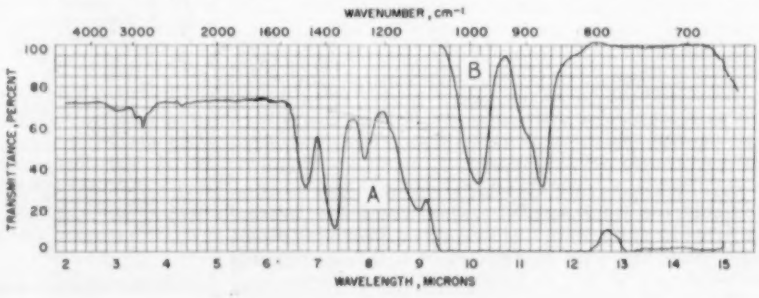

FIGURE 4. *Infrared spectrum of titanium tetrachloride.*

Curve A, measured in 50-mm cell; curve B, measured in 0.25-mm cell.

showed an intense absorption by vanadium oxytrichloride at 390 mμ, which caused a visible yellow color in concentrations as low as 1 ppm. Silicon compounds were determined by emission spectroscopy of an aqueous solution of the titanium tetrachloride, since infrared spectrophotometry proved too insensitive.

It is believed that this is the first time that chlorinated acetyl chlorides have been identified as persistent contaminants in commercial titanium tetrachloride. In very dilute solution, the three chlorides are indistinguishable spectrophotometrically. At somewhat higher concentrations (5 ppm), chloroacetyl chloride was found to have a second peak at 5.64 μ, which was about one-fourth as intense as the peak at 5.55 μ; dichloroacetyl chloride showed a second peak at 5.64 μ of the same intensity as that at 5.55 μ. Trichloroacetyl chloride showed no secondary peaks in this range of concentrations. Whereas solutions of mono- and dichloroacetyl chlorides in titanium tetrachloride rapidly turn yellow, a solution of trichloroacetyl chloride (bp, 118° C) at a concentration of 0.1 percent (1,000 ppm) remains colorless for at least a week.

At no time in the course of these experiments was the characteristic hydroxyl absorption band at about 2.8 μ observed. Apparently the reaction of titanium tetrachloride with small amounts of water does not yield $Ti(OH)Cl_3$, but instead a compound with a

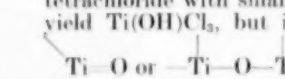

Ti—O or —Ti—O—Ti— linkage must be formed rapidly and completely on hydrolysis.

5. Vibration Spectrum of Titanium Tetrachloride

Except for the very early work of Marvin [1],[2] there has been no infrared absorption spectrum reported for titanium tetrachloride. Numerous observations [2 to 8] of the Raman spectrum have established values for the fundamental vibrations, tabulated in table 3, and Rumpf [9] has reported very weak Raman lines, which perhaps correspond to harmonic or combination vibrations at 631.5, 784.5, and 926 cm^{-1}, although these lines might arise from hydrolysis products.

TABLE 3. *Fundamental vibrations from the Raman spectrum*

Worker and year	$\nu_1(a_1)$	$\nu_2(e)$	$\nu_3(f_2)$	$\nu_4(f_2)$
	cm^{-1}	cm^{-1}	cm^{-1}	cm^{-1}
Daure [2] 1928	385	113	480	134
Daure [3] 1929	390	120	500	140
Trumpy [4] 1930	386	119	491	139
Bhagavantam [5] 1930	382	120	494	145
Cabannes and Rousset [6] 1933	386	120	497	144
Delwaulle and François [7] 1945	389	120	{490 / 506}	140
Average values given by Kohlrausch [8]	386	120	495	141

Marvin's spectrum, which extended from 2 to 16 μ, excluded the fundamental region which lies beyond 20 μ (below 500 cm^{-1}). He reported bands at about 3160, 1610, 982, 875, and 822 cm^{-1} with considerable uncertainty, because of the doubtful sodium chloride dispersion data at his disposal. His sample was evidently quite impure.

Titanium tetrachloride has the symmetric tetrahedral structure [10] of point group T_d. Its fundamental vibrations are divided into symmetry species as follows: $1a_1+1e+2f_2$. Only the two triply degenerate f_2 fundamentals are infrared active but all are Raman active. Higher vibrational transitions must contain a component of species F_2 in order to be infrared active and a component of species A_1, E, or F_2 to be Raman active. Table 4 contains frequencies and assignments for bands observed in the present work and also for the three Raman lines reported by Rumpf. The frequencies given by Kohlrausch are used in calculating expected frequencies.

TABLE 4. *Assignment of vibration frequencies of titanium tetrachloride*

Origin	Symmetry species	Wave number	
		Expected	Observed [a]
		cm^{-1}	cm^{-1}
$\nu_3(f_2)+\nu_4(f_2)$	$A_1+E+F_1+F_2$	636	631.5 (R)
$2\nu_3(a_1)$	A_1	772	784.5 (R)
$\nu_3(a_1)+\nu_4(f_2)$	F_2	881	874 S
$2\nu_3(a_1)+\nu_2(e)$	E	892	897 M, SH
$2\nu_3(a_1)+\nu_4(f_2)$	F_1	913	926 (R)
$2\nu_3(f_2)$	A_1+E+F_2	980	980 S
$\nu_2(e)+2\nu_3(f_2)$	$A_1+A_2+2E+F_1+F_2$	1,110	1,111 VW
$2\nu_3(a_1)+\nu_4(f_2)$	F_2	1,267	1,259 VW
$\nu_1(a_1)+2\nu_3(f_2)$	A_1+E+F_2	1,376	1,361 VW
$3\nu_3(f_2)$	$A_1+F_1+2F_2$	1,485	1,479 VW

[a] (R), Raman line; S, strong; M, medium; VW, very weak; SH, shoulder.

The agreement between observed and calculated frequencies seems good in view of the uncertainties in the original Raman data. The two strongest bands in the infrared spectrum are assigned to the only two binary vibrations expected in this region. No bands assignable as difference combinations were observed, and no quaternary combinations were observed. $2\nu_1+\nu_2$ (897 cm^{-1}) is of species E and should be infrared inactive. However, normally inactive bands are sometimes observed in spectra of liquids because of the perturbations produced by neighboring molecules.

6. References

[1] H. H. Marvin, Phys. Rev. **34,** 161–186 (1912).
[2] Pierre Daure, Compt. rend. **187,** 940–941 (1928).
[3] Pierre Daure, Ann. phys. [10] **12,** 375–441 (1929).
[4] B. Trumpy, Z. Physik **66,** 790–806 (1930).
[5] S. Bhagavantam, Indian J. Phys. **5,** 35–48; 59–71 (1930); **7,** 79–86 (1932).
[6] J. Cabannes and A. Rousset, Ann. phys. [10] **19,** 229–303 (1933).
[7] Marie-Louise Delwaulle and Félix François, Compt. rend. **220,** 173–174 (1945); J. Phys. Radium [8] **7,** 15–32 (1946).
[8] K. W. F. Kohlrausch, Der Smekal-Raman Effekt. Ergänzungsband (Julius Springer, Berlin, 1938; Edwards Brothers, Ann Arbor, Mich., 1944, p. 146).
[9] Marie-Élisa P. Rumpf, Compt. rend. **202,** 950–952 (1936).
[10] G. Herzberg, Infrared and Raman spectra of polyatomic molecules (D. van Nostrand Co., Inc., New York, N. Y., 1945).

WASHINGTON, April 30, 1954.

[2] Figures in brackets indicate the literature references at the end of this paper.

Journal of Research of the National Bureau of Standards Vol. 53, No. 4, October 1954 Research Paper 2534

Some Properties of Porcelains and Phase Relations in the Ternary Systems of Beryllia and Zirconia With Titania, Ceria, and Chromia

S. M. Lang, R. S. Roth, and C. L. Fillmore [1]

The following physical properties were determined for some BeO-TiO_2-ZrO_2 and BeO-CeO_2-ZrO_2 porcelain specimens of less than 0.10 percent equivalent water absorption: Maturing range, 1,450° to 1,750° C; shrinkage, 13.9 to 18.7 percent; bulk density, 3.0 to 5.8 g/cm³; room-temperature sonic elastic properties—Young's modulus, 18.7 to 43.6×10^6 lb/in.², shear modulus, 8.0 to 18.1×10^6 lb/in.², Poisson's ratio, 0.17 to 0.28, and bulk modulus, 5.3 to 12.1×10^6 lb/in.²—for each specimen tested for transverse strength; room-temperature static strength properties—transverse, 12.0 to 23.4×10^3 lb/in.², and compressive, 112 to 271×10^3 lb/in.²—and Young's modulus, 18.7 to 46.8×10^6 lb/in.²; and, at 1,800° F (982° C), static transverse strength, 9.1 to 18.1×10^3 lb/in.², Young's modulus, 21.5 to 38.3×10^6 lb/in.², and strain rates under various stresses. Because of the loss of chromia from the samples during preliminary heating trials, no specimens of BeO-Cr_2O_3-ZrO_2 mixtures were prepared for these tests. The conjecture is made that porous oxide porcelains with requisite strength properties may prove of considerable interest in the search for materials of greater thermal-shock resistance than that associated with dense, practically impervious oxide porcelains with high-strength properties.

It is proposed that the phase diagram of the BeO-TiO_2-ZrO_2 system includes an invariant point at about 20-BeO, 35-TiO_2, and 45-ZrO_2 (wt %) and 1,630° C; an invariant point at about 20-BeO, 55-TiO_2, and 25-ZrO_2 (wt %) and 1,610° C; and primary crystallization fields of BeO, tetragonal ZrO_2 solid solution, ZrO_2-TiO_2 solid solution, and TiO_2 solid solution.

The limited X-ray data indicate that the BeO-CeO_2-ZrO_2 system is a simple one with an invariant point at approximately 40-BeO, 30-CeO_2, and 30-ZrO_2 (wt %) and 1,845° C, and primary crystallization fields of BeO, tetragonal ZrO_2 solid solution, and CeO_2 solid solution.

Based upon extremely limited data and considerable amount of speculation, a suggested configuration of the liquidus surfaces of the BeO-Cr_2O_3-ZrO_2 system would be one that contains three invariant points and primary crystallization fields of BeO, tetragonal ZrO_2, BeO·Cr_2O_3, BeO·3Cr_2O_3, and Cr_2O_3. Beryllium chromate (BeO·Cr_2O_3), the chromia analog of chrysoberyl, was identified; crystallographic parameters of this orthorhombic compound were tentatively determined as being $a=10.0$ A, $b=3.8$ A, and $c=4.5$ A.

1. Introduction

Many investigations have been conducted, and many reports published, on special oxide ceramics to replace metals for high-temperature service. Although no completely acceptable ceramics have been developed for such a critical use as turbine blades, the need is so urgent that continued research is justified.

Previous work at the National Bureau of Standards [1, 2, 3, 4] [2] on the properties of pure oxides, singly and in combination, shows that the best ceramics for use under severe service conditions usually involve combinations of BeO and ZrO_2, due in large part to the apparent thermal conductivity of beryllia and to the strength of zirconia. In order to produce impervious specimens, required to attain reproducibility of maximum strength test values, it is necessary to introduce at least a third component to beryllia-zirconia mixtures.

This report describes exploratory physical-property studies for mixtures in the systems BeO-TiO_2-ZrO_2, BeO-CeO_2-ZrO_2, and BeO-Cr_2O_3-ZrO_2. In addition, a limited investigation was conducted to determine the approximate equilibrium relations that exist in these systems.

[1] Formerly, a National Bureau of Standards staff member.

[2] Figures in brackets indicate the literature references at the end of this paper.

2. Materials, Equipment, and Procedures

Commercially available materials of high purity were used in the preparation of all specimens: *beryllia* (BeO), low-calcined material of nominal 99.7 percent purity; *titania* (TiO_2), TAM "Titanox A-MO", nominal titania content 98.7 percent, calcined at 1,100° C; *ceria* (CeO_2), calcined material of nominal 99+ percent purity; *chromia* (Cr_2O_3), chemically pure reagent-grade material; and *zirconia* (ZrO_2), low-calcined material of nominal 99-percent purity, recalcined at 1,440° C. As prepared for use, the materials were, in all instances, sufficiently finely divided to pass the No. 325 U. S. Standard Sieve.

For convenience, the test procedures employed [2, 3, 4] are given briefly. Carbon tetrachloride was used for absorption determinations, and the results were converted to equivalent water-absorption values. Matured bodies were considered to be those having less than 0.1 percent of equivalent water absorption. Shrinkage values were calculated from micrometer measurements before and after heating. Apparent density values were obtained by calculations based upon the volume as determined by a mercury volumeter and the dry weight of the specimen. A few calculated bulk density values were obtained from the dry weight of the samples by measuring the length, width, and breadth of specimens specifically prepared for transverse-strength tests. The ends

of the ½-in.-diameter specimens for the compressive-strength tests were ground parallel, so that the height-to-diameter ratio was approximately 2. The test pieces were placed between graphite-oil lubricated, cold-rolled steel blocks, and the compressive stress was applied at about 31,250 lb/in.²/min by a 75,000-lb-capacity hydraulic press.

Transverse moduli of rupture and of elasticity were determined statically at room temperature and at 1,800° F (982° C), using a specially designed transverse-strength test furnace [3]. The specimens were stressed at 2-min intervals at calculated increments of 1,500 lb/in². When it was noted, during the 1,800° F tests, that the deflection following loading continued after the first minute, it was assumed that permanent deformation, or "plastic flow," had occurred. This deformation could be verified when the test pieces were examined for permanent curvature following rupture. In order to investigate the relative magnitude of the deformation, some bars were subjected to a short-time (1 hr) stress-strain test at 1,800° F. Beginning at 6,000-lb/in.² calculated stress, stress increments of 1,500 lb/in.² were added to the bars at hourly intervals, or until rupture occurred, during which time the deflection was measured at prescribed intervals.

This paper is believed to be the first in which the room temperature elastic properties, Young's modulus, shear modulus, Poisson's ratio, and bulk modulus, are reported for each of a series of porcelain-type specimens. The prepared transverse-test specimens and equipment recently developed [5] were used for these tests. Young's modulus values were calculated, using the flexural vibration frequencies determined along the width and depth of the bars and, in a few instances, longitudinally through the length. In most cases, the values obtained for sound bars were within one-half percent of each other and were always within 1 percent. Where internal flaws, such as cracks, were present, the variations obtained were large. Shear modulus values were calculated, using the determined torsional vibration frequencies. Poisson's ratio and the bulk modulus were calculated for each specimen by the formulas:

$$\sigma = \frac{E}{2G} - 1 \qquad (1)$$

$$K = \frac{E}{3(1+\sigma)}, \qquad (2)$$

where σ is Poisson's ratio, E is Young's modulus, G is the shear modulus, and K is the bulk modulus.

The reported phase relations for the three systems were determined mainly by interpreting X-ray diffraction patterns of the interiors of some of the maturing range and transverse-strength test specimens. Liquidus surface configurations were obtained by isothermal tests of mixtures at various temperature levels. A few melting-point and softening-range determinations were made. It was assumed that the published equilibrium relations of the various subordinate binary systems were correct. Because of the nature of the investigation, it was not deemed advisable to determine any phase relations in anything more than an approximate manner.

Assignment of mole ratios to the various mixtures[3] is used solely because a compound will nearly always correspond to an integral molecular ratio. If sufficient mole-ratio mixtures are heated, the chances of missing a compound are minimized, regardless of the investigational procedure employed.

3. The System BeO-TiO_2-ZrO_2

3.1. Phase Relations

a. The System BeO-TiO_2

The equilibria were described by von Wartenberg et al. [6] as including two compounds, 3BeO·TiO_2 and BeO·TiO_2, melting congruently at 1,800° and 1,720° C, respectively. In the work at NBS [4] no evidence was found of a compound in this system. A single eutectic exists at about 85 weight percent of TiO_2 and 1,670° C, and a narrow region of TiO_2-BeO solid solution extends from just beyond the eutectic at about 90 weight percent of TiO_2 to pure TiO_2. The absence of compound formation is supported by the results of a limited study at Pennsylvania State College [7], which also indicate that a solid solution may exist at high temperatures.

b. The System BeO-ZrO_2

It was first proposed [8] that this is a simple system with one eutectic at about 2,180° C and 65 weight percent of ZrO_2. The compound 3BeO·2ZrO_2, melting at 2,550° C, and two eutectics were then reported [9]; but later [10], the system was shown as a simple one with the eutectic at about 75 weight percent of ZrO_2 and 2,240° C. Similar data, placing the eutectic at 2,210° C, were published the same year [11], and a diagram again showing the 3B·2Z compound was published in 1933 [12]. In 1937 von Wartenberg et al. [6] reported a single, sharp eutectic at about 66 mole percent of BeO and 2,200° C. Mixtures of ZrO_2 and BeO for use in crucibles were discussed by Ryschkewitsch [13]. In the work at NBS, Geller et al. [1] found no evidence of a compound between BeO and ZrO_2.

c. The System TiO_2-ZrO_2

The melting relations were reported by von Wartenberg and Gurr [10] as indicating one eutectic at about 20 mole (27.8 wt) percent of ZrO_2 and 1,760° C. Vaporization was insignificant, but they reported considerable reduction of TiO_2, so that the diagram obtained was not strictly that between ZrO_2 and TiO_2. A limited study by Bussem, Schusterius, and Ungewiss [14] indicated no compound formation but some solid-solution development. They showed that 10 weight percent of zirconia at 1,460°, and 16 weight percent at 1,520° C, may dissolve in the rutile structure without change. The system was found by Sowman and Andrews [15] to be one of partial solid solutions with no inter-

[3] The short form of indicating the mole compositions of mixtures is used throughout the text. The code is B=BeO, Ti=TiO_2, Ce=CeO_2, Cr=Cr_2O_3, and Z=ZrO_2. The short form, i. e., 1B:2Ti:3Z, then reads: 1 mole of BeO plus 2 moles of TiO_2 plus 3 moles of ZrO_2 and does not indicate a compound.

mo ate compounds and the eutectic to be located at 50 - 55 weight percent of ZrO_2 and about 1,600° C. At is temperature the maximum solubility of ZrO_2 in O_2 was found to be 21 weight percent; that of Ti in ZrO_2 was found to be 37 weight percent. A per ectic was indicated at 60 weight percent of ZrO and 1,900° C between cubic zirconia and a tet agonal zirconia solid solution. Later work by Sowman [16] indicated that the 1:1 mixture, after heat treatment, consists of either a distorted form of tetragonal zirconia or a new compound. Brown and Duwez [17, 18] proposed a diagram indicating the existence of the ZrO_2-TiO_2 compound. Independently, Coughanour, Roth, and DeProsse [19] located and described the optical and X-ray properties of the incongruently melting 1:1 compound. Their diagram shows a eutectic at about 80 mole (72.2 wt) percent of TiO_2 and 1,760° C and an invariant point at about 55 mole (44.2 wt) percent of TiO_2 and 1,820° C. Solid solutions are formed at the eutectic temperature in which about 15 mole percent of ZrO_2 (at 78.6 wt percent of TiO_2) will enter the rutile structure and about 10 mole percent of TiO_2 (at 49.3 wt percent of TiO_2) will enter the compound structure. There was no reaction of the tetragonal zirconia solid solution with the compound. At the invariant point temperature (1,820° C), the melting data indicate that about 38 mole (28.4 wt) percent of TiO_2 forms a solid solution with tetragonal zirconia. Although not shown on the diagram, it was found that about 10 mole (6.7 wt) percent of TiO_2 forms a solid solution with monoclinic zirconia.

d. The System BeO-TiO_2-ZrO_2

No literature references could be found describing the phase relations for this system. In the present study, some ternary mixtures were successively heated at 1,600°, 1,625°, 1,650°, 1,675°, 1,750°, and 1,800° C for 30 min at each temperature and were visually examined after each heating for evidences of melting. Petrographic and X-ray diffraction examinations were made using a few fused samples.

Mixture 4B:4Ti:1Z, which melts at about 1,615° ±10 deg C, appears to be located near the probable eutectic composition. No ternary compounds were found to exist, and the system contains primary crystallization fields for BeO, tetragonal ZrO_2 solid solution, TiO_2 solid solution, and ZrO_2·TiO_2 solid solution, this probably being small. These data are shown on figure 1.

Figure 2 shows an isothermal section based upon X-ray examinations of specimens that had been heated at 1,550° C during the maturing range tests. Each sample was sectioned so that an interior surface could be used to prepare the X-ray diffraction patterns. Within the firing-time interval used for these specimens, the solid-state reactions seem to attain an equilibrium condition in all compositions throughout the ternary system. However, when samples of a few mixtures at or near the binary join were melted during the tests to determine liquidus surface, equilibrium was not attained. The diffraction patterns show four instead of three phases

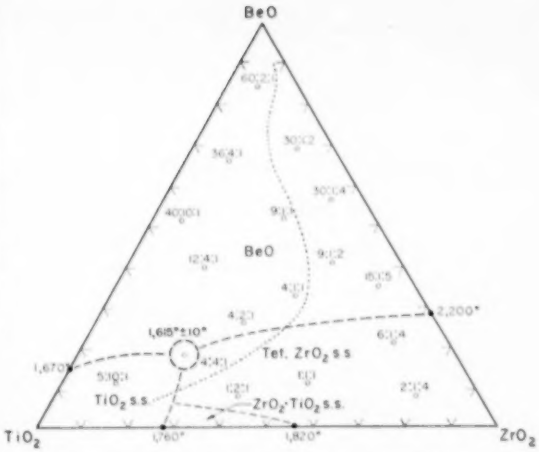

FIGURE 1. *The system* BeO-TiO_2-ZrO_2.

This figure shows the approximate location and temperature of the invariant point and the probable phase boundaries. Compositions of the mixtures are indicated on the figure in molar ratios but are placed graphically according to weight percentages. All of the mixtures, whose compositions are located between the heavy-dash line and the BeO-TiO_2 join, could be matured to imperviousness but only when the specimens were small. Mixture 1:2:1 indicates it to be the molecular ratio 1BeO:2TiO_2:1ZrO_2 and is not intended to infer a compound formulation.

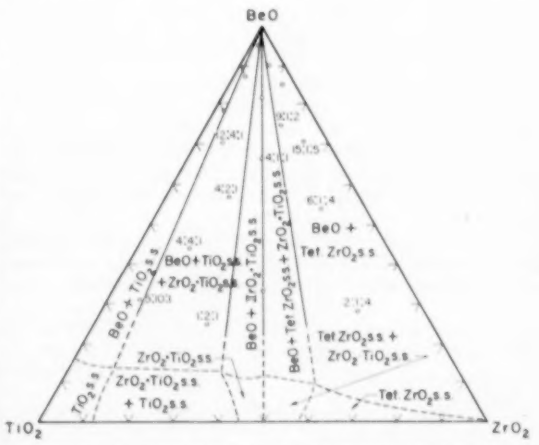

FIGURE 2. *Isothermal section of the system* BeO-TiO_2-ZrO_2 *at 1,550° C.*

The equilibria shown between zero and 20 mole percent of BeO are based only upon the reported equilibria for the TiO_2-ZrO_2 system. The mole ratio mixtures are located on the diagram on a mole percent basis. Mixture 1:2:1 indicates it to be the molecular ratio 1BeO:2TiO_2:1ZrO_2 and is not intended to infer a compound formulation.

present in these mixtures, indicating that the ZrO_2·TiO_2 compound had not crystallized completely during cooling.

3.2. Ceramic Bodies

Table 1 gives the property values determined for specimens fired in an electrically heated furnace and used for preliminary maturing range studies (about ½ in. high) and for those fired in a gas-heated furnace

TABLE 1. *Maturing-range studies and compressive-strength results of some* BeO-TiO_2-ZrO_2 *porcelains*

Composition						Results of maturing-range studies [a]					Properties of compressive-strength specimens [b]					
Molecular			Weight			Maturing [c] range	Properties at maturity				Firing temperature	Shrinkage (±0.05)	Absorption (±0.005)	Bulk [d] density (±0.005)	Height: diameter ratio	Strength at [illegible] temperature [illegible]
BeO	TiO_2	ZrO_2	BeO (±0.01)	TiO_2 (±0.01)	ZrO_2 (±0.01)		Firing temperature	Shrinkage (±0.05)	Absorption (±0.005)	Bulk [d] density (±0.005)						
			%	%	%	°C.	°C.	%	%	g/cm³	°C.	%	%	g/cm³		lb/in.²
1	1	1	10.97	35.02	54.01	O.F. 1,550	.....	.....	.....	.....	.....	.....	.....	.....	.....	.....
1	2	1	8.12	51.88	40.00	O.F. 1,500	.....	.....	.....	.....	.....	.....	.....	.....	.....	.....
2	1	4	8.03	12.83	79.14	O.F. 1,550	.....	.....	.....	.....	.....	.....	.....	.....	.....	.....
4	1	1	33.01	26.35	40.64	1,500 to 1,550	1,550	15.6	0.00	3.82	1,525	17.5	0.01	3.87	1.98	260×10³
4	2	1	26.12	41.71	32.17	1,500 to 1,550	1,550	16.7	.00	3.96	1,525	18.7	.01	4.02	1.97	244
4	4	1	18.43	58.87	22.70	1,500 to 1,550	1,550	16.8	.00	3.92	1,550	18.3	.01	3.95	1.95	231
5	10	1	11.94	76.29	11.77	1,500 to 1,550	1,550	16.8	.00	3.85	1,550	18.1	.01	3.90	1.97	239
6	1	4	20.77	11.05	68.18	O.F. 1,550	.....	.....	.....	.....	.....	.....	.....	.....	.....	.....
9	1	1	52.58	18.65	28.77	1,500 to 1,550	1,550	16.3	.01	3.43	1,525	17.8	.00	3.42	2.02	227
9	1	2	40.83	14.49	44.68	O.F. 1,650	.....	.....	.....	.....	.....	.....	.....	.....	.....	.....
12	4	1	40.41	43.01	16.58	1,500 to 1,600	1,500	17.8	.00	3.63	1,525	21.4	.01	3.63	2.05	271
15	1	5	35.03	7.46	57.51	O.F. 1,550	.....	.....	.....	.....	.....	.....	.....	.....	.....	.....
30	1	2	69.70	7.42	22.88	O.F. 1,500	.....	.....	.....	.....	.....	.....	.....	.....	.....	.....
30	1	4	56.72	6.04	37.24	O.F. 1,550	.....	.....	.....	.....	.....	.....	.....	.....	.....	.....
36	4	1	67.04	23.79	9.17	1,450 to 1,550	1,500	18.7	.00	3.27	1,525	20.4	.01	3.27	1.98	241
40	10	1	52.26	41.30	6.44	1,450 to 1,600	1,550	18.3	.00	3.41	1,550	20.5	.01	3.39	1.99	259
60	2	1	84.14	8.95	6.91	1,550 to 1,600	1,550	18.1	.00	3.03	1,550	23.0	.01	2.96	1.94	221

[a] All specimens for this determination were heated in an electrically heated furnace (ThO_2 resistor-type) for 1 hr. at the temperatures indicated.
[b] All specimens for this determination were heated in a gas-fired furnace for 1 hr. at the temperatures indicated.
[c] Maturing range is defined as that temperature interval resulting in an equivalent water-absorption value of 0.10 percent or less. "O.F. 1,550° C." indicates that a specimen had overfired at 1,500° C. and that at the next lower temperature of heating, a 50-deg-C. interval, a specimen had not reached a matured condition.
[d] Values calculated from the dry weight of the specimens and from the volume determined, using a mercury volumeter.
[e] The numerical average of three test values.

and used for the compressive-strength tests (about 1¼ in. high). Although both were made in the same manner, it should be noted that shrinkage and bulk density values obtained for the larger specimens fired in the gas-heated furnace were higher than those for the smaller specimens fired in the electrically heated furnace at the same apparent temperatures. The area of the ternary diagram (fig. 1) between the heavy dash-line and the BeO–TiO_2 join indicates the mixtures that could be matured to an impervious condition.

Table 2 gives the maturing data, the flexural strength, and elasticity both at room temperature and at 1,800° F (982° C) determined statically, and Young's modulus, shear modulus, Poisson's ratio, and bulk modulus determined sonically at room temperature. It should be noted that the value of Poisson's ratio for BeO-TiO_2-ZrO_2 porcelains ranges between 0.17 and 0.24.

When the bars for these tests were first made, it was found that those that did not contain at least 70 weight percent of BeO had cracked during the maturing treatment. Unfortunately, these cracks were all internal, and they were not found until the specimens had been ground to size for the transverse-strength tests. Another set of specimens was made, which behaved identically. When a third set of specimens was made in which 2 weight percent

TABLE 2. *Flexural strength and elasticity of some* BeO-TiO_2-ZrO_2 *porcelains*

Mole [a] composition	Number of specimens [b]	Maturing data [c]		Bulk density [d]		Room temperature [e]				Strength in bending (flexural) at — [f]					
						Sonic elastic properties				Room temperature			1,800° F (982° C)		
BeO:TiO_2:ZrO_2		Firing temperature	Absorption	Calculated	Mercury	Young's modulus	Shear modulus	Poisson's ratio	Bulk modulus	Number of specimens	Transverse strength	Young's modulus	Number of specimens	Transverse strength	Young's modulus
		°C	%	g/cm³	g/cm³	lb/in.²	lb/in.²		lb/in.²		lb/in.²	lb/in.²		lb/in.²	lb/in.²
4:4:1C	3	1,550	0.99	3.66	3.68	18.7×10^6	8.0×10^6	0.17	5.3×10^6	1	$(6.0)\times10^3$	18.7×10^6	2	11.9×10^3	21.5×10^6
5:10:1C	1	1,550	.80	3.58	3.60	20.4	8.6	.18	5.8				1	9.1	23.5
9:1:1	6	1,525	.01	3.55	3.55	36.4	14.8	.23	9.9	2	12.0	39.5	3	15.0	29.0
12:4:1	4	1,525	.02	3.51	3.52	37.0	14.9	.24	9.9	2	14.3	38.3	1	16.5	31.8
12:4:1	4	1,525	.01	3.56	3.57	38.8	15.7	.24	10.4	1	18.1	36.9	2	15.1	26.7
36:4:1	4	1,500	.01	3.24	3.24	43.6	18.1	.20	12.1	2	16.6	44.6	1	16.5	38.3
36:4:1C	6	1,500	.36	3.09	3.11	40.6	16.7	.22	11.1	2	15.1	38.1	4	11.5	30.8
40:10:1	2	1,550	.01	3.36	3.36	43.0	17.7	.22	11.8	1	18.9	41.9	1	12.1	31.1
60:2:1	7	1,550	.35	2.96	2.99	41.2	17.3	.19	11.5	2	14.5	46.8	4	10.8	29.2

[a] The weight compositions of these molar mixtures are given in table 1. Those marked "C", i. e., 4:4:1C, indicate an admixture of 2 weight percent of CaO to the base composition.
[b] Because of cracking, only a limited number of specimens were obtained.
[c] All specimens were heated in a gas-fired furnace for 1 hr at the temperatures indicated.
[d] These values were calculated from the dry weight and the measured dimensions, and from the volumes determined, using a mercury volumeter.
[e] Young's modulus and the shear modulus were calculated by using the various flexural and the torsional vibration frequencies, respectively. Poisson's ratio and the bulk modulus were calculated from these moduli.
[f] These values were determined statically.

of CaO was added to the base mixture, a larger percentage of usable specimens was obtained. It was expected that the CaO admixture would form a stabilized, cubic zirconia instead of a monoclinic or tetragonal zirconia phase. It was not known at that time that the compound ZrO_2-TiO_2 exists. When the compound was identified and its properties determined [19], it was reasoned that the crystallographic transformation of the compound was responsible for the observed cracking of the specimens rather than the phase transformation of zirconia.

Although the crystallographic data are not thoroughly understood at present, it is known that the unit-cell dimension of the *c*-axis of ZrO_2-TiO_2 undergoes a large change (from 5.447 to 5.483 A) in the interval between 800° and 1,200° C. This could easily account for the cracking of the large, bar-shaped specimens formed in the first and second trials. Although it is a matter of conjecture, because time did not permit investigation, it is believed that ZrO_2-TiO_2 formed from CaO-stabilized, cubic zirconia undergoes to only a small extent, if at all, the crystallographic phase transformation associated with material formed from either monoclinic or tetragonal zirconia.[4]

Table 3 gives the results of the short-time (1 hr) stress-strain tests at 1,800° F for some BeO-TiO_2-ZrO_2 porcelains, and their strain rates under 6,000-, 9,000-, and 12,000-lb/in.^{2} stress for 5-, 10-, 20-, 30-, and 60-min intervals. At 12,000-lb/in.^{2} stress, the strain rates for these were intermediate between those of the BeO-Al_2O_3-ZrO_2 [3] and the BeO-Al_2O_3-TiO_2 [4] porcelains.

4. The System BeO-CeO_2-ZrO_2

4.1. Phase Relations

a. The System BeO-CeO_2

In two papers, von Wartenberg and coworkers [6,20] reported this system to be a simple one, with the eutectic at about 80 weight percent of CeO_2 and 1,960° C. The volatilization of CeO_2 was said to be very slight, but that of Ce_2O_3, which forms easily and melts at about 1,690° C, as appreciable over 2,000° C.

b. The System BeO-ZrO_2

The equilibria are described in section 3.1, b.

c. The System CeO_2-ZrO_2

This system has been given as a simple one with a minimum at about 40 weight percent of ZrO_2 and 2,400° C [10] and, also at about 2,300° C. [20]. Considerable solid solution in the system, involving change of the zirconia lattice to a cubic fluorite-type lattice, has been reported [8, 21]. Recently, it was shown that a tetragonal, not cubic, zirconia solid-solution phase is formed [22, 23, 24]. Duwez and Odell [24] proposed a diagram to satisfy the following equilibria relations: (1) A tetragonal zirconia solid solution containing approximately 10 mole percent of CeO_2, and transformation to a monoclinic solid-solution form below 1,000° C, (2) extensive cubic solid solution from about 24 to 100 mole percent of CeO_2 at 2,000° C, (3) a narrow two-phase region at 2,000° near 20 mole percent of CeO_2, and (4) extension of the two-phase region with lowering of temperature, so that the cubic CeO_2 solid-solution range extends from about 65 mole percent at 1,375° to about 90 mole percent of CeO_2 at 1,100° C.

d. The System BeO-CeO_2-ZrO_2

At temperatures above 1,970° C, Ruff and coworkers [25] made isothermal studies of the melting of ternary mixtures containing at least 50 mole percent of ZrO_2. Curtis [23] investigated specimens of a few ternary mixtures containing at least 80 mole percent of ZrO_2 and found that a body composed of about 10 mole percent of BeO, 10 mole percent of CeO_2, and 80 mole percent of ZrO_2 appeared to have the best thermal-shock resistance.

Figure 3 shows an isothermal section of this system based upon X-ray examination of specimens that had been heated at 1,750° C during the maturing-

[4] Unpublished data have been obtained by Coughanour and Roth to check this theory. They found that ZrO_2-TiO_2, formed from CaO-stabilized, cubic zirconia has a *c*-axis of 5.459 A when quenched from 1,550° C and 5.440 A when furnace-cooled from 1,475° C. This difference represents approximately one-half of the *c*-axis change observed, using pure ZrO_2-TiO_2, and, in general, agrees with both the proposed theory and the results of this investigation.

TABLE 3. *Short-time (1 hr) stress-strain tests and interval strain rates for some* BeO-TiO_2-ZrO_2 *porcelains at 1,800° F (982° C)*

All rates of strain are $n \times 10^{-6}$ (in./in.)/min.

Mole % composition BeO: TiO_2: ZrO_2	Number of specimens	Strain rates at 1,800° F and—[5]						Interval-strain rates at 1,800° F and—													
								6,000-lb/in.^{2} stress for—					9,000-lb/in.^{2} stress for—					12,000-lb/in.^{2} stress for—				
		6,000-lb/in.^{2} stress	7,500-lb/in.^{2} stress	9,000-lb/in.^{2} stress	10,500-lb/in.^{2} stress	12,500-lb/in.^{2} stress	13,500-lb/in.^{2} stress	0 to 5 min	0 to 10 min	0 to 20 min	0 to 30 min	0 to 60 min	0 to 5 min	0 to 10 min	0 to 20 min	0 to 30 min	0 to 60 min	0 to 5 min	0 to 10 min	0 to 20 min	0 to 30 min	0 to 60 min
4:4:1C	1	1.5	...	1.5	...	(x)	....	3.0	(2.4)	2.6	2.1	1.5	2.8	2.6	2.1	1.9	1.5	...	...	...	...	....
9:1:1	1	2.8	2.3	2.6	2.7	(x)	....	5.6	5.0	4.1	3.7	2.8	3.8	3.6	3.2	3.1	2.6	...	...	...	...	....
12:4:1	1	2.3	...	2.8	2.9	3.2	3.4	5.5	4.4	3.3	3.0	2.3	4.5	4.0	3.1	3.1	2.8	3.8	3.7	3.7	3.5	3.2
36:4:1	2	1.0	1.0	1.0	1.1	1.2	(x)	2.1	(1.7)	2.0	1.2	1.0	1.5	(0.9)	1.1	1.1	1.0	...	1.3	1.3	1.4	1.2
36:4:1C	2	1.0	...	1.3	1.3	1.4	(x)	3.0	2.3	1.9	1.5	1.0	2.5	2.0	1.8	1.6	1.3	2.4	2.3	1.8	1.7	1.4
40:10:1	1	1.7	1.6	1.6	1.7	(x)	....	3.2	3.0	2.6	2.4	1.7	2.3	(2.0)	2.2	1.9	1.6	...	...	...	...	....
60:2:1	2	1.5	1.3	1.7	2.1	(x)	....	4.4	2.4	2.3	2.1	1.5	(1.9)	2.4	1.9	1.8	1.7	...	...	...	...	....

[5] The weight compositions of these molar mixtures are given in table 1. Those marked "C", i.e., 4:4:1C, indicate an admixture of 2 weight percent of CaO to the base composition. The maturing temperatures and the properties of the matured porcelains are given in table 2.

[6] Beginning at 6,000-lb/in.^{2} stress, each stress was maintained for 1 hr, or until rupture occurred. The (x) indicates that the specimen had broken after that stress was applied but before the hourly period had elapsed.

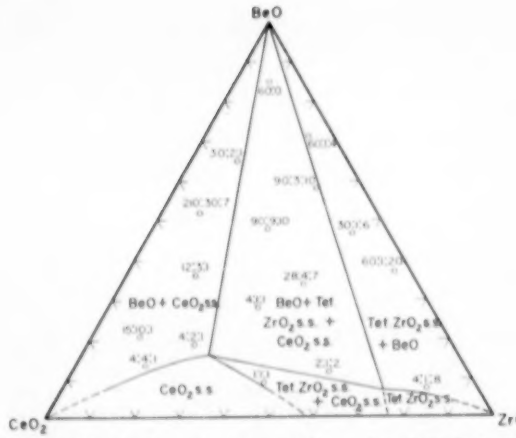

FIGURE 3. *Isothermal section of the system* BeO-CeO_2-ZrO_2 *at 1,750° C.*

The compositions of the mixtures are indicated on the figure in molar ratios, but are placed graphically according to weight percentages. Mixture 4:1:8 indicates it to be the molecular ratio $4BeO:1CeO_2:8ZrO_2$ and is not intended to infer a compound formulation.

range tests. Each sample was sectioned so that an interior surface could be used to prepare the X-ray diffraction patterns. The data indicate that this is a system of partial solid solutions with no binary or ternary compounds. Although BeO has not been reported as forming solid solutions with either CeO_2 or ZrO_2, it is apparent that it did enter both of the CeO-ZrO_2 solid solutions. For example, after being heated at 1,750° C, mixture 1B:1Ce:1Z contains no free BeO but only tetragonal ZrO_2 and cubic CeO_2 solid solutions. Similarly, mixture 4B:4Ce:1Z is almost a single-phase cubic CeO_2 solid solution containing only a very small amount of free BeO. It seems likely, therefore, that BeO should form a solid solution with CeO_2 in the binary as well as it does in the ternary system.

For the specimens used in this study, the phases identified at room temperature were the same as those shown at the 1,750° C isothermal section, with the following exceptions: Mixtures 4B:1Ce:8Z, 30B:1Ce:6Z, 60B:1Ce:4Z, and 60B:1Ce:20Z. At room temperature, mixture 60B:1Ce:20Z is composed of monoclinic ZrO_2 solid solution and BeO. The effect of a larger CeO_2 content (as in the other three mixtures) is that BeO and both monoclinic and tetragonal ZrO_2 solid solutions are present. With these data and that from other investigations [12, 23, 24], showing the 1,000° C transformation of tetragonal to monoclinic ZrO_2 solid solution, it is likely that at 1,750° C the four mixtures contain only tetragonal ZrO_2 solid solution and BeO.

When ternary mixtures were heated successively at 1,750°, 1,800°, and at 1,845° C for periods of 30 min at each temperature, the only liquid formation that could be determined by visual examination at room temperature had occurred in mixture 90B:9Ce:10Z, which had been heated at 1,845° C. From the data determined for the solid-state reactions at 1,750° C, it is evident that this is a simple ternary system. If the ternary eutectic were to be located at the 90B:9Ce:10Z composition, it would violate the laws of the phase rule, assuming that the phase diagrams of the binary systems, as previously published, are correct. However, it has been shown in this investigation that a solid solution probably exists at the CeO_2 side of the BeO-CeO_2 system. If this is true, it seems reasonable to assume that the reported

TABLE 4. *Maturing-range studies and compressive-strength results of some* BeO-CeO_2-ZrO_2 *porcelains*

Composition						Results of maturing-range studies [a]					Properties of compressive-strength specimens [b]						
Molecular			Weight			Maturing [c] range	Properties at maturity				Firing temperatures	Shrinkage (±0.05)	Absorption (±0.005)	Bulk [d] density (±0.005)	Height-diameter ratio	Strength at room temperature (±5,000)	Number of specimens
BeO	CeO_2	ZrO_2	BeO (±0.01)	CeO_2 (±0.01)	ZrO_2 (±0.01)		Firing temperature	Shrinkage (±0.05)	Absorption (±0.005)	Bulk [d] density (±0.005)							
			%	%	%		° C	° C	%	%	g/cm³	° C	%	%	g/cm³		lb/in.²	
1	1	1	7.81	53.73	38.46	O.F. 1,750											
2	1	2	10.68	36.73	52.59	O.F. 1,700						1,750	12.0	2.6	4.71	1.80	112	2
4	1	1	25.31	43.53	31.16	1,600 to 1,750	1,750	15.6	0.00	4.90		1,750	16.6	0.06	4.63	1.89	184	3
4	1	8	7.96	13.68	78.36	1,600 to 1,750	1,700	13.9	.01	5.14								
4	2	1	17.63	60.66	21.71	1,600 to 1,700	1,650	14.7	.01	5.37		1,700	17.1	.06	5.25	1.89	211	1
4	4	1	10.98	75.51	13.51	1,600 to 1,750	1,750	14.4	.01	5.80		1,750	18.4	.04	5.87	1.83	166	4
12	3	1	31.95	54.94	13.11	1,550 to 1,750	1,700	15.9	.00	4.71								
15	10	1	16.91	77.54	5.55	1,650 to 1,750	1,750	14.4	.00	5.48								
28	4	7	31.11	30.58	38.31	1,550 to 1,750	1,700	15.6	.01	4.53								
30	1	6	45.16	10.36	44.48	1,550 to 1,700	1,650	17.2	.00	3.99		1,650	17.7	.07	3.92	2.03	247	1
30	2	1	61.62	28.26	10.12	1,550 to 1,700	1,700	18.0	.00	3.67								
60	1	1	83.56	9.58	6.86	1,550 to 1,700	1,700	18.1	.00	3.14		1,650	17.9	1.8	2.89	1.88	199	1
60	1	4	69.30	7.95	22.75	1,550 to 1,700	1,700	18.0	.01	3.42		1,650	18.4	0.23	3.24	1.86	247	1
60	1	20	36.28	4.16	59.56	O.F. 1,700												
90	3	10	56.29	12.91	30.80	1,550 to 1,750	1,750	17.6	.01	3.74								
90	9	10	44.74	30.78	24.48	1,550 to 1,750	1,750	16.8	.00	4.13		1,700	17.1	.09	3.85	1.87	233	1
210	30	7	46.58	43.78	7.64	1,550 to 1,700	1,700	16.7	.00	4.15								

[a] All specimens for this determination were heated in an electrically heated furnace (ThO_2 resistor-type) for 1 hr at the temperatures indicated.

[b] All specimens for this determination were heated in a gas-fired furnace for 1 hr at the temperatures indicated. At least three of each mixture were heated originally, some had cracked during heating.

[c] Maturing range is defined as that temperature interval resulting in an equivalent water-absorption value of 0.10 percent or less. "O.F. 1,750° C" indicates that a specimen had overfired at 1,750° C and that at the next lower firing temperature, a 50-deg-C interval, a specimen had not reached a matured condition.

[d] Values calculated from the dry weight of the specimens and from the volume determined, using a mercury volumeter.

BeO-CeO_2 eutectic composition is incorrect. If it is located between 0 and 40 weight percent of CeO_2, the equilibrium diagram of the BeO-CeO_2-ZrO_2 system can be given with the ternary eutectic at about the composition of mole mixture 90B:9Ce:10Z. It is for these reasons that no equilibrium diagram is given for the BeO-CeO_2-ZrO_2 system.

4.2. Ceramic Bodies

Table 4 gives the property values determined for specimens fired in an electrically heated furnace and used for the preliminary maturing-range studies, and those of the compressive-strength specimens, fired in a gas-heated furnace. Except for mixtures 1B:1Ce:1Z and 2B:1Ce:2Z, in the area of the heavy-dash line near the CeO_2-ZrO_2 eutectic, and 60B:1Ce:20Z near the BeO-ZrO_2 eutectic, all of the mixtures shown on figure 3 could be matured to an impervious condition.

Table 5 gives the maturing data, the flexural strength and elasticity, determined statically, both at room temperature and at 1,800° F, and Young's modulus, shear modulus, Poisson's ratio, and bulk modulus determined sonically at room temperature. The value for Poisson's ratio ranges from 0.21 to 0.28 for these BeO-CeO_2-ZrO_2 porcelains.

In this, as well as in the similar system containing TiO_2, considerable difficulty was encountered in forming satisfactorily sound bars for the transverse-strength and elasticity tests. Here again, it was found that the cracks that had developed were all internal and were not found until the specimens had been ground to size for the various tests. Only those few bars from the first lot to be formed, which were found to be satisfactory, were used. No attempts were made to form more of the mixtures to usable specimens. It is apparent from figure 3 that the majority of the mixtures used in this study lie within the fields containing tetragonal zirconia at 1,750° C. In some of the mixtures, this reverts to the monoclinic form during cooling. Both the

TABLE 5. *Flexural strength and elasticity of some* BeO-CeO_2-ZrO_2 *porcelains*

Mole [a] composition BeO:CeO_2:ZrO_2	Number of specimens [b]	Maturing data [c]		Room temperature [d]		Room temperature [e]				Strength in bending (flexural) at—[f]					
				Bulk density		Sonic elastic properties				Room temperature			1,800° F (982° C)		
		Firing temperature	Absorption	Calculated	Mercury	Young's modulus	Shear modulus	Poisson's ratio	Bulk modulus	Number of specimens	Transverse strength	Young's modulus	Number of specimens	Transverse strength	Young's modulus
		°C	%	g/cm³	g/cm³	lb/in.²	lb/in.²		lb/in.²		lb/in.²	lb/in.²		lb/in.²	lb/in.²
1:1:1	4	1,750	(1.8 to 0.00)	(5.29 to 5.61)	(5.33 to 5.64)	(22.2 to 26.7×10⁶)	(8.7 to 10.4×10⁶)	0.27	(5.8 to 6.9×10⁶)	2	14.2×10³	22.4×10⁶	2	14.2×10³	20.1×10⁶
2:1:2	4	1,750	1.2	5.08	5.06	22.9	8.8	.28	5.9	2	13.6	23.3	2	15.8	17.9
4:1:1	4	1,750	0.04	4.66	4.67	30.4	12.0	.26	8.0	2	17.3	30.3	2	18.1	23.2
4:2:1	3	1,700	.01	5.35	5.40	33.0	13.0	.27	8.6	1	18.8	34.7	2	16.1	25.1
4:4:1	4	1,750	.08	5.82	5.86	31.3	12.2	.28	8.2	2	15.6	30.8	2	13.0	20.4
12:3:1	1	1,700	.01	4.70	4.72	38.2	15.2	.25	10.2				1	18.0	24.8
15:10:1	2	1,750	.01	5.51	5.58	35.1	13.8	.27	9.2	1	19.7	35.8	1	19.5	26.2
30:2:1	2	1,700	3.1	3.35	3.36	30.1	12.3	.22	8.2	1	12.0	29.5	1	12.1	23.9
60:1:1	1	1,650	4.4	2.83	2.82	34.0	14.1	.21	9.4				1	12.0	25.3
60:1:4	4	1,650	0.77	3.21	3.22	37.1	15.1	.23	10.1	2	23.4	38.4	2	16.6	28.9
80:9:10	1	1,700	1.8	3.79	3.79	30.7	12.3	.25	8.2				1	16.6	26.7

[a] The weight compositions of these molar mixtures are given in table 4.
[b] Because of firing cracking, only a limited number of specimens were obtained.
[c] All of the specimens were heated in a gas-fired furnace for 1 hr at the temperatures indicated.
[d] These values were calculated from the dry weights and the measured dimensions, and from the volumes determined, using a mercury volumeter.
[e] Young's modulus and the shear modulus were calculated by using the various flexual and the torsional vibration frequencies, respectively. Poisson's ratio and the bulk modulus were calculated from these moduli.
[f] These values were determined statically.

TABLE 6. *Short-time (1 hr) stress-strain tests and interval strain rates for some* BeO-CeO_2-ZrO_2 *porcelains*

All rates of strain are $n \times 10^{-6}$ (in./in.)/min.

Mole [a] composition BeO:CeO_2:TiO_2	Strain rates at 1,800° F. (982° C.) and—[b]						Interval strain rates at 1,800° F. and—															
							6,000-lb/in.² stress for—					12,000-lb/in.² stress for—					15,000-lb/in.² stress for—					
	6,000-lb/in.² stress	9,000-lb/in.² stress	12,000-lb/in.² stress	13,500-lb/in.² stress	15,000-lb/in.² stress	16,500-lb/in.² stress	0 to 5 min	0 to 10 min	0 to 20 min	0 to 30 min	0 to 60 min	0 to 5 min	0 to 10 min	0 to 20 min	0 to 30 min	0 to 60 min	0 to 5 min	0 to 10 min	0 to 20 min	0 to 30 min	0 to 60 min
1:1:1	0.9	0.6	0.7	(x)	----	----	2.9	2.3	1.5	1.3	0.9	2.3	1.6	0.9	0.7	0.7	--	--	--	--	--
2:1:2	1.0	.6	.9	0.9	1.1	(x)	3.3	2.6	1.8	1.3	1.0	1.6	1.1	.9	.9	.9	1.9	1.6	1.3	1.3	1.1
4:1:1	0.8	1.0	1.0	----	1.3	1.1	(1.4)	1.8	1.2	1.1	0.8	(1.9)	1.9	1.4	1.2	1.0	2.6	2.3	1.9	1.6	1.3
4:2:1	.8	1.0	0.8	.8	0.7	0.9	3.4	2.2	1.5	1.3	.8	1.7	1.1	1.2	1.0	0.8	1.0	0.8	0.9	0.8	0.7
4:4:1	1.2	0.4	1.2	(x)	----	----	3.1	2.8	2.0	1.8	1.2	(1.8)	1.9	1.8	1.7	1.2	--	--	--	--	--
60:1:4	1.5	1.7	(x)	----	----	----	4.1	3.4	2.6	2.1	1.5	--	--	--	--	--	--	--	--	--	--

[a] The weight compositions of these molar mixtures are given in table 4. The maturing temperature and the properties of the matured porcelains are given in table 5. Only one specimen of each of these mixtures was used for the short-time stress-strain tests.
[b] Beginning at 6,000 lb/in.², each stress (at 1,500-lb/in.² increments) was maintained for 1 hr or until rupture occurred. The (x) indicates that the specimen had broken after that stress was applied but before the hourly period had elapsed.

tetragonal to monoclinic transformation and the known high expansion of tetragonal zirconia (coefficient of 12 to 13.5×10^{-6}) [22] are considered to have been of sufficient magnitude to have caused the physical deterioration of the samples. Because of the limited time available to this project, no attempts were made to eliminate these conditions by transforming the zirconia to the stable cubic form by the addition of CaO.

Except for mixtures 2B:1Ce:2Z and 4B:1Ce:8Z, all of those studied showed varying reduction of CeO_2. Usually, this could be seen only when the interior of a specimen was examined. However, it is well known that very small amounts of Ce_2O_3 (less than 0.01%) have extremely strong coloring effects. The amount of reduction in these samples is considered as being very small because no evidence of Ce_2O_3 could be found by petrographic or X-ray analyses.

Table 6 gives the results of the short-time (1 hr) stress-strain tests at 1,800° F. for some of these porcelains and their interval-strain rates under 6,000-, 12,000-, and 15,000-lb/in.^{2} stress for 5-, 10-, 20-, 30-, and 60-min intervals. At 12,000-lb/in.^{2} stress, the strain rates for these BeO-CeO_2-ZrO_2 porcelains were rather low, about 1.5×10^{-6} (in./in.)/min, and were very similar to those of the BeO-Al_2O_3-TiO_2 porcelains [4].

5. The System BeO-Cr_2O_3-ZrO_2

5.1. Phase Relations

a. The System BeO-Cr_2O_3

Minimum melting at about 30 weight percent of BeO and 2,230° C has been reported [6] for this system. Although $BeO+Cr_2O_3$ mixtures were not investigated in the present study, the compound beryllium chromate (BeO-Cr_2O_3), the chromia analog of chrysoberyl (BeO-Al_2O_3), was identified in most of the BeO-Cr_2O_3-ZrO_2 mixtures heated at 1,800° C (see section 5.2).

It was found that this orthorhombic compound is isostructural with chrysoberyl and has the following approximate crystallographic parameters: $a=10.0$ A, $b=5.8$ A, $c=4.5$ A, as compared to those of chrysoberyl: $a=9.39$ A, $b=5.47$ A, and $c=4.24$ A. No attempts were made to synthesize the pure compound.

b. The System BeO-ZrO_2

The equilibria are described in section 3.1, b.

c. The System Cr_2O_3-ZrO_2

A rather flat and long minimum melting region at about 30 to 60 weight percent of ZrO_2 and about 2,320° C has been reported for this system [9].

d. The System BeO-Cr_2O_3-ZrO_2

No literature references could be found describing the phase relations for the beryllia-chromia-zirconia system. In this investigation, an X-ray examination was made, using an interior surface of each mixture heated at 1,800° C. The compositions studied are located within the subordinate ternary system BeO-$BeO{\cdot}Cr_2O_3$-ZrO_2. Beryllia, monoclinic zirconia, and beryllium chromate are found in all mixtures except 1B:1Cr:1Z and 4B:4Cr:1Z. In these, only monoclinic zirconia and $BeO{\cdot}Cr_2O_3$ are present. There are no apparent solid solutions formed between any binary or ternary combination of beryllia, monoclinic zirconia, and beryllium chromate, and there are no known ternary compounds.

Figure 4 shows a possible liquidus surface configuration for this system based upon extremely limited data and a considerable amount of speculation. The compound $BeO{\cdot}Cr_2O_3$ should melt congruently if it is assumed that the BeO-Cr_2O_3 system contains approximately the same equilibria relations as are present in the BeO-Al_2O_3 [4] system. By a similar analogy the compound $BeO{\cdot}3Cr_2O_3$ also may be present and may melt congruently. It seems reasonable to assume, from previous work on pure-oxide systems [1, 2, 3, 4], that the lowest melting invariant point in this system should be about 150 to 200 deg C above the lowest maturing-range temperature; i. e., at about 2,000° C (see section 5.2 for maturing data).

5.2. Ceramic Bodies

Reports of the volatility of Cr_2O_3 in binary mixtures [6, 9] indicate that it occurs at temperatures of approximately 2,000° C or higher, except when binary invariant points occur at lower temperatures. In this investigation it was found that an appreciable amount of Cr_2O_3 was lost from the specimens at temperatures as low as 1,600° to 1,700° C. This occurred on all exposed specimen surfaces, as evidenced by the relatively light surface color as compared to the dark interior color. In addition, recrystallized Cr_2O_3 was found as dark-green or green-gray contamination areas in various portions of the furnace refractories.

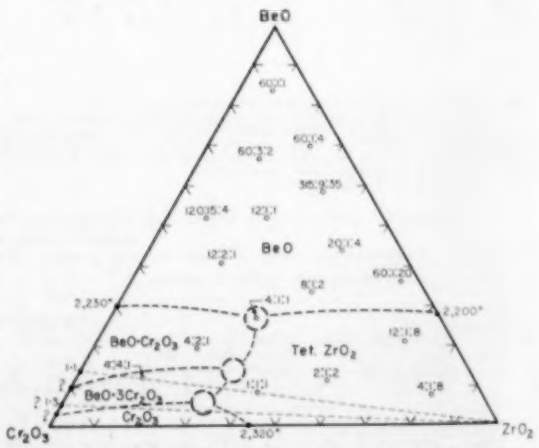

FIGURE 4. *Possible equilibria relations for the* BeO-Cr_2O_3-ZrO_2 *system.*

The equilibria of this system are based upon extremely limited data and a considerable amount of speculation. Beryllium chromate ($BeO{\cdot}Cr_2O_3$), the chromia analog of chrysoberyl, was found in all of the mixtures studied. The compositions of the mixtures are indicated on the figure in molar ratios, but are placed graphically according to weight percentages. Mixture 1:1:1 indicates it to be the molecular ratio $1BeO{:}1Cr_2O_3{:}1ZrO_2$ and is not intended to infer a compound formulation.

When heated at 1,800° C only two mixtures, 8B:1Cr:1Z and 12B:1Cr:1Z, were found to have matured. Because of the volatilization of the chromia, it was not considered practical to attempt further heatings at that temperature or higher temperature heatings. The time allotted to the project permitted only one attempt at reducing the maturing temperature. A series of mixtures were prepared that contained an admixture of 2 weight percent of CaO. When the first trials showed that the maturing temperatures were reduced by less than 50 deg C, and that the chromia loss remained appreciable, further work in this system was discontinued.

6. Discussion

The principal factors limiting the use of ceramics under stress conditions at temperatures above the useful temperature range for metals are their poor thermal-shock resistance and impact strengths. From a theoretical viewpoint, the resistance to thermal shock may be expressed in the general form

$$W \sim \frac{\sigma_t}{\alpha E} \cdot F\left(\frac{Kt}{\rho C l^2}\right),$$

where σ_t is the tensile strength, E is Young's modulus, α is the coefficient of linear thermal expansion, F is an unknown function, K is the thermal conductivity, t is the time at which maximum stress is developed, ρ is the density, C is the specific heat, and l^2 is the dimensional area.

Considering two specimens of the same material and size, one practically impervious and one slightly porous, it can be assumed that the coefficient of linear thermal expansion, Poisson's ratio, and the specific heat will be the same for both, and that for the porous specimen the tensile strength, the thermal conductivity, and the density will be lower. A reduction in Young's modulus with increased porosity is probable for a given body, as shown by the following values for the $1BeO:1CeO_2:1ZrO_2$ mixture:

Specimen	Absorption	Bulk density	Young's modulus
	%	g/cm^3	$lb./in.^2$
1	0.00	5.64	25.7×10^3
2	.23	5.49	23.6
3	1.63	5.33	22.2
4	1.83	5.28	22.5

It seems reasonable to expect that the value of the function, F, will not be appreciably different for a porous specimen and for a practically impervious specimen. Therefore, the expression $\sigma_t/\alpha E$ is the dominant consideration. The conjecture is made that porous oxide porcelains with requisite strength properties may prove of considerable interest in the search for materials of greater thermal-shock resistance than that associated with dense, practically impervious porcelains with high strength properties.

Although most of the mixtures studied in this investigation have fairly good strength properties, both at room temperature and at 1,800° F, additional work would be required if a considerable number of specimens of any one mixture are desired, all with nearly identical properties. This is illustrated by the variations shown by specimens of mixture 12B:4Ti:1Z, given in table 2, when similar samples were fired in the same furnace, at the same apparent temperature, but on different days.

7. Summary

7.1. The System BeO-TiO_2-ZrO_2

The configuration of the liquidus surfaces indicates the phase equilibrium relations to be those of a simple eutectic system with primary crystallization fields for BeO, tetragonal ZrO_2, ZrO_2-TiO_2, and TiO_2 solid solutions. The lowest melting ternary mixture studied occurs at about mole ratio $4BeO:4TiO_2:1ZrO_2$ and 1.615° ±10 deg. C.

Those mixtures whose compositions are within the triangular area bounded by BeO, ZrO_2-TiO_2, and TiO_2, and which contain at least 15 to 20 weight percent of BeO, could be matured to imperviousness, but only when the sample size was small (⅝ in. in diameter by ½ in. high). Considerable difficulty was encountered in fabricating large, usable samples (6 in. long by ¾ in. wide by $\frac{5}{16}$ in. thick) probably because of the length change, parallel to the c-axis, that occurs during the crystallographic transformation of ZrO_2-TiO_2 between 800° and 1,200° C. Some usable test specimens could be made when 2 weight percent of CaO was added to the base mixtures. The range of physical property values for the BeO-TiO_2-ZrO_2 porcelains investigated is given in table 7.

7.2. The system BeO-CeO_2-ZrO_2

The limited data available indicates this to be a simple system with primary crystallization fields of BeO, tetragonal ZrO_2 solid solution, and CeO_2 solid solution. No liquidus surface equilibrium diagram is given because the lowest melting invariant point was not located at a composition consistent with the phase rule. The data indicate that the invariant point temperature is at least as high as 1,845° C.

All of the mixtures studied, except those few near the reported BeO-ZrO_2 and the CeO_2-ZrO_2 eutectic compositions, could be matured to imperviousness, but only when a small specimen was used. Large, strength-test samples were difficult to obtain in usable form probably because of the large expansion of tetragonal zirconia and, for some samples, because of the crystallographic transformation of tetragonal zirconia to the monoclinic form during cooling. The range of physical property values for the BeO-CeO_2-ZrO_2 porcelains investigated is given in table 7.

7.3. The system BeO-Cr_2O_3-ZrO_2

Although the binary system BeO-Cr_2O_3 was not studied, beryllium chromate (BeO-Cr_2O_3), the chromia analog of chrysoberyl, was identified in all of the ternary mixtures. The crystallographic parameters of this orthorhombic compound are tentatively given as being $a=10.0$ A, $b=5.8$ A, and $c=4.5$ A. The compositions studied are located within

TABLE 7. *Summary and comparison of the physical properties of some* $BeO\text{-}TiO_2\text{-}ZrO_2$ *and* $BeO\text{-}CeO_2\text{-}ZrO_2$ *porcelains*

Physical properties	Units	$BeO\text{-}TiO_2\text{-}ZrO_2$ porcelains	$BeO\text{-}CeO_2\text{-}ZrO_2$ porcelains
Maturing range	°C	1,450 to 1,600	1550 to 1,750
Matured specimens:			
Temperature	°C	1,500 to 1,550	1,650 to 1,750
Shrinkage	%	16.3 to 18.7	13.9 to 18.1
Absorption	%	0.00 to 0.01	0.00 to 0.01
Density, bulk	g/cm³	3.00 to 3.96	3.14 to 5.80
Room-temperature properties:			
Statically tested:			
Compressive strength	lb/in.²	203 to 271×10³	112 to 247×10³
Transverse strength	lb/in.²	12.0 to 18.9×10³	12.0 to 23.4×10³
Young's modulus	lb/in.²	18.7 to 46.8×10⁶	22.4 to 38.4×10⁶
Sonically tested:			
Young's modulus	lb/in.²	18.7 to 43.6×10⁶	22.2 to 38.2×10⁶
Shear modulus	lb/in.²	8.0 to 18.1×10⁶	8.7 to 15.2×10⁶
Poisson's ratio		0.17 to 0.24	0.21 to 0.28
Bulk modulus	lb/in.²	5.3 to 12.1×10⁶	5.8 to 10.2×10⁶
1,800° F properties:			
Statically tested:			
Transverse strength	lb/in.²	9.1 to 16.5×10³	12.0 to 18.1×10³
Young's modulus	lb/in.²	21.5 to 38.3×10⁶	17.9 to 28.9×10⁶
Strain rates under—			
6,000-lb/in.² stress	(in./in.)/min	1.0 to 2.8×10⁻⁵	0.8 to 1.5×10⁻⁵
12,000-lb/in.² stress	(in./in.)/min	1.2 to 3.2×10⁻⁵	0.7 to 1.2×10⁻⁵
15,000-lb/in.² stress	(in./in.)/min		0.7 to 1.3×10⁻⁵

the subordinate ternary system $BeO\text{-}BeO\cdot Cr_2O_3\text{-}ZrO_2$.

Based upon extremely limited data and a considerable amount of speculation, it is suggested that the $BeO\text{-}Cr_2O_3\text{-}ZrO_2$ equilibrium diagram should contain three invariant points, each above 2,000° C, with primary crystallization fields for BeO, tetragonal ZrO_2, $BeO\cdot Cr_2O_3$, $BeO\cdot 3Cr_2O_3$, and Cr_2O_3.

Only two ternary mixtures attained an impervious structure when heated as high as 1,800° C for 1 hour. An admixture of 2 weight percent of lime, CaO, to some of these resulted in only a slight lowering of the maturing temperatures and no noticeable reduction of the chromia losses. Because of these appreciable chromia losses, no work was done to fabricate test specimens;

7.4. General Considerations

Of possible interest to the designers of high-temperature components are the room-temperature elastic properties (Young's modulus, shear modulus, Poisson's ratio, and bulk modulus) that are presented, it is believed for the first time, for a series of porcelain-type ceramics. It should be noted that the commonly accepted value of Poisson's ratio (0.30) for oxide porcelains is considerably higher than those determined for the $BeO\text{-}TiO_2\text{-}ZrO_2$ and $BeO\text{-}CeO_2\text{-}ZrO_2$ porcelains.

One of the more interesting sidelights of the investigation is the suggestion that porous oxide porcelains with requisite strength properties may prove of considerable interest in the search for materials of greater thermal-shock resistance than that associated with dense, practically impervious oxide porcelains with high-strength properties.

The authors express their appreciation to the late R. E. Moreland, who performed many of the physical property tests after fabricating many of the specimens; to S. Spinner, for the sonic testing; and to R. F. Geller, who outlined the original program.

8. References

[1] R. F. Geller, P. J. Yavorsky, B. L. Steierman, and A. S. Creamer, J. Research NBS **36,** 277 (1946) RP1703.
[2] S. M. Lang, L. H. Maxwell, and R. F. Geller, J. Research NBS **43,** 429 (1949) RP2034.
[3] S. M. Lang, L. H. Maxwell, and M. D. Burdick, J. Research NBS **45,** 366 (1950) RP2147.
[4] S. M. Lang, C. L. Fillmore, and L. H. Maxwell, J. Research NBS **48,** 298 (1952) RP2316.
[5] S. Spinner, J. Am. Ceram. Soc. **37,** 229 (1954).
[6] H. von Wartenberg, H. J. Reusch, and E. Saran, Z. anorg. u. allgem. Chem. **230,** 257 (1937).
[7] E. C. Henry, Pennsylvania State College, Quarterly Progress Report, Memorandum Report No. 19 (Feb. 15, 1949).
[8] O. Ruff, F. Ebert, and E. Stephan, Z. anorg. u. allgem. Chem. **180,** 221 (1929).
[9] H. von Wartenberg and H. Werth, Z. anorg. u. allgem. Chem. **190,** 178 (1930).
[10] H. von Wartenberg and W. Gurr, Z. anorg. u. allgem. Chem. **196,** 374 (1931).
[11] O. Ruff, F. Ebert, and H. von Wartenberg, Z. anorg. u. allgem. Chem. **196,** 335 (1931).
[12] H. von Wartenberg and H. Werth, Z. anorg. u. allgem. Chem. **213,** 321 (1933).
[13] E. Ryschkewitsch, Chem. App. **24,** 137 (1937.).
[14] W. Bussem, C. Schusteriuz, and A. Ungewiss, Ber. duet. keram. Ges. **18,** 433 (1937).
[15] H. G. Sowman and A. I. Andrews, J. Am. Ceram. Soc. **34,** 298 (1951).
[16] Personal communication from H. G. Sowman to R. S. Roth.
[17] F. H. Brown and P. Duwez, Jet Propulsion Lab., California Institute of Technology, Prog. Rept. No. 20–180 (Aug. 20, 1952).
[18] F. H. Brown and P. Duwez, J. Am. Ceram. Soc. **37,** 129 (1954).
[19] L. W. Coughanour, R. S. Roth and V. A. DeProsse, J. Research NBS **52,** 37 (1954) RP2470.
[20] H. von Wartenberg and K. Eckhardt, Z. anorg. u. allgem. Chem. **232,** 179 (1937).
[21] O. Ruff and F. Ebert, Z. anorg. u. allgem. Chem. **180,** 19 (1929).
[22] R. F. Geller and P. J. Yavorsky, J. Research NBS **35,** 87 (1945) RP1662.
[23] C. E. Curtis, J. Am. Ceram. Soc. **30,** 180 (1947).
[24] P. Duwez and F. Odell, J. Am. Ceram Soc. **33,** 274 (1950).
[25] O. Ruff, F. Ebert, and W. Loerpabel, Z. anorg. u. allgem. Chem. **207,** 310 (1932).

WASHINGTON, May 25, 1954

Journal of Research of the National Bureau of Standards Vol. 53, No. 4, October 1954 Research Paper 253

Effects of Recent Knowledge of Atomic Constants and of Humidity on the Calibrations of the National Bureau of Standards Thermal-Radiation Standards

Ralph Stair and Russell G. Johnston

The National Bureau of Standards thermal-radiation standards, as established and maintained since 1913, are based primarily upon the emission of a blackbody, using the Stefan-Boltzmann constant of total radiation $\sigma = 5.70 \times 10^{-12}$ watt/(cm^2 deg^4).

The present status of this constant is reviewed in relation to the recent experimental evidence for more accurate values of the velocity of light and for the other atomic constants effecting the value of σ. It is concluded that any change in the Stefan-Boltzmann constant is unimportant at this time.

An investigation is reported on the effect of the atmospheric water vapor on the transmitted radiant intensities of these lamps at the working distance of 2 meters. The usual variations in laboratory humidities will affect the certified calibrations of these standard lamps less than 0.3 percent and hence may be neglected in all radiometric work wherein they are employed.

One section of the paper is given to general instructions for the use of these standards in precision work.

1. Introduction

A convenient standard of thermal radiation was early recognized as an important requirement in scientific laboratories engaged in researches involving the use of radiant energy. Toward this end such a standard was set up at the Bureau by W. W. Coblentz four decades ago [1, 2][1] This standard continues to be used for all radiometric work, not only in this country but throughout much of the scientific world.

The choice of a carbon-filament lamp for this standard was a wise one. This type of lamp was in general use for illuminating purposes in this country during the early years of the present century. No other type has been found to equal the carbon-filament lamp in ruggedness and stability, although many styles and types of lamps have been developed by industry through the years. A study was made both of lamps under carefully controlled laboratory conditions [3] and of a number of lamps returned after years of service in various laboratories. This study established that these standards retain their original calibration with no significant change for more than 200 hours if not mechanically or electrically abused. A supply of these lamps acquired by the Bureau in World War I days has been extremely useful in the preparation of standards for use in many governmental and other scientific laboratories. They are preferred to some of the more recently manufactured carbon-filament lamps.

This standard [1, 2, 3] is based upon the radiation from a blackbody operated in the range of temperatures between about 1,000° and 1,150° C. For the original calibration it was assumed that the Stefan-Boltzmann constant of total radiation was $\sigma = 5.70 \times 10^{-12}$ watt/(cm^2 deg^4). Auxiliary measurements made directly, using an absolute thermopile [2], wherein electric-energy dissipation provided the basis of the calibration showed no systematic differences from those with the blackbody. Other measurements with a nocturnal-radiation instrument constructed for the United States Weather Bureau likewise showed agreement with the original blackbody calibrations.

[1] Figures in brackets indicate the literature references at the end of this paper.

2. Present Status of the Radiation Constants

The fundamental law of the blackbody, the Stefan-Boltzmann law, relates the total radiant flux, W, from a unit area of a blackbody to the absolute temperature by the relationship

$$W = \sigma T^4.$$

The precise value of the Stefan-Boltzmann constant of total radiation is based mainly upon factors associated with atomic structure according to the relationship

$$\sigma = \frac{2\pi^5 c^2 h}{15 c_2^4},$$

where

c = the velocity of light in cm/sec;
h = Planck's constant of action in erg sec;
c_2 = the second radiation constant in cm deg K;
σ = the Stefan-Boltzmann constant in w/(cm^2 deg^4 K).

In the recently published least-squares summaries of fundamental constants [4, 5], the value given for c is 2.99793×10^{10} cm/sec, h is 6.6252×10^{-27} erg sec, c_2 is 1.4388 cm deg, and σ is 5.6686×10^{-12} w/(cm^2 deg^4 K). Hence as a result of recent investigations the value of σ is placed approximately 0.55 percent lower than that employed in 1914.[2] This difference, however, is near the level of the experimental error

[2] Because the temperature scale in the region of 1,100° C, that is near the values of temperature employed in the blackbody calibrations of the original standards of thermal radiation, requires alteration by an insignificant amount [18, 19], no correction for temperature appears to be required at this time.

assessed in the original calibration. Because measurements with an absolute thermopile, in which only electrical constants entered, were in precise agreement with the blackbody determinations [1, 2], if any correction to the data were made at this time it probably should be based on a mean value between the two, namely, of an order of less than 0.3 percent. Taking into account the level of precision normally obtainable in radiometric work, it must be concluded that no correction to the original data is warranted at this time because of new information and changes in the value of the velocity of light or of the other atomic constants entering into radiant-energy emission.

3. Effect of Humidity

A knowledge of the precise radiant-energy output of these standards under conditions of variable humidity has recently been desired in a number of laboratories. Although it was pointed out by Coblentz [1] in 1914 that the radiation transmitted by the glass bulb of these lamps was confined principally to wavelengths less than 3.5 microns, and would therefore be affected but little by variations in atmospheric humidity and hence no correction for water-vapor absorption would be necessary, nevertheless, questions have arisen from time to time regarding the magnitude of this absorption. This possibly results from the fact that a number of water-vapor absorption bands are present in the near infrared spectral region. The present investigation was undertaken, therefore, to ascertain the amount of the attenuation of the radiant flux from the NBS standards of thermal radiation to see if any correction should be applied to the data.

3.1. Instruments and Method

As it was known that any humidity effect upon the calibration of the NBS standards of thermal radiation must be small, as indicated above, special precautions were taken in setting up an experiment to measure precisely the radiant energy from a group of lamps as a function of atmospheric humidity in a manner little affected either by temperature changes, or air currents within the laboratory, or by stray light from the sun or other sources. Toward this end a plywood box, approximately 24 by 36 by 120 in. painted a dull black inside and fitted with a suitable arrangement of diaphragms, was set up to house the 2-m optical path between the standard lamp and the thermopile. The box was arranged with a suitable window through which a self-recording hydrothermograph could be viewed without disturbing the humidity or temperature conditions within the box. Motor-driven fans were employed to stir the air within the box from time to time to insure relatively constant temperature and humidity conditions throughout.

Desired changes in humidity were accomplished partly by working at different seasons when different outside weather conditions existed. Thus the lowest humidities were obtained on clear, cold days during the winter, with outside air being brought into the box through a filter-trap, which was further cooled by dry ice. Additional absorption of water vapor within the box was accomplished by the use of P_2O_5 and other commercial driers. The highest humidities were obtained during the summer season by additional heating of the enclosure with electric coils and by adding live steam.

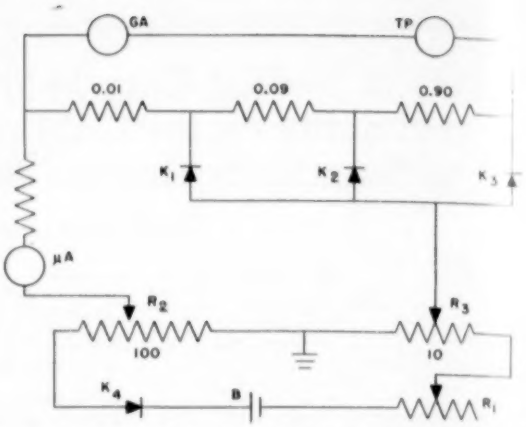

FIGURE 1. *Electric circuit employed in the potentiometer for the radiant-energy measurements.*

In the tests each lamp was subjected to a complete series of measurements without touching its adjustment in the socket, because it had been found that a significant error is sometimes attributable to a slight misalinement of the source relative to the thermopile.

In this work the standards were set up according to the general instructions applicable to their use. A special Lindeck type potentiometer [6] having a sensitivity of 0.005 to 0.5 μv per scale division, when used with a high-grade microammeter (ranges 0 to 50 μa and higher), was employed for measuring the lamp output. Thus the scale readings of microamperes corresponded directly to microvolts. This instrument, whose essential circuit elements are shown in figure 1, was employed in preference to the direct use of a galvanometer to avoid errors resulting from changes in circuit resistance and galvanometer sensitivity.

3.2. Results

Measurements were made on five lamps over a wide range in humidity. For each measurement the temperature and relative humidity were recorded. Then from the curves of figure 4, which was prepared from the Smithsonian meteorological tables [7] giving the density of water vapor at saturation as a function of temperature, the amount of precipitable water (the absolute humidity of the atmosphere) was determined in grams per cubic meter. The summer measurements on two lamps covering a humidity range of about 10 to 26 g of water per cubic meter are shown in figure 2, whereas the winter

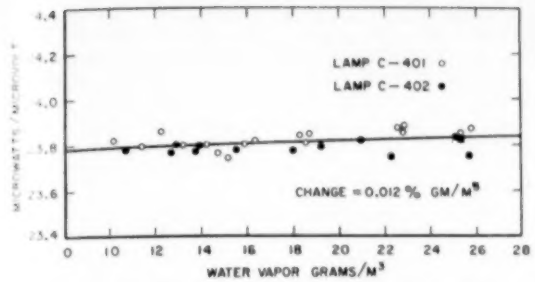

FIGURE 2. *Variation of transmitted radiant energy through 2 meters as a function of humidity.*

Summer measurements at high humidities, using thermopile 2028.

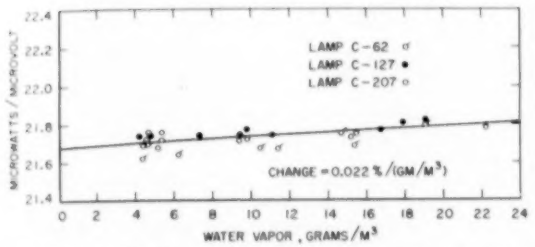

FIGURE 3. *Variation of transmitted radiant energy through 2 meters as a function of humidity.*

Winter measurements at low humidities, using thermopile 2030.

data on three lamps given in figure 3 cover a lower range extending from about 4 to 22 g/m³. The lowest value (4 g/m³) corresponds to the condition of the atmosphere for a room temperature near 70° F and a relative humidity of about 20 percent. The highest value of 26 g/m³ corresponds to a temperature of approximately 85° F and a relative humidity of about 90 percent. A value of 10 corresponds to a room temperature of 70° to 75° F and a relative humidity of approximately 55 percent—the value normally expected in Washington during July, at which time the original blackbody calibrations were made.[3] The differences in microwatts (per square centimeter) per microvolt in the two cases (see figs. 2 and 3) result because of the use of different thermopiles having unequal sensitivities.

An analysis by least squares, of the data for the five lamps studied, given in figures 2 and 3, shows a mean change of 0.017 percent per gram of water per cubic meter. As the work in the original calibration of the lamp standards is thought to have been performed under conditions of a humidity of approximately 10 g of water per cubic meter, any correction of the original data should be made on the basis of that humidity. The data illustrated in figure 4 indicate that the range in humidities ordinarily encountered in laboratories in this country will seldom exceed a change of more than 5 g/m³ from the basic value of 10 g on which the original measurements were made. As a difference of 5 g/m³ in humidity corresponds to a change in radiant energy of only 0.085 percent, no consideration need be taken of normal atmospheric humidities in the use of these standards in ordinary radiometric work.

[3] The distance at which the original standard lamps were calibrated, namely, 2.0 m, was not the same as that used for the calibration of the detectors by the blackbody. The latter distance varied from about 40 to 70 cm, and the air path was thoroughly dried by the use of P_2O_5.

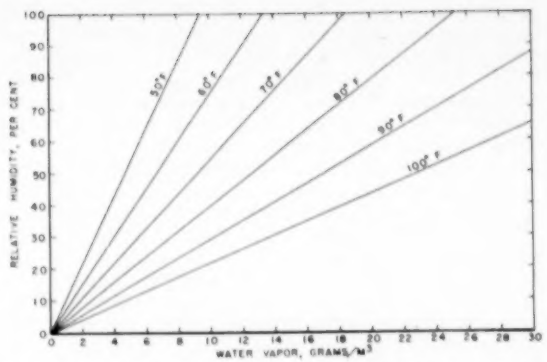

FIGURE 4. *Total atmospheric humidity as a function of relative humidity and temperature.*

From Smithsonian Meterological Tables.

A word of caution should be given at this point, however. Although no correction need be made for humidity in the use of these standards, the worker is often concerned with the measurement of radiant energy from sources rich in short ultraviolet or long infrared rays. In the former case, although water vapor may not be troublesome, transmission factors of radiometric windows require careful attention. In the infrared, especially at wavelengths longer than 4,000 mμ, the absorption of water vapor, CO_2, and other gases [8, 11], as well as the transmittance of window material [12] and the spectral efficiency of radiometer detecting surfaces [13], must be taken into account.

4. Operation of the Standards

As noted above, the carbon-filament lamp is employed as a standard because of its proved stability [14]. Calibration and operation at voltages (and currents) below the normal rated value add much to its life and general stability. Proper handling and care, further insure its reliability.

In operations wherein a galvanometer is employed directly, extraneous currents may be kept balanced by the use of an auxiliary control current from a special battery-operated shunt arrangement [15] to improve accuracy and linearity of the response (galvanometer deflection). Where a potentiometer setup can be employed, slightly higher accuracy may be obtained. The use of a light modulator and low-impedance tuned a-c amplifier may be found to give sufficiently accurate results and is to be highly recommended where noisy conditions prevail or where

speed of operation is important. The potentiometer or galvanometer is to be preferred for quiet locations where accuracy or precision in results is at a premium. The lamps employed (rated at about 50 w) are first seasoned, then marked for orientation (because the radiation is not the same in all directions), and then calibrated for the density of radiant flux at a fixed distance (usually 2 m) in the specified direction.

In operation, the lamp is screwed into an ordinary metal socket that is held upright by some convenient support, which cannot reflect light into the radiometer. The entire lamp bulb is to be exposed to the radiometer. Sufficient time must be given (say 5 min) for the glass base, which supports the filament, to become thoroughly warmed, otherwise errors will be introduced into the radiant-energy measurements The distance of the lamp is measured from the radiometer to the center (glass tip if present, the etched mark, or other special mark noted in the NBS report on a particular standard lamp) of the lamp bulb.

A black cloth, about 1 m^2, should be placed about 1 m to the rear of the lamp. An opaque shield about 1 by 1 m, having an opening about 10 cm wide and 15 cm high, is placed at a distance of about 25 cm in front of the lamp. To screen this opening, a shutter, about 20 by 20 cm, is placed between this shield and the lamp. Facing the opening in the shield, the radiometer is placed at a distance of 2 m from the lamp. The shield and shutter may be made of air-separated sheets of cardboard, asbestos board, metal, or other suitable materials.

Before the lamp is lighted, the shutter should be opened and closed to determine the amount of stray thermal radiation falling upon the radiometer. This test may be applied at any time, provided the lamp has been given sufficient time to come to room temperature. The wall and screen to the rear of the lamp may be cooler than the shutter, which will cause a negative deflection. The correction to the observed lamp deflection is, in that case, positive. It is desirable to make the calibration in a dimly lighted room to avoid errors from sunlight that is continually varying with cloudiness, thus varying stray radiant energy within the room as well as the temperature of the walls, and also causing air currents near the radiometer.

The measurement of the current through the lamp is, of course, sufficient to determine the radiant flux, the voltage being useful mainly to determine whether the lamp has remained constant.

To conserve the calibration, which gradually changes with use, these lamps should be kept as reference standards only, and other lamps used as working standards in all cases where extensive radiometric comparisons are made.

These instructions and standards of radiation apply to radiometers used in air. If a window is used on the radiometer, for example, as in a vacuum radiometer, then a correction has to be made for the radiant flux absorbed by the window [16, 17], for the particular lamp used as a standard, and for the source measured. This absorption is a function of the temperature of the lamp filament. For example, it was found that for a glass or quartz window about 1.5 mm in thickness, the transmission amounted to about 83 percent when a certain standard lamp was operated on 0.35 amp, and increased to 84 percent when the lamp was operated on 0.40 amp. Using a fluorite (CaF_2) window, the transmission is higher (about 91.5 percent) and varies somewhat less with the current ordinarily used in the lamp. For example, using a certain standard lamp, the transmission through a fluorite window varied from 91.0 percent on 0.25 amp to 92 percent on 0.4 amp, with an average value of 91.6 percent on 0.35 amp.

The transmission of the window varies also with the spectral quality of the radiant flux emitted by the source under investigation. This must also be taken into consideration.

The thermal-radiation sensitivity of a surface thermopile varies with the degree of evacuation; when highly evacuated this sensitivity may be several times as great as in air. Because at low air pressures the sensitivity is variable with the pressure, great care must be taken to test the sensitivity of the thermopile under the exact conditions existing during its use.

The identical area of the radiometer receiver should be exposed to the standard of radiation as is used in the measurements of the unknown source.

5. Example of a Thermopile Calibration

The thermopile was exposed, at 2 m, to the standard of radiation that was operated on 0.350 amp, under which conditions the radiant flux was 84.9×10^{-6} w/cm² or 20.3×10^{-6} g cal/cm²/sec. As the thermopile was covered with a fluorite window, only 91.6 percent was transmitted, or $0.916\times84.9\times10^{-6}=77.8\times10^{-6}$ w/cm². Under these conditions, the galvanometer gave a scale deflection of 3.15 cm. Hence, a deflection of 1 cm indicated that $77.8\times10^{-6}\div3.15=24.7\times10^{-6}$ w/cm² was incident on the thermopile element.

Suppose that the radiant flux of a source rich in infrared rays is being measured, in which the fluorite window transmits only 80 percent of the total. Under this condition, a deflection of 1 cm indicated $24.7\times10^{-6}\div0.80=30.9\times10^{-6}$ w/cm² was incident on the thermopile window.

If the radiometer window is of quartz, then the spectral correction for losses by reflection is about 8.5 percent for all wavelengths from the ultraviolet to 2 μ in the infrared, where absorption begins.

Owing to the large heat capacity of the filament there is no appreciable difference in the radiation emitted by this type of lamp on 60-cps a-c and on d-c generators. The use of lower frequencies is questionable. In order to maintain a constant voltage it is preferable to use a storage battery. However, by the use of a small-voltage regulator and a small-variable-voltage transformer, satisfactory voltage and current control may be obtained on standard 110 v, 60-cps circuits.

6. References

[1] W. Coblentz, Measurements on standards of radiation in absolute value, Bul. BS **11**, 98 (1914) S227.

[2] W. Coblentz and W. B. Emerson, Studies of instruments for measuring radiant energy in absolute value: An absolute thermopile, Bul. BS **12**, 503 (1916) S261.

[3] W. W. Coblentz and R. Stair, The present status of the standards of thermal radiation maintained by the Bureau of Standards, BS J. Research **11**, 79 (1933) RP578.

[4] J. A. Bearden, M. D. Earle, J. M. Minkowski, and J. S. Thomsen, Present status of the atomic constants, Phys. Rev. **93**, 629 (1954).

[5] J. W. M. DuMond and E. R. Cohen, Least squares adjustment of the atomic constants, 1952, Rev. Mod. Phys. **25**, 691 (1953).

[6] Forrest K. Harris, Electrical measurements (John Wiley & Sons, Inc., New York, N. Y., 1952).

[7] Robert L. List, Smithsonian meteorological tables, 6th ed., table 108, p. 382 (1951).

[8] W. W. Coblentz, Radiometric investigation of water of crystallization, light filters, and standard absorption bands, Bul. BS **7**, 619 (1911) S168.

[9] A. Adel, Atmospheric absorption of infrared solar radiation, Astrophys. J., **89**, 1 (1939); **91**, 1 (1940); **94**, 375, 379, and 451 (1941).

[10] W. S. Benedict and Earle K. Plyler, Absorption spectra of water vapor and carbon dioxide in the region of 2.7 microns, J. Research NBS **46**, 246 (1951) RP2194.

[11] W. S. Benedict, H. H. Claassen, and J. H. Shaw, Absorption spectrum of water vapor between 4.5 and 13 microns, J. Research NBS **49**, 91 (1952) RP2347.

[12] Nora M. Mohler and John R. Loofbourow, Optical filters, Am. J. Phys. **20**, 499 and 579 (1952).

[13] Earle K. Plyler and Joseph J. Ball, Infrared absorption of deposited blacks, J. Opt. Soc. Am. **38**, 988 (1948).

[14] E. B. Rosa and G. W. Middlekauff, Carbon filament lamps as photometric standards, Proc. Am. Inst. Elec. Engrs. **29**, 1191 (1910).

[15] W. W. Coblentz, R. Stair, and J. M. Hogue, A balanced thermocouple and filter method of ultraviolet radiometry, with practical applications, BS J. Research **7**, 723 (1931) RP370.

[16] W. W. Coblentz, Absorption, reflection and dispersion constants of quartz, Bul. BS **11**, 471 (1913) S237.

[17] W. W. Coblentz, Infrared transmission and refraction data on standard lens and prism material, BS Sci. Pap. **16**, 701 (1920) S401.

[18] H. F. Stimson, The International Temperature Scale of 1948, J. Research NBS **42**, 209 (1949) RP1952.

[19] Robert J. Corruccini, Differences between the International Temperature Scales of 1948 and 1927, J. Research NBS **43**, 133 (1949) RP2014.

WASHINGTON, June 10, 1954.

[1] Synthesis of D-Galactose-1-C^{14} and D-Talose-1-C^{14}

Horace S. Isbell, Harriet L. Frush, and Nancy B. Holt

An efficient procedure is presented for the preparation of α-D-galactose-1-C^{14} and α-D-talose-1-C^{14} from D-lyxose and C^{14}-labeled cyanide. The epimeric acids from the cyanohydrin synthesis were separated as calcium D-galactonate-1-C^{14} pentahydrate and D-talono-γ-lactone-1-C^{14} in yields of 67 and 28 percent, respectively. The calcium D-galactonate-1-C^{14} was converted quantitatively to D-galactono-γ-lactone-1-C^{14} and this was reduced, in 86-percent yield, to D-galactose-1-C^{14}. The over-all radiochemical yield of D-galactose-1-C^{14} from $NaC^{14}N$ was thus 57 percent. D-Talono-γ-lactone-1-C^{14} was reduced to α-D-talose-1-C^{14} in 56-percent yield, an over-all radiochemical yield of 16 percent.

1. Introduction

D-Galactose, one of the most important natural sugars, occurs in numerous polysaccharides, in certain glycosides (e. g., cerebrosides), in lactose, and in other substances of biological importance. Prior to the present study, D-galactose-1-C^{14} had been prepared in 21-percent yield from D-lyxose and $NaC^{14}N$ [1],[2] but the sugar was not generally available to research workers; the epimeric sugar, D-talose-1-C^{14}, had not been prepared. In order to make D-galactose-1-C^{14} available for tracer studies in biological systems, and to facilitate its preparation by others, a study was made of its synthesis by techniques similar to those described in previous publications from this laboratory [2, 3, 4, 5, 6, 7]. α-D-Galactose-1-C^{14} and α-D-talose-1-C^{14} have now been synthesized in good yield by the following procedure:

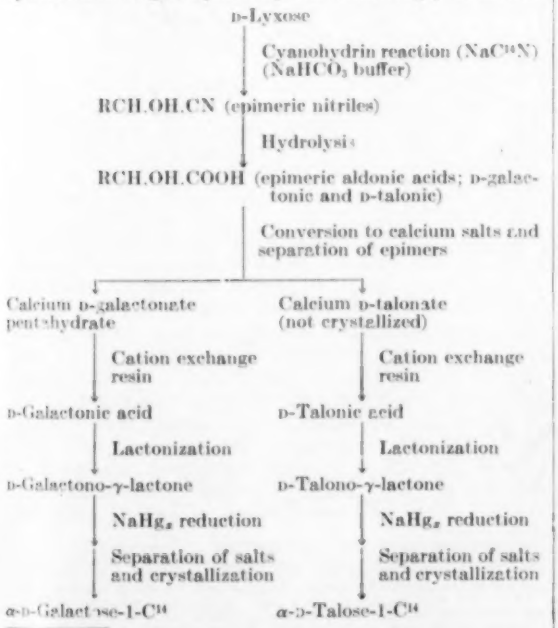

[1] Part of a project on the development of methods for the synthesis of radioactive carbohydrates, sponsored by the Atomic Energy Commission.

[2] Figures in brackets indicate the literature references at the end of this paper.

2. Discussion of the Experimental Method

It was found that in the reaction of cyanide with D-lyxose, general acid catalysts favor formation of the galactonic epimer. Accordingly, the preparation of the radioactive cyanohydrins was conducted in the presence of sodium bicarbonate. The epimeric acids were conveniently separated by means of the calcium salts, one of which, calcium D-galactonate-1-C^{14} pentahydrate, crystallizes readily. The salts were converted to the corresponding acids, and these were lactonized and then reduced to the corresponding sugars. In a preparation beginning with 7.5 millicuries of $NaC^{14}N$, calcium D-galactonate-1-C^{14} pentahydrate and D-talono-γ-lactone-1-C^{14} were obtained in radiochemical yields of 67 and 28 percent, respectively. The calcium D-galactonate-1-C^{14} was converted to D-galactono-γ-lactone-1-C^{14}, and this was reduced to the sugar by means of sodium amalgam in the presence of sodium acid oxalate [3]. The radiochemical yield of α-D-galactose-1-C^{14} from calcium D-galactonate-1-C^{14} pentahydrate was 86 percent, and the over-all yield from $NaC^{14}N$ was 57 percent.[3] Similarly, the radiochemical yield of α-D-talose-1-C^{14} from D-talono-γ-lactone-1-C^{14} was 56 percent, and the over-all yield was 16 percent.

3. Experimental Details

3.1. Preparation of Calcium D-Galactonate-1-C^{14} Pentahydrate

A solution consisting of 20 ml of water, 10 mM of sodium hydroxide and 12 mM of $NaC^{14}N$, having an activity of 7,500 microcuries, was frozen in a 100-ml round-bottomed glass-stoppered flask, and a carbon dioxide-saturated solution containing 13 mM of D-lyxose [8] and 10 mM of sodium bicarbonate in 10 ml of water was added. The flask was stoppered and kept in gentle motion until the ice had melted. After storage for 5 days at 0° C, the mixture was heated at 80° C under a stream of air with the addition of water from time to time, until ammonia was no longer detectible in the vapor (about 12 hr). The solution was diluted with 25 ml of water and passed

[3] If allowance is made for calcium D-galactonate-1-C^{14} reclaimed by carrier technique after the reduction, the yield in the reduction step becomes 98 percent, and the over-all yield, 66 percent. The reclaimed material was of low activity, and suitable for use as a carrier in a subsequent preparation.

through 70 ml of cation exchange resin.[4] The column was washed until the activity was negligible, and the total effluent was evaporated to 100 ml under reduced pressure; an aqueous suspension of calcium hydroxide was then added in sufficient amount to give a faint, but permanent, pink color in the presence of phenolphthalein indicator. The solution, filtered and evaporated under reduced pressure, yielded a sirup that crystallized readily upon addition of methanol and seed crystals. After 3 days, a crop of calcium D-galactonate-1-C^{14} pentahydrate was separated and recrystallized once by dissolving it in the minimum amount of hot water, cooling the solution, and cautiously adding methanol. The crystals, when separated and dried, weighed 1.838 g (equivalent to 7.07 mM) and had an activity of 4,435 μc. By the successive use of four 700-mg quantities of nonradioactive D-galactose as carrier an additional 583 μc was separated. Thus the total yield of calcium D-galactonate-1-C^{14} pentahydrate was 5,018 μc, or 66.9 percent. The residues, containing 2,400 μc of radioactivity, were used for the preparation of D-talono-γ-lactone-1-C^{14}, as described in section 3.4.

3.2. Preparation of D-Galactono-γ-lactone-1-C^{14}

A 1.42-g quantity of calcium D-galactonate-1-C^{14} pentahydrate having an activity of 3,600 μc[5] was dissolved in 100 ml of water, and the solution was passed through a column containing 70 ml of cation exchange resin. The column was thoroughly washed, and the total effluent was concentrated under reduced pressure to 25 ml. The solution was then transferred in equal parts to 5 reduction tubes.[6] In order to lactonize the D-galactonic-1-C^{14} acid, the tubes were placed in a bath at 80° C, and each solution was concentrated in a current of air; from time to time the residues were dissolved in ethylene glycol monomethyl ether (Methyl Cellosolve), and the evaporation was continued. During this treatment, the needle-like crystals of D-galactonic acid, first observed, were slowly converted to the typical wedge-shaped crystals of the lactone. When the lactonization seemed to be complete, as evidenced by the lack of amorphous material and needle crystals (about 3 days), the tubes were stored in a desiccator until used for production of the sugar.

3.3. Reduction of D-Galactono-γ-lactone-1-C^{14} to α-D-Galactose-1-C^{14}

Prior to the preparation of D-galactose-1-C^{14}, the experiments given in table 1 were conducted with nonradioactive D-galactono-γ-lactone in order to ascertain optimum conditions for reduction of the lactone. In each experiment, the crystalline sodium acid oxalate and the lactone were placed in a reduction tube immersed in an ice bath. Twenty milliliters of ice water was added, and vigorous stirring was begun. The 5-percent amalgam[7] was then added in one portion through the side arm. Stirring was continued until the amalgam had completely reacted (about 2 hr). The solution was filtered, and the amount of sugar formed was determined by the modified Scales method [9]. The data of table 1 show that 1 mM of D-galactono-γ-lactone was reduced most effectively by 4.6 g of 5-percent sodium amalgam in the presence of 2 g of sodium acid oxalate (approximately a 50-percent excess); hence these proportions were used in the reduction of the labeled lactone.

TABLE 1. *Reduction of D-galactono-γ-lactone[a] by sodium amalgam in the presence of sodium acid oxalate*

Experiment	Sodium acid oxalate	$NaHg_x$ (5-percent)	Yield of D-galactose (by analysis)
	g	g	%
1	1.0	2.3	70.2
2	2.0	4.6	95.3
3	2.4	5.5	89.2

[a] 1.0 mM of lactone in 20 ml of ice water.

The 5 aliquots of D-galactono-γ-lactone-1-C^{14} described in section 3.2 (each containing 1.1 mM with 720 μc of activity) were reduced separately[8] by use of 5 g of 5-percent sodium amalgam and 2.3 g of sodium acid oxalate. After 2 hr, the mercury was separated, and the products from the 5 tubes were combined and diluted with 5 volumes of methanol. The resulting crystalline salts were separated by filtration and discarded after they were found to be nonradioactive. The alcoholic filtrate was concentrated under reduced pressure to 20 ml, cooled in ice water, and neutralized with aqueous sodium hydroxide until it had a faint, but permanent, pink color in the presence of phenolphthalein indicator. An equal volume of methanol was added, the mixture was refiltered, and the residue, likewise found to be nonradioactive, was discarded. After the filtrate had been concentrated to about 15 ml and diluted with 2 parts of methanol, a third crop of salts with negligible radioactivity was removed by filtration and discarded. The filtrate was concentrated to remove most of the methanol and then passed through a column containing 50 ml of a mixture of equal parts of cation[9] and anion[10] exchange resin. Five milliliters of cation exchange

[4] Amberlite IR 120–H, analytical grade, Resinous Products Division of Rohm & Haas Co., Philadelphia, Pa.

[5] The calcium D-galactonate-1-C^{14} pentahydrate employed here was part of that described in section 3.1, to which a small amount of material from another preparation was added. The level of activity (2.54 μc/mg) is slightly higher than that of section 3.1 (2.41 μc/mg).

[6] The reduction apparatus employed here has been fully described [5]; it consists of a heavy-walled glass tube, 200 by 25 mm, having a 24/40 standard-taper joint. A side arm, 50 by 15 mm, attached just below the joint, facilitates addition of the amalgam. A stainless-steel, standard taper stopper, equipped with oilless bearings, supports a stainless-steel stirrer, which just touches the bottom of the tube.

[7] The amalgam was prepared in small pellets by pouring it in molten condition through a heated alundum thimble, having a small hole in the bottom, into a 2-ft "shot tower" of mineral oil. The pellets were stored under mineral oil, and just before use, were blotted dry, weighed, and rinsed with benzene.

[8] Since this work was completed, a larger stainless-steel reduction apparatus has been employed, which makes portion-wise reduction unnecessary.

[9] Amberlite IR 100–H, analytical grade, Resinous Products Division of Rohm & Haas Co., Philadelphia, Pa.

[10] Duolite A–4, Chemical Process Co., Redwood City, Calif.

re was also placed at the top and at the bottom of the mixed resins. The absence of free acid in the effluent showed that sufficient resin was present to remove all salts. The column was washed until the activity was negligible, and the effluent was concentrated to 20 ml under reduced pressure. The solution was then filtered through a slender column containing 0.1 g of a decolorizing carbon, and the filtrate was freeze-dried. After the residue had been dissolved in 3 ml of methanol, and 2-propanol added to the point of incipient turbidity, crystallization of D-galactose-1-C^{14} began immediately. At the end of 3 days, the mother liquor was removed with a capillary pipet, and the crystals were carefully washed in place with ethanol. To recrystallize, the material was dissolved in 1 ml of water by warming, 5 ml of methanol was added, and then 2-propanol almost to the point of saturation. After 48 hr, the crystals were separated as described before and dried; they weighed 760 mg and contained 2,780 μc of activity. By use of three 500-mg portions of nonradioactive D-galactose as carrier, an additional 300 μc of activity was recovered from the mother liquor. Hence the radiochemical yield of D-galactose-1-C^{14} was 3,080 μc, or 85.6 percent of the activity of the original calcium D-galactonate-1-C^{14} pentahydrate (3,600 μc).

When the column of mixed resin used for the purification of the sugar was extracted with 250 ml of 10-percent aqueous acetic acid, 435 μc of activity was recovered. The solution was concentrated under reduced pressure almost to dryness, and finally was freeze-dried. An aqueous solution of the residue was de-cationized, neutralized with a solution of calcium hydroxide, filtered, and used to dissolve 500 mg of nonradioactive calcium D-galactonate pentahydrate. After concentration of the solution under reduced pressure, and addition of methanol, a crop of calcium D-galactonate-1-C^{14} pentahydrate was obtained, which, once recrystallized, contained 366 μc of activity. This material was used as a carrier in a later prepara ion. If allowance is made for the reclaimed calcium D-galactonate-1-C^{14} pentahydrate, the yield of D-galactose-1-C^{14} from the calcium salt becomes 98.3 percent.

3.4. D-Talono-γ-lactone-1-C^{14}

The liquor that remained after separation of the last traces of crystalline calcium D-galactonate-l-C^{14} pentahydrate in the experiment described in section 3.1 was diluted with 25 ml of water and passed through a column containing 25 ml of cation exchange resin. The effluent was concentrated under reduced pressure, and the resulting sirup was finally transferred to a test tube by means of Methyl Cellosolve. The D-talonic-l-C^{14} acid in the sirup was lactonized by immersing the tube in a water bath at 60° C, and passing a current of air over the warm liquid; a few drops of Methyl Cellosolve were added at 2-hr intervals. After 8 hr the residue was taken up in about 5 ml of 2-propanol. Crystalline D-talono-γ-lactone (200 mg) was added, the mixture was warmed to dissolve the carrier, and the solution was seeded and set aside for 24 hr. The first crop of D-talono-γ-lactone-l-C^{14}, after one recrystallization from 2-propanol, weighed 606 mg, and had an activity of 1,625 μc. The combined mother liquors, when treated with 2 additional 200-mg quantities of carrier, yielded 482 μc. The total radiochemical yield was thus 2,107 μc, corresponding to 28 percent of the $NaC^{14}N$ used in the cyanohydrin synthesis.

3.5. Preparation of α-D-Talose-1-C^{14}

Prior to the reduction of the labeled lactone, suitable conditions for the production of the sugar were determined by means of the experiments reported in table 2.

TABLE 2. *Reduction of D-talono-γ-lactone [a] by sodium amalgam in the presence of sodium acid oxalate*

Experiment	Sodium acid oxalate	$NaHg_x$ (5-percent)	Yield of D-talose (by analysis)
	g	*g*	*%*
1	1.6	2.3	54.7
2	3.2	4.6	75.0
3	4.8	6.9	76.1
4	6.4	9.2	75.0
5	6.4	[b] 18.4	66.7

[a] 0.5 mM of lactone in 20 ml of ice water.
[b] Added in two portions.

Experiments 2, 3, and 4 of table 2 gave nearly the same yield of sugar. The conditions of experiment 2 were adopted for the reduction of the labeled material, as they called for less of the reagents. In a typical preparation, 430 mg of D-talono-γ-lactone-1-C^{14} having an activity of 378 μc, was reduced in two portions by use of 13 g of 4.2-percent amalgam [11] and 7.5 g of sodium acid oxalate for each portion. The product was treated in essentially the same manner as the product from the reduction of D-galactono-γ-lactone-1-C^{14}. The sugar solution, after deionization, was concentrated to 50 ml under reduced pressure and was then freeze-dried. The residue was dissolved in 0.5 ml of ethanol, *n*-butanol was added to the point of incipient turbidity, and the solution was seeded with α-D-talose previously prepared [10]. After several days, the mother liquor that remained was withdrawn with a capillary pipet, and the crystalline α-D-talose-1-C^{14} was washed with a few drops of 2-propanol. The product, recrystallized once from the minimum amount of water by the addition of 2-propanol, weighed 170 mg, and had an activity of 142 μc. By use of 600 mg of carrier in 2 portions, an additional 70 μc of α-D-talose-1-C^{14} was separated from the combined mother liquors. The total yield was thus 212 μc, or 56 percent of the D-talono-γ-lactone-1-C^{14} used.

[11] The sodium content was somewhat less than that of the amalgam used in the reductions in table 2; a proportionately larger amount was employed.

4. References

[1] Y. J. Topper and D. Stetten, Jr., J. Biol. Chem. **193** 149 (1951).

[2] H. S. Isbell, U. S. Patent 2,606,918 (1952).

[3] H. S. Isbell, U. S. Patent 2,632,005 (1953).

[4] H. S. Isbell, J. V. Karabinos, H. L. Frush, N. B. Holt, A. Schwebel, and T. T. Galkowski, J. Research NBS **48,** 163 (1952) RP2301.

[5] H. L. Frush and H. S. Isbell, J. Research NBS **50,** 133 (1953) RP2400.

[6] H. L. Frush and H. S. Isbell, J. Research NBS 51, 67 (1953) RP2446.

[7] H. L. Frush and H. S. Isbell, J. Research NBS 51, 307 (1953) RP2458.

[8] F. J. Bates and associates, Polarimetry, saccharimetry and the sugars, NBS Circular 440, p. 469 (1942).

[9] H. S. Isbell, W. W. Pigman, and H. L. Frush, J. Research NBS **24,** 241 (1940) RP1282.

[10] W. W. Pigman and H. S. Isbell, J. Research NBS **19,** 189 (1937) RP1021.

Washington, May 13, 1953.

Determination of Carbon-14 in Solutions of C^{14}-Labeled Materials by Means of a Proportional Counter [1]

A. Schwebel, H. S. Isbell, and J. D. Moyer

A study is reported of the determination of carbon-14 in C^{14}-labeled substances by counting, with a proportional gas-flow counter, the radioactive disintegrations arising from a material that is dissolved in a suitable solvent. A number of solvents were found to be satisfactory. Formamide is recommended for the assay of carbohydrates and other materials with which it is a compatible solvent. Ethylene glycol is suitable for the assay of highly alkaline substances, and, in conjunction with sequestering agents, for the assay of alkaline earth carbonates. Other useful solvents are dimethyl formamide and 90-percent phosphoric acid. The counting efficiency in different solvents was found to be inversely proportional to the density of the solution and highly reproducible. The study shows that solutions of C^{14}-labeled materials can be counted easily and precisely with a proportional counter.

1. Introduction

Relatively little work has been done on the counting with proportional counters of C^{14}-labeled compounds in solution [1, p. 101].[2] Direct measurement of the radioactivity of solid sources is complicated by variations in self-absorption, backscattering, and forescattering, and (in counting on plastic backings) by the presence of static charges that distort the field. These variations do not occur with solutions, which are strictly reproducible, and have little tendency to hold static charges. Other complications arise, however, and one cannot obtain satisfactory assays with most solvents. In a prior publication from the Bureau the use of formamide solutions for the determination of carbon-14 in labeled materials was described [2]. The present paper presents further studies of the method and of the application of other solvents.

2. Discussion of the Experimental Technique

2.1. Counting Apparatus

Figure 1 illustrates a typical proportional gas-flow counter. The instrument is designed so that a continuous stream of a "self-quenching" gas flows at about atmospheric pressure through the counting chamber, which contains the material to be analyzed. Radiation from the material under analysis produces ionization in the chamber; this leads to a momentary discharge across the high-voltage field maintained between the wall of the chamber and a wire anode. The change in potential caused by the discharge is converted into a current pulse that activates a recording mechanism by means of a vacuum-tube amplifier [3, p. 29]. Instruments of this type are available commercially and are readily adapted for assay of liquid samples. They are much more stable and sensitive than thin-window Geiger counters; hence they are particularly suitable for measurement of low-energy beta radiation, such as that from carbon-14.

To adapt commercially available proportional counters for the assay of liquid samples it is necessary to fit them with a suitable cell to hold the liquid. Figure 2 shows the stainless-steel cell used in the present study. It has an inside diameter of 36 mm and a depth of 1.1 mm. When full, it holds 1.1 ml of solution. In the analysis approximately 1 ml of solution is placed in the cell. The amount is not critical because even 0.5 ml gives an "infinitely thick" layer of the solution with respect to penetra-

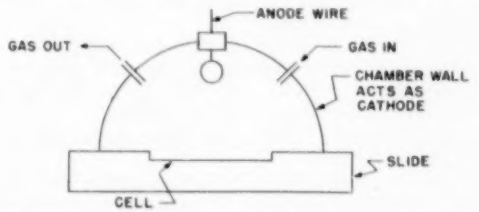

FIGURE 1. *Diagram of proportional gas-flow counter.*

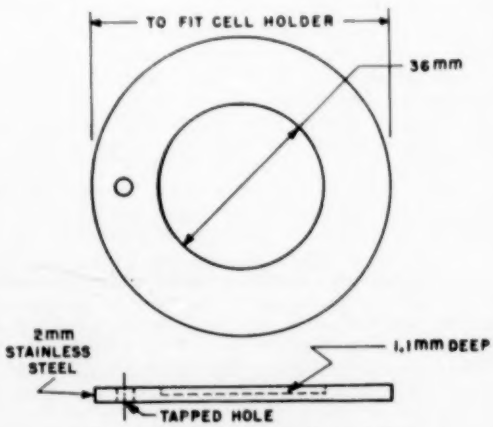

FIGURE 2. *Cell for counting solutions.*

[1] Part of a project on the development of methods for the synthesis of radioactive carbohydrates, sponsored by the Atomic Energy Commission. This paper is based on the work described in a previous AEC report.

[2] Figures in brackets indicate the literature references at the end of this paper.

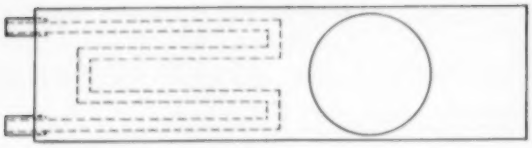

FIGURE 3. *Top view of water-cooled slide.*

tion of the radiation from carbon-14. The cell is handled without contamination by use of a bolt that fits the tapped hole and serves as a removable handle.

In instruments in which the counting chamber is surrounded by electronic tubes and other parts that liberate heat, the temperature of the solution rises with long counting periods. The rise in temperature causes evaporation of volatile constituents in the solution under analysis, and this leads to erroneous results. This difficulty may be overcome by the use of a cooling device. In the present study the counter slide of a commercial instrument [3] was drilled as shown in figure 3, and a stream of cold water was circulated through the passage. With instruments in which the counting chamber remains at room temperature, a cooling device is not necessary.

2.2. Solvent

A satisfactory solvent for counting of C^{14}-labeled materials in solution by means of a proportional counter should have the following characteristics:

1. It should be an adequate solvent for the material to be analyzed.
2. Its vapor pressure should be low, to avoid a change in the concentration of the solute with time.
3. Its vapors should not form a conducting path across the high-voltage wire insulation.
4. It must have little or no tendency to creep over the edge of the cell.

In the present study, many liquids were tried. Water caused insulation breakdown; monomethyl and monoethyl ethers of ethylene glycol (Methyl Cellosolve and Ethyl Cellosolve, respectively) evaporated slightly and also showed a marked tendency to creep; 75-percent sulfuric acid was found to be useful, but on long standing it crept slightly; 90-percent phosphoric acid was fairly satisfactory whereas purified formamide, dimethyl formamide,[4] and ethylene glycol gave excellent results. Solutions of acetamide in formamide were found to be satisfactory, and undoubtedly other solvents could be used. Ordinarily, commercial formamide contains sufficient ammonia to cause insulation breakdown in the counter. For use as a counting liquid it should be purified by drying with anhydrous sodium sulfate and distilling under reduced pressure. The middle, ammonia-free fraction is satisfactory, for counting purposes, and can be kept for months without deterioration.

The amount of water that can be present in the solvent without interference depends, in part, on the operating conditions, especially the temperature, the rate of gas flow, and the design of the counter. With an instrument in which the counting chamber is not enclosed in a case with the electronic mechanism, up to 10 percent of water can be present in a formamide solution without interference. With the water-cooled slide shown in figure 3, satsifactory results were obtained with formamide solutions containing up to 15 percent of water, but ordinarily the water content should be kept as low as possible to minimize error due to evaporation.

[3] Nuclear Measurements Corporation, Indianapolis, Ind., model PC-1.
[4] Suggested by W. H. Smith of the Bureau.

2.3. Analytical Procedures

The solution to be assayed can be prepared by any convenient method. Readily soluble materials are dissolved directly in the counting liquid. Aqueous solutions are prepared for assay by taking a definite volume (up to 0.1 ml) in a mixing pipet and then adjusting the volume to 1 ml with formamide or other suitable solvent. The separation of insoluble precipitates or a second liquid phase must be avoided. To minimize errors that might arise from adsorption of the radioactive material on the cell or from concentration of the sample on the surface of the counting liquid, highly active materials are diluted with a suitable quantity of the corresponding nonradioactive material when the solution is prepared for counting. After the solution has been placed in the counter, the system is thoroughly flushed with the counting gas, and the count is taken. For maximum precision, background determinations are made before and after each measurement.

2.4. Precision of Measurements

Tables 1 and 2 show the reproducibility of measurements made on a C^{14}-labeled sugar in formamide and in ethylene glycol, using three proportional counters differing slightly in counting efficiency. The counts for the two solutions are not directly comparable because the solutions differ in concentration and density. In accordance with the conventional statistical treatment [3, p. 43] of the disintegration rate of a radioactive substance, one would expect a standard deviation of ± 309 for 95,000 counts. The standard deviations obtained for the experimental data are only slightly higher than this value. Thus C^{14}-labeled compounds can be reproducibly counted in solutions of either formamide or ethylene glycol.

The count for the formamide solution with instrument No. 3 increased slightly as the measurements progressed. A change of this character might arise from an instrument drift, or from evaporation of the solvent with a corresponding increase in the concentration of the solute. Instrument 3 was cooled by circulating water at about 25° C, whereas instruments 1 and 2 were cooled with water at about 15° C. Thus it seems possible that the increase was caused by evaporation of the solvent. The increase was small and would be insignificant with a normal counting period.

TABLE 1. *Reproducibility of successive 8-min counts of* D-*galactose-1-*C^{14} *in formamide solution* [a]

Proportional counter 1		Proportional counter 2		Proportional counter 3	
Count	Deviation from mean	Count	Deviation from mean	Count	Deviation from mean
94,144	+412	94,886	+512	89,678	−1,223
93,952	+220	94,349	−25	90,014	−887
93,542	−190	94,170	−204	89,897	−1,004
94,054	+322	94,272	−102	90,868	−33
93,542	−190	93,900	−474	90,401	−500
94,413	+681	94,566	+192	91,047	+146
93,402	−330	94,540	+166	90,313	−588
93,325	−407	95,002	+628	90,677	−224
93,542	−190	94,323	−51	91,000	+99
93,926	+194	95,116	+742	90,773	−128
93,632	−100	94,382	+8	91,851	+950
93,645	−87	94,067	−307	90,579	−322
93,389	−343	94,362	−12	91,178	+277
93,542	−190	94,566	+192	90,942	+41
93,606	−126	94,221	−153	91,993	+1,092
93,414	−318	94,349	−25	90,774	−127
93,926	+194	94,578	+204	91,277	+376
93,555	−177	94,285	−89	91,121	+220
94,643	+911	94,170	−204	92,055	+1,154
93,696	−36	94,131	−243	91,672	+771
93,773	+41	93,798	−576	.....	.....
93,286	−446	94,208	−166	.....	.....
93,964	+232	94,221	−153	.....	.....
93,978	+246	94,387	+13	.....	.....
93,414	−318	94,515	+141	.....	.....
Avg. 93,732	.....	94,374	.....	90,901	.....
Standard deviation	339		301		649

[a] The solution contained 0.415 mg of D-galactose-1-C^{14} per milliliter.

2.5 Calibration

To convert the observed counts per second (cps) to the absolute disintegration rate (dps), or to microcuries per milliliter of solution, it is necessary to standardize the procedure by counting a solution containing a C^{14}-labeled substance of known radioactivity under conditions comparable to those used in the analysis. In the present study several materials were used for standardization. The radioactivity was determined by oxidizing the material [1, p. 92], transferring the carbon dioxide to an ionization chamber, and comparing the drift rate of a vibrating-reed electrometer with the drift rate obtained from the carbon dioxide in a sample of the NBS Carbon-14 Beta Ray Standard. Known concentrations of the standardized materials in formamide or other solvent were then counted in the cell of figure 2.

Any comparison of counting rates must take into account the density of the solution because the absorption of beta radiation is proportional to the density of the absorbing medium [3, p. 159]. For this reason the counting efficiency (cps/dps) in a given counter should be inversely proportional to the density of the solution counted.

Table 3 presents data for D-mannitol-1-C^{14} dissolved in a variety of solvents, and table 4 presents results obtained with a variety of C^{14}-labeled materials dissolved in the same solvent. The results given in these tables show that the product of the counting efficiency and the density is substantially constant, regardless of the substance counted or the solvent. This gives rise to a constant calibration factor that can be used for converting the count of an unknown sample to microcuries of C^{14} per milliliter. Thus, for all C^{14}-labeled materials, the product of cps, density and calibration factor gives microcuries of C^{14} per milliliter. The calibration

TABLE 2. *Reproducibility of successive 8-min counts of* D-*galactose-1-*C^{14} *in ethylene glycol solution* [a]

Proportional counter 1		Proportional counter 2		Proportional counter 3	
Count	Deviation from mean	Count	Deviation from mean	Count	Deviation from mean
97,830	−59	98,227	−183	95,727	+108
98,074	+185	97,894	−516	96,369	+750
98,227	+338	98,458	+47	96,208	+589
97,254	−635	97,754	−656	96,697	+1,078
97,984	+95	98,662	+252	95,806	+187
98,496	+607	98,803	+393	94,994	−625
97,830	−59	98,933	+521	95,120	−499
97,946	+57	98,752	+342	95,394	−225
97,920	+31	98,304	−106	94,950	−669
97,997	+108	98,624	+214	95,813	+194
97,638	−251	98,406	−4	94,678	−941
98,150	+261	98,330	−80	95,299	−320
97,562	−327	98,483	+73	95,503	−116
97,613	−276	97,920	−490	95,569	−50
97,587	−302	98,150	−260	96,147	+528
97,715	−174	98,317	−93	95,511	−108
97,958	+69	97,993	−417	95,646	+27
97,933	+44	98,560	+150	95,366	−253
98,022	+133	98,278	−132	95,698	+79
98,009	+120	98,560	+150	95,523	−96
97,702	−187	98,304	−106	95,848	+239
97,933	+44	98,483	+73	95,220	−389
98,598	+709	98,586	+176	95,796	+177
98,278	+389	98,355	−55	95,397	−222
98,010	+121	98,445	+35	95,819	+200
98,458	+569	98,304	−106	96,030	+411
97,894	+5	98,496	+86	95,440	−179
98,947	−942	98,009	−401	95,758	+139
97,958	+69	98,304	−106	.....	.....
97,920	+31	98,432	+22	.....	.....
97,907	+18	98,854	+444	.....	.....
97,998	−391	98,278	−132	.....	.....
97,331	−558	98,394	−16	.....	.....
97,869	−20	98,778	+368	.....	.....
98,048	+159	99,238	+828	.....	.....
97,920	+31	98,419	+9	.....	.....
98,064	+171	98,227	−183	.....	.....
97,830	−59	98,291	−119	.....	.....
97,779	−110	.....	.....	.....	.....
Avg. 97,889	.....	98,410	.....	95,619	.....
Standard deviation	316	.....	314	.....	409

[a] The solution contained 0.424 mg of D-galactose-1-C^{14} per milliliter.

TABLE 3. *Counting efficiency with* C^{14}*-labeled* D-*mannitol in various solvents; correlation of counting efficiency and density*

Solvents	Density at 20° C	Counting efficiency	Counting efficiency times density	Calibration factor, $\frac{\mu c}{cps \times density}$
		%		
Formamide	1.133	1.000	1.133	2.385×10^{-3}
Formamide+5% H_2O [a]	1.127	1.009	1.137	2.377
Formamide+10% H_2O [a]	1.121	1.013	1.136	2.379
Formamide+20% H_2O [a]	1.110	1.025	1.138	2.375
Dimethyl formamide	0.949	1.19	1.129	2.394
Ethylene glycol	1.107	1.02	1.129	2.394
Ethylene glycol+NaI [b]	1.622	0.697	1.131	2.390
Average	.....	.....	1.133	2.385
Standard deviation	.....	.....	0.004	0.007

[a] 5, 10, or 20 ml of water diluted to 100 ml with formamide.
[b] Solution contained 8 g of NaI and 10 ml (11 g) of ethylene glycol.

TABLE 4. *Counting efficiency with various C^{14}-labeled compounds in the same solvents*

C^{14}-labeled solute [a]	Density of solution	Disintegration rate[b] per milliliter	Counting rate	Counting efficiency times density	Calibration factor, $\frac{\mu c}{cps \times density}$
	mg/ml	*dps*	*cps*		
D-Mannitol (0.400 μc/mg)	1.0	1,133	14,800	148.4	1.136	2.379×10^{-3}
D-Mannitol (0.0107 μc/mg)	25.6	1,139	10,140	100.6	1.130	2.392
D-Mannitol (0.00727 μc/mg)	55.0	1,145	14,800	146.5	1.133	2.385
D-Mannono-γ-lactone	17.4	1,138	2,640	26.4	1.138	2.375
Sodium D-α-glucoheptonate	24.1	1,139	5,085	50.4	1.129	2.394
Sodium carbonate [c]	4.0	1,112	18,100	184.4	1.133	2.385
Average				1.133	2.385
Standard deviation				0.003	0.007

[a] All of the materials were dissolved in formamide except the sodium carbonate. The latter was dissolved in water and an aliquot was diluted 25-fold with ethylene glycol containing 2 percent of sodium hydroxide.
[b] Based on the NBS Carbon-14 Beta Ray Standard.
[c] To avoid loss of $C^{14}O_2$ by CO_2 exchange, the gas for use in the counter was passed through a column of Ascarite.

factor for the instrument used in the present study was 0.002385. This value is characteristic of the instrument and dimensions of the counting cell. It does not vary appreciably from day to day, but major adjustments in the instrument may cause appreciable change. Hence it is necessary to check the calibration from time to time.

The densities of solutions containing small quantities of a solute in a particular solvent do not vary widely. Hence for routine measurements it is not necessary to determine the density of all solutions. Frequently, no substantial error is introduced by use of the density of the solvent for the density of the solution. Density determinations can be avoided by use of a conversion factor obtained by counting a solution of known activity having essentially the same density as that of the unknown. Under these conditions the ratio of microcuries to counts per second obtained for the standard can be used to convert the cps of the unknown to the corresponding microcuries of carbon-14 per milliliter of solution.

The measurement with ethylene glycol containing sodium iodide, reported in table 3, was made to determine whether the presence of an element of high atomic number caused deviations that might arise from backscattering. No such effect was found.

2.6. Applicability of the Method

Counting of carbon-14 in solution is most useful for the assay of highly active samples such as those encountered in synthetic and chemical studies. Although relatively large samples are required, the material may usually be reclaimed by removal of the solvent. The method permits use of volumetric techniques and eliminates the problems inherent in the combustion of samples, in the deposition of films, and in the plating of solids. The method is limited to nonvolatile materials. Even traces of labeled hydrogen cyanide formed by the hydrolysis of cyanide contaminate the counter and must be avoided. Most of the sugars and sugar derivatives dissolve in formamide and are readily assayed in that solvent. Dimethylformamide is suitable for some materials not soluble in formamide, and ethylene glycol can be used for basic materials that decompose formamide. Thus carbon dioxide can be absorbed in a water solution of either sodium or potassium hydroxide and assayed in aqueous ethylene-glycol solution. In the assay of carbonates the counting gas must be free of carbon dioxide in order to avoid exchange with the labeled carbonate. Alkaline earth carbonates are dissolved in a water solution of the sequestering agent, tetrasodium salt of ethylene diamine tetraacetic acid, and counted after dilution with ethylene glycol.

3. Summary

A simple, rapid, and precise method is presented for the assay of C^{14}-labeled substances. The material to be assayed is dissolved in a suitable solvent, and the radiation from the solution is measured with a commercial gas-flow proportional counter. The characteristics of suitable solvents are discussed, and it is shown that formamide and ethylene glycol are particularly useful. The counting efficiency was found to be inversely proportional to the density of the solution counted. By counting a substance of known activity under the conditions used for unknown substances, a factor is obtained for converting the count to microcuries of carbon-14 in the sample.

4. References

[1] M. Calvin, C. Heidelberger, J. C. Reid, B. M. Tolbert and P. F. Yankwich, Isotopic carbon, (John Wiley & Sons, Inc., New York, N. Y., 1949).
[2] A. Schwebel, H. S. Isbell, and J. V. Karabinos, Science **113,** 465 (1951).
[3] E. Pollard and W. L. Davidson, Applied nuclear physics, (John Wiley & Sons, Inc., New York, N. Y., 1951).

WASHINGTON, June 25, 1954.

Journal of Research of the National Bureau of Standards Vol. 53, No. 4, October 1954 Research Paper 2538

Extension of the Arc Spectra of Palladium and Platinum (6500 to 12000 A)

Karl G. Kessler, William F. Meggers, and Charlotte E. Moore

The arc spectra of palladium and platinum have been reinvestigated photographically in the red and infrared, and extended approximately 2000 angstroms beyond the former limit of observation. The spectra were excited in conventional direct-current arcs between pure-metal electrodes and recorded by modern sensitized emulsions with the aid of diffraction gratings of 640-cm radius. Improved wavelength values and intensity estimates are given for 63 Pd I lines between 6598.42 and 11556.27 A, and for 74 Pt I lines between 6648.32 and 10757.78 A. All of the observed Pd I lines have been explained as transitions between known atomic energy levels, but only 42 of the 74 Pt I lines can be explained in like manner. It is concluded that further progress in the structural analysis of the Pt I spectrum is dependent on making an improved description in the visible and ultraviolet.

1. Introduction

Inspiration for this investigation was provided by the current compilation of NBS Circular 467 on atomic energy levels [1].[1] Such analyses are usually handicapped by the limited range of photographic observation of spectra, especially in the infrared. Thirty years ago one of the present authors [2] recorded some infrared lines in the arc spectra of the platinum elements by sensitizing ordinary photographic emulsions with dicyanin. Although considerable extensions of the arc spectra were thus made, the greatest wavelength then detected photographically with palladium was 9234.02 A, and with platinum, 8762.48 A.

In 1935 new types of photographic emulsions and sensitizing dyes for infrared photography were described [3], and good infrared sensitive photographic plates became commercially available for the first time. By using these plates the arc spectra of many elements were promptly observed to a new limit in the infrared several thousand angstroms beyond the previous limit set by dicyanin. Such observations for some noble metals were recently made for rhodium [4] and ruthenium [5], and are here presented for palladium and platinum. In most cases, as in rhodium, extension of the infrared spectrum has been rewarded by the discovery of new energy levels, and the possibility that this might happen also in palladium and platinum could not be neglected. The present paper has three collaborators: the first made the spectrograms, the second measured the wavelengths, and the third interpreted the spectra.

2. Materials and Methods

Solid, cylindrical electrodes, approximately 6 mm in diameter and 8 mm long, were made by pressing the purest powdered palladium or platinum metal in a Dietert hydraulic press. These electrodes were pinched in slotted copper rods that served as electrode holders. Electric arcs were produced between a pair of electrodes by currents of 6 to 7 amp from a 220-v d-c circuit. In the case of platinum, the arc was extremely unstable and could not be maintained in the slotted copper holders, but the stability was satisfactory when the short platinum electrodes were held by water-cooled brass clamps.

To record the red and near infrared spectra of these metal arcs, three types of sensitized photographic plates were used. The wavelength range 6500 to 8800 A was photographed with Eastman I-N plates, 8500 to 10500 A with Eastman I-Q plates, and 10000 to 12000 A with Eastman I-Z plates. Before use, these plates were hypersensitized by bathing in dilute solutions of ammonia, followed by rinsing in alcohol and rapid drying with an air blower.

The previous infrared spectrograms obtained with dicyanin-stained plates [2] were made with a concave grating, of 640-cm radius, ruled with 7,500 lines per inch; the scale of the spectrum was 10.4 A/mm. Because the commercial infrared-sensitive photographic plates are vastly more sensitive, it was possible to make the new spectrograms with increased dispersion. Accordingly, the range recorded on I-N plates was observed with a grating ruled 30,000 lines per inch and an average reciprocal dispersion of 1.6 A/mm. The ranges covered by I-Q and I-Z plates were photographed with a grating ruled 15,000 lines per inch and reciprocal dispersion of 4.5 A/mm. Both gratings have radii of 640 cm and are illuminated with parallel light in Wadsworth mountings.

The Eastman I-N plates were so extraordinarily sensitive that arc spectra were completely recorded with continuous background in 30 min. Relatively, the I-Q and I-Z plates are much less sensitive, so that exposure times of 2 to 4 hr. were required to record spectra with background. Furthermore, the sensitivity of I-Z plates declines rapidly beyond 11000 A, the background vanishes even with 4-hr exposures, and the estimated relative intensities of observed spectral lines are consequently too low for the longest waves.

The red and infrared arc spectra of palladium and

[1] Figures in brackets indicate the literature references at the end of this paper.

platinum were photographed in the first order of both gratings, and for the measurement of wavelengths the arc spectrum of iron was recorded in juxtaposition. In the I-N region the wavelengths were usually measured relative to the first-order spectrum of iron, but in the I-Q and I-Z ranges the standards were generally taken from the second- and third-order iron spectra, respectively. The spectrograms were measured on a 20-inch Gaertner comparator reading directly to 1 micron.

3. Results

The experimental results of this investigation consist of measured wavelengths and estimated relative intensities of palladium and platinum lines recorded photographically in the red and infrared. The wavelengths result from averaging 2 to 4 independent determinations; their average uncertainty is of the order of ± 0.01 A. Estimated intensities are based largely on the strongest spectrogram; they are given on an open scale ranging from 1 to 2000, to represent approximate relative energies (except beyond 11000 A, where sensitivity of detection falls off rather rapidly). Some of the intensity numbers are accompanied by letters that have been recommended by the Joint Commission for Spectroscopy [6] for the qualitative description of spectral lines. Briefly, *h* stands for hazy, *H* for very hazy, *l* for shaded to longer waves, and *s* for shaded to shorter waves.

In the range of wavelengths reported here, the only spectral impurities detected in palladium and platinum were potassium and calcium. However, the arc spectra of noble metals, especially in the long-wave range, are always contaminated by superposed spectra of atmospheric constituents and metallic compounds. In addition, the arc spectrum of platinum in air is accompanied by fairly complete atomic spectra of nitrogen, oxygen, and a strong background of irregularly spaced lines that represent certain unidentified molecules. That background is usually present in all arc spectra of noble metals, and can therefore be recognized and ignored by recording side by side the arc spectra of two different noble metals and by measuring only the lines that are not common to both.

3.1. Palladium (46 Pd)

Among the six noble metals, palladium is outstanding in possessing the simplest arc spectrum. Following previous workers, Shenstone [7] in 1930 compiled and thoroughly analyzed the arc spectrum of palladium. That compilation lists about 350 Pd I lines with wavelengths ranging from 1945.98 to 9234.02 A. Most of those lines were quoted from published [2] and unpublished data by Meggers. Recently, Shenstone [8] made a new examination of the Pd I spectrum and contributed 75 new lines, mostly in the ultraviolet down to 1683.65 A.

In the present paper only new data for 63 red and infrared lines of the Pd I spectrum are given in table 1. Between 6508 and 8761 A the new list is almost identical with that published by Meggers [2] in 1925, except that the intensity scale has been increased, and the accuracy of wavelengths has been improved. A few faint lines in the early list were not confirmed, but 17 new lines were observed, and the Pd I spectrum has been extended to 11556.27 A in the infrared. All the new lines were immediately explained as transitions between atomic energy levels already published by Shenstone [8], and it must be concluded that the analysis of the Pd I spectrum is practically complete, so that further effort to extend it may not be justified. Incidentally, two forbidden transitions (6915 and 7147 A) between terms of like parity, first discovered by Shenstone [8], were nicely confirmed by the present observations.

TABLE 1. *Extension of the first spectrum of palladium*, Pd I

[*h*, hazy; *H*, very hazy; *l*, shaded to longer waves; *s*, shaded to shorter waves]

Wavelength	Intensity and character	Wave number, *K*		Spectral-term combination	Wavelength	Intensity and character	Wave number, *K*		Spectral-term combination
		Observed	Computed				Observed	Computed	
A		cm^{-1}	cm^{-1}		*A*		cm^{-1}	cm^{-1}	
6508.42	30	15360.47	60.5	$5p\ ^3D_3^\circ - 6s\ ^3D_1$	6774.53	200	14757.10	57.0	$5s^2\ ^3F_4 - 5p\ ^1F_3^\circ$
6591.44	5	15167.00	67.1	$5p\ ^1F_3^\circ - 5d\ ^3F_4$	6784.51	1000	14735.39	35.4	$5p\ ^3P_2^\circ - 6s\ ^3D_3$
6597.06	1	15154.08	54.1	$5p\ ^1F_3^\circ - 5d\ ^3F_3$	6833.41	80*h*	14629.95	29.9	$5p\ ^3D_3^\circ - 5d\ ^3D_2$
6603.03	1	15140.38	40.4	$5p\ ^1F_3^\circ - 5d\ ^3D_2$	6878.36	3	14534.34	34.3	$5p\ ^1P_1^\circ - 5d\ ^1P_0$
6623.27	20	15094.11	94.2	$5p\ ^3D_3^\circ - 6s\ ^1D_2$	6915.0	5*Hs*	144457.3	57.1	$5p\ ^3D_1^\circ - 6p\ ^1P_1^\circ$
6625.28	10	15089.53	89.6	$5p\ ^1F_3^\circ - 5d\ ^3D_3$	6916.53	200*hl*	14454.13	54.1	$5p\ ^3D_1^\circ - 5d\ ^3P_1$
6662.87	20	15004.40	04.4	$5p\ ^3D_1^\circ - 5d\ ^3P_0$	6917.53	5	14452.04	52.0	$5p\ ^3D_1^\circ - 5d\ ^3P_2$
6681.56	5	14962.43	62.5	$5p\ ^1F_3^\circ - 5d\ ^3P_2$	7016.47	200	14248.25	48.3	$5p\ ^3P_0^\circ - 6s\ ^3D_1$
6685.70	3	14953.17	53.0	$5p\ ^1F_3^\circ - 5d\ ^3G_4$	7026.88	2	14227.15	27.2	$5p\ ^1D_2^\circ - 5d\ ^3D_2$
6686.80	20	14950.71	50.7	$5p\ ^3P_2^\circ - 6s\ ^3D_2$	7037.58	10	14205.51	05.5	$5p\ ^3D_1^\circ - 5d\ ^3S_1$

TABLE 1. *Extension of the first spectrum of palladium*, Pd I—Continued

[*h*, hazy; *H*, very hazy; *l*, shaded to longer waves; *s*, shaded to shorter waves]

Wavelength	Intensity and character	Wave number, *K*		Spectral-term combination	Wavelength	Intensity and character	Wave number, *K*		Spectral-term combination
		Observed	Computed				Observed	Computed	
A		cm^{-1}	cm^{-1}		*A*		cm^{-1}	cm^{-1}	
7052.04	3	14176.38	76.4	$5p\ {}^1D_2^3 - 5d\ {}^3D_3$	8599.13	300	11625.89	26.0	$5p\ {}^3D_3^3 - 6s\ {}^3D_2$
7060.29	50	14159.82	59.8	$5p\ {}^1P_1^3 - 5d\ {}^3D_2$	8644.48	100	11564.90	65.0	$5p\ {}^1D_2^3 - 6s\ {}^3D_1$
7115.82	7	14049.32	49.3	$5p\ {}^1D_2^3 - 5d\ {}^3P_2$	8695.12	60	11497.55	97.6	$5p\ {}^1P_1^3 - 6s\ {}^3D_1$
7147.5	2*Hs*	13987.0	87.0	$5p\ {}^1P_1^3 - 6p\ {}^3P_1$	8761.39	600	11410.58	10.7	$5p\ {}^3D_3^3 - 6s\ {}^3D_3$
7149.00	50*hl*	13984.12	84.0	$5p\ {}^1P_1^3 - 5d\ {}^3P_1$	8922.04	6*h*	11205.12	04.9	$6s\ {}^3D_2 - 27_{\frac{1}{2}}$
7150.13	2	13981.91	81.9	$5p\ {}^1P_1^3 - 5d\ {}^3P_2$	8984.04	40	11127.79	27.7	$5s^2\ {}^3F_2 - 5p\ {}^1F_3^3$
7242.91	5	13802.80	02.8	$5p\ {}^1D_2^3 - 5d\ {}^3S_1$	9038.75	5	11060.44	60.3	$5s^2\ {}^3F_2 - 5p\ {}^1D_2^3$
7278.44	4	13735.42	35.4	$5p\ {}^1P_1^3 - 5d\ {}^3S_1$	9233.85	1000	10826.75	26.7	$5s^2\ {}^3F_4 - 5p\ {}^3F_4^3$
7310.08	200	13675.97	76.0	$5p\ {}^3F_3^3 - 6s\ {}^1D_2$	9380.32	200	10657.69	57.6	$5s^2\ {}^3F_2 - 5p\ {}^3D_1^3$
7368.12	1000	13568.24	68.2	$5p\ {}^3F_3^3 - 6s\ {}^3D_2$	9433.02	70	10598.15	98.2	$5s^2\ {}^3F_3 - 5p\ {}^3F_2^3$
7391.92	400	13524.56	24.6	$5p\ {}^3F_2^3 - 6s\ {}^3D_1$	9793.76	150	10207.78	07.8	$5p\ {}^3F_2^3 - 6s\ {}^3D_2$
7486.93	300	13352.93	52.9	$5p\ {}^3F_3^3 - 6s\ {}^3D_3$	9852.14	3	10147.30	47.1	$5s^2\ {}^3F_2 - 5p\ {}^3F_3^3$
7763.99	2000	12876.43	76.4	$5p\ {}^3F_4^3 - 6s\ {}^3D_3$	10509.75	7*h*	9512.36	12.4	$6s\ {}^3D_3 - 24_{\frac{1}{2}3}$
7786.63	500	12838.99	39.0	$5p\ {}^3P_1^3 - 6s\ {}^3D_2$	10890.26	80	9180.00	80.0	$5s^2\ {}^3F_3 - 5p\ {}^3D_3^3$
7915.79	800	12629.50	29.6	$5p\ {}^1F_3^3 - 6s\ {}^1D_2$	10985.03	30	9100.80	00.7	$5s^2\ {}^3F_2 - 5p\ {}^3F_2^3$
7961.03	200	12557.73	57.8	$5s^2\ {}^3F_3 - 5p\ {}^1D_2^3$	11175.09	10	8946.02	46.1	$5p\ {}^1F_3^3 - 6s\ {}^3D_3$
8132.81	400	12292.49	92.4	$5s^2\ {}^3F_4 - 5p\ {}^3D_3^3$	11409.45	8	8762.26	62.3	$5s^2\ {}^3F_3 - 5p\ {}^3D_2^3$
8249.19	50	12119.07	19.1	$5p\ {}^3D_1^3 - 6s\ {}^1D_2$	11556.27	5	8650.94	50.9	$5p\ {}^3D_1^3 - 6s\ {}^3D_2$
8300.82	1000	12043.69	43.7	$5p\ {}^3D_2^3 - 6s\ {}^3D_2$					
8353.58	200	11967.63	67.7	$5p\ {}^3D_1^3 - 6s\ {}^3D_1$					
8387.99	3*h*	11918.53	18.5	$6s\ {}^3D_3 - 5p\ {}^1G_4^3$					
8451.93	10	11828.37	28.4	$5p\ {}^3D_2^3 - 6s\ {}^3D_3$					
8532.76	300	11716.32	16.4	$5p\ {}^1D_2^3 - 6s\ {}^1D_2$					
8582.10	200	11648.96	49.0	$5p\ {}^1P_1^3 - 6s\ {}^1D_2$					
8585.33	20	11644.58	44.6	$5s^2\ {}^3F_3 - 5p\ {}^1F_3^3$					

3.2. Platinum (78 Pt)

Although nearly 1,000 lines have been reported for the arc spectrum of platinum, the data must be sought in five different sources, because no one has made a systematic and satisfactory description of this spectrum. Haussman [9] in a report on Zeeman effect and terms in the Pt I spectrum compiled a list of 377 classified lines, quoting wavelengths from Meggers [2], Meggers and Laporte [10], Kayser [11], and Exner and Haschek [12]. The only additional data are wavelengths of 56 ultraviolet lines (2241.20 to 1928.85 A) published by Livingood [13], but most of these remain unclassified.

The present paper is concerned primarily with improved description of the long-wave portion of the Pt I spectrum through the use of photographic plates of greater sensitivity and spectrographs of greater dispersive power. The pioneering work of Meggers [2] produced about 50 Pt I lines with wavelengths greater than 6648 A; now the number is increased to 74 as displayed in table 2. The photographic extension is nearly 2000 A, but the Pt I spectrum appears to be very sparce in the infrared, and no new lines could be detected beyond 10758 A with 4-hr exposures.

Only 42 of the Pt I lines in table 2 can be accounted for as combinations of Haussmann's [9] or Livingood's [10] terms. Attempts to classify the remainder by searching for new atomic energy levels among the unclassified lines were not successful. In fact, a critical examination of the old analyses of the Pt I spectrum raised many doubts about the interpretation of certain levels and the reality of others. A discussion of this will appear in Atomic Energy Levels [1]. It must be concluded that no further progress can be made with the structural analysis of the Pt I spectrum without a more complete and homogeneous description of this spectrum.

TABLE 2. *Extension of the first spectrum of platinum*, Pt I [a]

[h, hazy]

Wavelength	Intensity and character	Wave number, K		Spectral-term combination	Wavelength	Intensity and character	Wave number, K		Spectral-term combination
		Observed	Computed				Observed	Computed	
A		cm^{-1}	cm^{-1}		*A*		cm^{-1}	cm^{-1}	
6648.32	100	15037.24	37.2	$6^{\frac{1}{2}} - e\,^3D_3$	7786.77	80	12838.76	38.7	$19^{\frac{1}{2}} - e\,^5F_4$
6655.55	3	15020.91	20.9	$22^{\frac{1}{2}} - E_3$	7790.21	5h	12833.09	..	.....
6710.41	400	14898.11	98.2	$8^{\frac{1}{2}} - e\,^3D_2$	7830.42	6h	12767.19	..	.....
6760.01	1000	14788.80	88.6	$z\,^3F_4^{\frac{1}{2}} - e\,^3D_3$	7877.45	3h	12690.97	..	.....
6820.21	10	14658.26	.....	.....	7911.26	20h	12636.73	..	.....
6838.08	20	14619.96	20.0	$24^{\frac{1}{2}} - M_3$	7977.35	60	12532.04	32.1	$30^{\frac{1}{2}} - N_4$
6842.61	200	14610.28	10.3	$8^{\frac{1}{2}} - e\,^3D_2$	8093.86	7	12351.65	51.7	$20^{\frac{1}{2}} - e\,^5F_4$
6896.73	20	14495.63	..	.....	8204.47	90	12185.13	85.1	$z\,^5F_4^{\frac{1}{2}} - e\,^3D_3$
6908.82	7	14470.26	70.2	$24^{\frac{1}{2}} - e\,^1D_2$	8224.78	400	12155.04	55.0	$a\,^1G_4 - z\,^3F_3^{\frac{1}{2}}$
6956.85	4	14370.36	..	.....	8227.55	70	12150.95	50.9	$z\,^5D_2^{\frac{1}{2}} - e\,^3D_2$
6957.51	20	14368.99	..	.....	8259.03	7	12104.63	04.7	$32^{\frac{1}{2}} - N_4$
6975.70	15	14331.53	31.5	$b\,^1D_2 - z\,^3D_3^{\frac{1}{2}}$	8301.83	20	12042.23	42.2	$29^{\frac{1}{2}} - G_4$
6989.83	20h	14302.56	..	.....	8428.47	4	11861.29	61.3	$32^{\frac{1}{2}} - e\,^1D_2$
7012.03	2	14257.27	..	.....	8456.36	3h	11822.17	22.2	$31^{\frac{1}{2}} - e\,^3D_1$
7030.08	10	14220.67	..	.....	8619.91	4h	11597.85	97.9	$z\,^1F_3^{\frac{1}{2}} - N_4$
7056.28	5	14167.87	67.9	$27^{\frac{1}{2}} - M_3$	8722.99	6h	11460.81	..	.....
7065.57	10	14149.24	49.3	$b\,^1D_2 - 13^{\frac{1}{2}}$	8762.47	70	11409.17	09.2	$z\,^3D_3 - e\,^3D_3$
7078.09	8	14124.21	24.2	$17^{\frac{1}{2}} - e\,^5F_4$	8804.61	2	11354.57	54.5	$z\,^1F_3^{\frac{1}{2}} - e\,^1D_2$
7094.61	15	14091.32	..	.....	8981.87	8	11130.48	30.4	$b\,^1D_2 - 8^{\frac{1}{2}}$
7094.78	100	14090.98	..	.....	9004.06	7h	11104.29	..	.....
7113.73	400	14053.45	53.5	$a\,^3P_1 - z\,^3P_2^{\frac{1}{2}}$	9012.40	3h	11092.78	92.8	$32^{\frac{1}{2}} - H_3$
7122.92	3	14035.32	..	.....	9060.50	1	11033.89	..	.....
7125.05	5	14031.12	..	.....	9100.87	2	10984.94	85.0	$32^{\frac{1}{2}} - e\,^5F_3$
7131.64	15	14018.16	18.1	$27^{\frac{1}{2}} - e\,^1D_2$	9128.03	2h	10952.26	52.2	$32^{\frac{1}{2}} - Q_3$
7179.95	4	13923.84	23.9	$z\,^3P_3^{\frac{1}{2}} - e\,^3D_1$	9201.81	20	10864.44	64.5	$z\,^3P_1^{\frac{1}{2}} - e\,^3D_2$
7217.57	200	13851.26	51.3	$z\,^3D_3^{\frac{1}{2}} - e\,^3D_2$	9291.30	3h	10759.80	59.8	$35^{\frac{1}{2}} - e\,^1D_2$
7254.23	5h	13781.26	..	.....	9340.16	4	10703.52	03.5	$b\,^1D_2 - 6^{\frac{1}{2}}$
7407.44	3	13496.22	..	.....	9460.64	3h	10567.21	..	.....
7486.03	80	13354.54	54.6	$a\,^1G_4 - z\,^9D_3^{\frac{1}{2}}$	10005.95	7h	9991.31	91.3	$35^{\frac{1}{2}} - H_3$
7607.25	10	13141.74	41.8	$27^{\frac{1}{2}} - e\,^5F_3$	10539.57	2h	9485.45	..	.....
7614.83	8	13128.65	28.7	$27^{\frac{1}{2}} - E_3$	10546.35	20	9479.35	79.4	$18^{\frac{1}{2}} - e\,^3D_2$
7618.17	30h	13122.90	..	.....	10685.35	2	9356.04	..	.....
7626.20	4h	13109.08	09.0	$27^{\frac{1}{2}} - Q_3$	10705.51	4h	9338.42	..	.....
7637.65	7h	13089.43	..	.....	10757.78	8	9293.05	..	.....
7641.27	2	13083.23	..	.....					
7644.11	5	13078.37	..	.....					
7738.60	3h	12918.68	..	.....					
7749.76	40	12900.07	00.0	$29^{\frac{1}{2}} - e\,^1D_2$					
7761.63	2	12880.35	..	.....					
7780.53	70h	12849.06	..	.....					

[a] Shenstone has pointed out that many *LS*-designations lack significance because of the effect of *jj*-coupling in Pt. I. In "Atomic Energy Levels" [1] many of the earlier designation assignments are, therefore, being omitted.

4. References

[1] C. E. Moore, Atomic energy levels as derived from analyses of optical spectra, NBS Circular 467, III (in press).
[2] W. F. Meggers, BS Sci. Pap. **20,** 31 (1925) S499.
[3] C. E. K. Mees, J. Opt. Soc. Am. **25,** 80 (1935).
[4] R. J. Murphy, J. Research NBS **49,** 371 (1952) RP2374.
[5] K. G. Kessler and W. F. Meggers (unpublished).
[6] Transactions of the Joint Commission for Spectroscopy, J. Opt. Soc. Am. **43,** 423 (1953).
[7] A. G. Shenstone, Phys. Rev. **36,** 669 (1930).
[8] A. G. Shenstone, Proc. Roy. Soc. [A] **219,** 419 (1953).
[9] A. C. Haussmann, Astrophys. J. **66,** 333 (1927).
[10] W. F. Meggers and O. Laporte, Phys. Rev. **28,** 642 (1926).
[11] H. Kayser, Handbuch der Spektroscopie **6,** 304 (1912).
[12] F. Exner and E. Haschek, Die Spektren der Elemente **II,** 204 (Franz Deuticke, Leipzig und Wien, 1911).
[13] J. J. Livingood, Phys. Rev. **34,** 185 (1929).

WASHINGTON, June 6, 1954

Journal of Research of the National Bureau of Standards Vol. 53, No. 4, October 1954 Research Paper 2539

Influence of Molecular Shape on the Dielectric Constant of Polar Liquids

F. Buckley and A. A. Maryott

The Onsager theory of the static dielectric constant of polar liquids has been modified to allow for the influence of molecular shape. Equations have been derived for both prolate and oblate spheroids in which the permanent dipole is directed along the axis of symmetry. These equations have been applied to a number of pure polar liquids, exclusive of the hydrogen bonded liquids, where reliable data were available over extended ranges of temperature. A satisfactory interpretation of the variation of dielectric constant with temperature is obtained provided the volume of the molecular cavity is maintained fixed and independent of temperature rather than allowed to expand in proportion to the molar volume as assumed by Onsager. The required molecular shapes are in general accord with the actual molecular geometries. The behavior of dilute solutions and mixtures with a nonpolar solvent are also satisfactorily correlated using the same shape parameters. It appears to be unnecessary to consider specific interactions between neighboring molecules in order to account for the static dielectric behavior of these systems.

1. Introduction

The Onsager [1][1] theory has been notably successful in relating electric dipole moments as determined in the vapor phase with the "static" dielectric constants of polar liquids. Exceptions are liquids in which association occurs, usually through hydrogen bonding, as in water and the alcohols, or for which the dipole moment is variable, as in ethylene chloride. For a large number of the more normal liquids, such as ethers, ketones, nitriles, and alkyl and aryl halides, the calculated values of dipole moment fall with more or less equal frequency above and below the measured gas values. The Onsager relation thus represents a rather satisfactory average. However, the agreement between observed and calculated values is far from perfect and discrepancies of the order of 10 to 20 percent are relatively common.

Recent extensions of the dielectric theory of liquids have usually followed one of two patterns. In the one case, following Onsager, the environment surrounding and interacting with any given molecule is treated as a continuum having the macroscopic dielectric constant and the molecular model is altered to accommodate either optical anisotropy [2] or geometrical anisotropy [3, 4] or both [5, 6]. A second, more generalized and flexible approach was introduced by Kirkwood [7] and extended by others [8, 9, 10]. Interactions between the molecule and its immediate surroundings are treated by the specific methods of statistical mechanics and the medium becomes a continuum only outside of this region. However, a rigorous application of this procedure to liquids is usually prevented by a lack of detailed knowledge of the liquid structure. Consequently, it has been customary in practice to make certain simplifying assumptions, of a nature comparable to those inherent in the Onsager development, in order to obtain a "normalized" relation that should apply in the absence of specific close-range interactions. Experimental departures from the idealized equation are then assumed to be indicative of such interactions or association [2, 10, 11]. If this interpretation were justified, dielectric measurements would provide a very useful tool for investigating structure in liquids since independent evidence regarding these interactions is ordinarily lacking.

The simplicity and explicit nature of the Onsager approach make it desirable to investigate its utility in more detail than has been done heretofore. In particular, it is of interest to see whether any reasonable and simple modification of Onsager's molecular model can account for the dielectric behavior of polar liquids when subjected to wide changes in temperature or when progressively diluted with a nonpolar solvent. Under these conditions the effect of molecular interactions, if important, should vary markedly.

In this paper equations are developed for both prolate and oblate spheroids in a manner

[1] Figures in brackets indicate the literature references at the end of this paper.

314715—54——3

formally analogous to Onsager's treatment of the spherical case. A solution for the prolate spheroid comparable to that employed here has been published by Abbott and Bolton [3]. Analysis of a large body of data on the dielectric constants of pure liquids, mixtures, and dilute solutions, excluding hydrogen bonded substances, shows that deviations from the Onsager equation can be rather systematically interpreted in terms of the spheroidal models and that these shapes are at least in qualitative accord with the actual molecular geometries. For these systems it appears to be unnecessary, in general, to consider additional factors involving specific molecular interactions or dipole association.

2. Modified Onsager Equation

The Onsager molecular model consists of a polarizable point dipole having a moment $\vec{\mu}_0$ and an isotropic polarizability α located at the center of an otherwise empty spherical cavity of volume v. The cavity is surrounded by a continuum having the macroscopic dielectric constant ϵ. The field inside the cavity is conveniently separated into two parts, a reaction field $\vec{R}$ that is parallel to the instantaneous dipole axis and a cavity field $\vec{E}_c$ parallel to the externally applied field $\vec{E}$. In the absence of any applied field, the polarizable dipole is enhanced by its reaction field, so that the total moment $\vec{\mu}=\vec{\mu}_0+\alpha\vec{R}=\vec{\mu}_0/[1-(\alpha/v)g]$, where $R=g\mu/v$ and $g=(4\pi/3)(2\epsilon-2)/(2\epsilon+1)$. The cavity field, $\vec{E}_c=3\epsilon/(2\epsilon+1)\vec{E}$, both orients the permanent dipole and induces a moment that, when enhanced by its own reaction field, becomes $\vec{m}_i=\alpha\vec{E}_c/[1-(\alpha/v)g]$. The average total moment in the direction of $\vec{E}$ is then $\overline{m}=m_i+\mu\,\overline{\cos\theta}$, where θ is the angle between $\vec{\mu}$ and $\vec{E}$. This model leads to the following relation between the dielectric constant and the molecular quantities:

$$\frac{(\epsilon-1)(2\epsilon-1)}{9\epsilon}V=\frac{4\pi N}{3}\left[\frac{\alpha}{1-\frac{\alpha}{v}g}+\frac{\mu_0^2}{3kT\left(1-\frac{\alpha}{v}g\right)^2}\right], \tag{1}$$

where k is Boltzmann's constant, T the absolute temperature, V the molar volume, and N Avogadro's number. The left-hand side of this expression is often called the Onsager-Kirkwood polarization, P.

It is convenient to express differences between theory and experiment in terms of a deviation factor, G, defined as $\mu^2_{0(\text{calc.})}/\mu^2_{0(\text{gas})}$. A value of unity for G indicates agreement between the dipole moment calculated from the dielectric constant of the liquid and the measured gas value. The values of G will depend upon the choice of polarizability and the volume assumed for the cavity. Onsager chose the cavity volume to be the same as the average volume occupied by the molecule, i. e., $v=V/N$, since eq (1) then reduces to the Clausius-Mossotti equation for a nonpolar liquid, a relation which, though not exact, is a good approximation in such cases. Although the polarizability should include a small "atomic" contribution as well as the optical part, the former is seldom known with any degree of accuracy for polar substances even from measurements on the vapor and will be neglected in the analyses to follow. Values of G derived from eq (1), hereafter designated as G_{Onsager} ($G_{\text{On.}}$), have been obtained by using the relations $4\pi N\alpha/3=R_D$ (molar refraction for the Na_D line), and

$$\alpha/v=\frac{3R_D}{4\pi V}=\frac{3(n_D^2-1)}{4\pi(n_D^2+2)}.$$

If one alters the Onsager model only to the extent of replacing the spherical cavity by one of equal volume having the shape of either a prolate or an oblate spheroid with the permanent dipole directed along the axis of symmetry, one obtains an equation of the form

$$\frac{(\epsilon-1)(2\epsilon+1)}{9\epsilon}V=\frac{4\pi N}{3}\left[\frac{\alpha k_\alpha}{1-\frac{\alpha}{v}gk_R}+\frac{\mu_0^2}{3kT\left(1-\frac{\alpha}{v}gk_R\right)^2}\right]k_c, \tag{2}$$

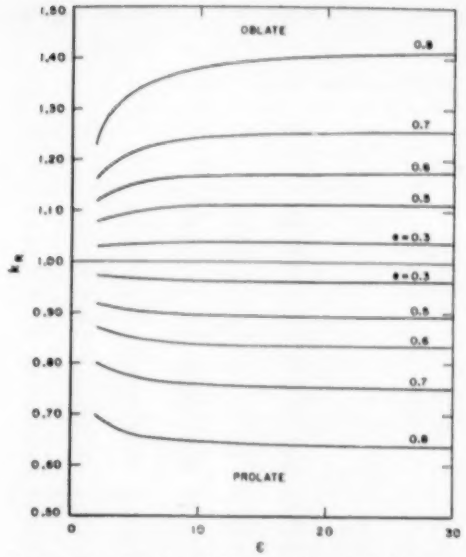

FIGURE 1. *Reaction field correction coefficient as a function of dielectric constant for various values of molecular eccentricity.*

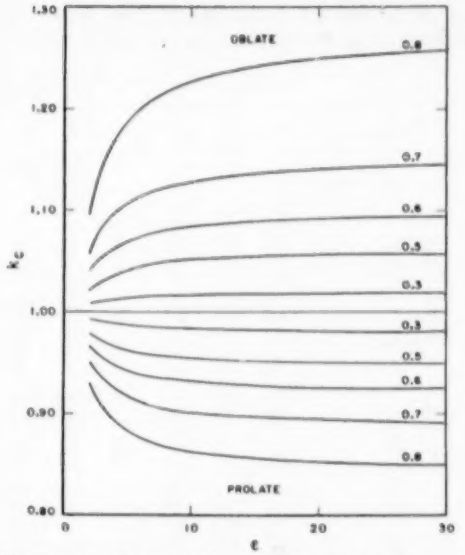

FIGURE 2. *Cavity field correction coefficient as a function of dielectric constant for various values of molecular eccentricity.*

The coefficients k_a, k_R, and k_c depend on the dielectric constant of the medium and the shape of the spheroid. k_R is the ratio of the reaction field of the spheroid to that of the equivalent sphere, and k_c is the corresponding ratio for the cavity fields. For the sphere, $k_a = k_R = k_c = 1$, and eq (2) reduces to Onsager's equation. Details of the mathematical development, as well as the explicit functions defining k_R, k_c, and k_a, are found in the appendix. To facilitate application of eq (2), it has been assumed that the product $k_a k_c = 1$. This approximation is adequate for the present purpose because $k_a k_c$ is generally close to unity and practically independent of temperature.

Figure 1 shows the variation in reaction-field coefficient k_R with dielectric constant for both prolate and oblate spheroids of various eccentricities ϵ. A similar plot of the cavity-field coefficient k_c is given in figure 2. For prolate spheroids, where k_R and k_c are both less than unity, the Onsager relation should give G factors less than unity. In like manner, oblate spheroids should lead to values of $G_{\text{On.}}$ greater than unity because both k_R and k_c are greater than unity.

3. Analysis of Data on Pure Liquids

Initial attempts to interpret deviations from Onsager's equation in terms of eq (2) for a number of pure polar liquids over rather extended ranges of temperature were only partially successful. In particular, G factors adjusted to unity at some temperature by suitable choice of shape and eccentricity did not remain substantially independent of temperature. These variations were not systematically correlated with any simple picture of dipole association. The difficulty appeared to be inherent in Onsager's assumption requiring the cavity volume to vary with the thermal expansion of the liquid and was largely overcome when the cavity volume was allowed to remain independent of temperature. Moreover, analyses made by the authors on a number of nonpolar liquids, as well as the published work of others [12], show that the fit of eq (1) is improved if this volume is maintained constant. Although the empirical evidence for a constant cavity volume is sufficiently convincing, it should be emphasized that in the electrostatic theory this equivalent volume is determined by the electrostatic properties of the molecule and might well be essentially independent of the temperature.

G factors for a number of pure polar liquids over a wide range of temperature, together with other pertinent data, are given in table 1.

TABLE 1. *Summary of the analysis of the dielectric data for pure liquids*[a]

Substance	T(°K)	ε	R_D/V	$G_{O\infty}$.	$G^{\circ}_{O\infty}$.	G_ϵ
PROLATE						
CH_3Cl	203	16.9	0.251	0.87	0.89	1.00
	213	15.8	.248	.88	.89	1.00
$\mu_0=1.87$[b]	223	14.9	.244	.88	.89	0.99
$R_D=11.7$	233	14.0	.240[c]	.88	.88	.99
$\epsilon=0.50$	243	13.3	.236	.89	.88	.99
	253	12.6	.233	.90	.88	.99
CH_2Br	173	16.9	.305	.70	.75	1.01
	193	14.9	.297	.72	.75	1.00
$\mu_0=1.80$	213	13.3	.289	.73	.75	1.00
$R_D=14.6$	233	11.9	.281[c]	.75	.75	.99
$\epsilon=0.71$	253	10.8	.274	.76	.75	.99
	273	9.82	.266	.78	.75	.99
CH_2I	213	9.74	.340	.57	.59	1.00
	233	8.87	.332[c]	.59	.59	1.00
$\mu_0=1.65$	253	8.13	.325	.60	.59	.99
$R_D=19.3$	273	7.53	.317	.62	.60	1.00
$\epsilon=0.85$	293	7.00	.309	.64	.60	1.00
	313	6.50	.301	.65	.60	.99
C_2H_5Br	173	17.1	.297	.77	.86	.99
	193	15.2	.290	.79	.87	1.00
	213	13.6	.283	.81	.87	1.00
$\mu_0=2.03$	233	12.3	.277	.83	.87	1.01
$R_D=19.1$	253	11.2	.270	.84	.88	1.01
$\epsilon=0.55$	273	10.2	.263	.86	.88	1.01
	293	9.31	.256[c]	.87	.87	.99
	313	8.44	.248	.87	.86	.98
C_2H_5I	193	11.6	.336	.62	.69	.92
	213	10.6	.329	.65	.70	.96
	233	9.74	.322	.66	.71	.96
$\mu_0=1.91$	253	9.01	.315	.69	.72	.98
$R_D=24.3$	273	8.38	.308	.71	.73	.99
$\epsilon=0.72$	293	7.82	.300[c]	.74	.74	1.00
	313	7.29	.293	.75	.74	1.00
	333	6.80	.286	.77	.75	1.00
C_2H_5CN	273	31.0	.230	.75	.76	1.01
$\mu_0=4.03$	293	27.2	.224[c]	.73	.73	.97
$R_D=15.8$	323	24.3	.216	.76	.73	.99
$\epsilon=0.73$						
n-C_3H_7Cl	183	12.2	.276	.84	.92	1.00
	203	11.0	.269	.87	.93	1.01
	223	9.94	.263	.88	.93	1.01
$\mu_0=2.05$	243	9.07	.257	.90	.93	1.01
$R_D=25.4$	263	8.32	.251	.92	.94	1.01
$\epsilon=0.40$	283	7.66	.246	.93	.94	1.01
	303	7.09	.240[c]	.94	.94	1.01
	323	6.56	.234	.95	.94	1.01
	343	6.05	.227	.96	.93	1.00
n-C_3H_7Br	183	11.1	.286	.71	.78	.97
	203	10.1	.280	.74	.79	.99
	223	9.26	.284	.76	.80	1.00
	243	8.52	.278	.78	.81	1.00
$\mu_0=2.08$	263	7.88	.272	.80	.82	1.01
$R_D=28.3$	283	7.32	.266	.82	.83	1.01
$\epsilon=0.65$	303	6.80	.260[c]	.83	.83	1.01
	323	6.35	.254	.86	.83	1.01
	343	5.93	.248	.86	.83	1.01
	363	5.54	.242	.87	.83	1.01
n-C_3H_7I	193	8.89	.325	.54	.59	.98
	213	8.18	.319	.56	.60	.99
	233	7.53	.313	.57	.60	1.00
	253	7.00	.306	.59	.61	1.00
$\mu_0=2.12$	273	6.54	.300	.61	.62	1.00
$R_D=33.5$	293	6.12	.294[c]	.62	.62	1.00
$\epsilon=0.87$	313	5.74	.288	.63	.62	1.00
	333	5.42	.282	.65	.63	1.00
	353	5.11	.276	.66	.63	1.00
C_6H_5Cl	223	7.28	.327	.68	.72	1.01
	243	6.76	.321	.70	.73	1.01
	263	6.26	.315	.71	.73	1.01
	283	5.82	.309	.72	.73	1.00
$\mu_0=1.70$	303	5.46	.303[c]	.73	.73	.99
$R_D=31.1$	323	5.15	.297	.75	.73	.99
$\epsilon=0.74$	343	4.89	.291	.76	.74	1.00
	373	4.52	.282	.78	.74	.99
	403	4.17	.272	.79	.73	.98
C_6H_5Br	274	5.74	.330	.64	.65	1.00
	298	5.39	.322[c]	.66	.66	1.01
$\mu_0=1.70$	313	5.18	.318	.67	.66	1.01
$R_D=34.0$	328	4.96	.314	.68	.66	1.01
$\epsilon=0.82$						
$C_6H_5NH_2$	273	7.38	.341	.94	.95	1.00
	283	7.13	.339	.94	.95	1.00
$\mu_0=1.53$	293	6.89	.336[c]	.95	.95	1.00
$R_D=30.6$	303	6.66	.333	.96	.95	1.00
$\epsilon=0.27$	313	6.43	.330	.96	.94	.99
	323	6.22	.327	.96	.94	.99
$C_6H_5NO_2$	283	37.6	.322	.97	.98	1.25
	303	33.9	.317[c]	.96	.96	1.23
	323	30.6	.312	.95	.93	1.19
$\mu_0=4.25$	343	27.6	.306	.94	.90	1.16
$R_D=32.7$	363	24.9	.301	.92	.87	1.12
$\epsilon=0.62$	383	22.7	.296	.91	.85	1.09
	403	20.8	.290	.91	.84	1.08
	423	19.3	.285	.91	.83	1.05
	473	16.0	.270	.91	.80	1.01
C_6H_5CN	273	27.6	.313	.64	.65	0.97
	291	25.9	.309[c]	.65	.65	.98
$\mu_0=4.42$	313	24.0	.303	.68	.67	.99
$R_D=31.6$	323	23.3	.300	.69	.67	1.00
$\epsilon=0.76$	333	22.7	.297	.70	.68	1.01
	343	22.1	.295	.72	.69	1.03
OBLATE						
CH_2NO_2	283	39.1	0.236	1.03	1.05	1.00
	303	35.9	.230[c]	1.05	1.05	1.00
$\mu_0=3.44$	323	32.9	.224	1.07	1.05	1.00
$R_D=12.5$	343	30.1	.218	1.08	1.05	1.00
$\epsilon=0.31$	363	27.6	.213	1.09	1.03	1.00
CH_2Cl_2	173	17.0	.301	1.09	1.23	1.00
	193	15.0	.294	1.11	1.22	1.00
	213	13.4	.287	1.13	1.22	1.00
$\mu_0=1.56$	233	12.0	.280	1.15	1.22	1.01
$R_D=16.6$	253	10.9	.273	1.17	1.22	1.01
$\epsilon=0.09$	273	9.92	.266	1.19	1.22	1.01
	293	9.09	.259[c]	1.21	1.22	1.01
	313	8.27	.252	1.21	1.20	1.00
$CHCl_3$	213	6.76	.294	1.46	1.56	1.00
	233	6.12	.287	1.46	1.53	1.00
	253	5.61	.280	1.47	1.52	1.00
$\mu_0=1.01$	273	5.22	.274	1.50	1.52	1.02
$R_D=21.4$	293	4.81	.267[c]	1.49	1.49	1.01
$\epsilon=0.81$	313	4.47	.260	1.50	1.48	1.01
	333	4.12	.253	1.47	1.43	1.00
$(CH_3)_2CCl_2$	253	12.2	.250	1.31	1.36	1.01
	263	11.5	.246	1.31	1.35	1.01
$\mu_0=2.13$	283	10.4	.239	1.32	1.34	1.00
$R_D=25.9$	303	9.37	.233[c]	1.32	1.31	0.99
$\epsilon=0.67$						
$(CH_3)_2O$	298	5.02	.189[c]	1.16	1.16	1.03
	318	4.54	.179	1.17	1.15	1.03
$\mu_0=1.30$	338	4.07	.169	1.17	1.13	1.01
$R_D=13.3$	358	3.59	.156	1.17	1.10	0.99
$\epsilon=0.58$	378	3.12	.137	1.19	1.10	1.01
	398	2.37	.102	1.20	1.08	1.00
$(C_2H_5)_2O$	233	5.86	.237	1.63	1.71	1.00
	253	5.30	.230	1.62	1.67	1.01
	273	4.80	.224	1.60	1.63	1.01
$\mu_0=1.15$	293	4.34	.217[c]	1.57	1.57	0.99
$R_D=22.5$	313	3.97	.209	1.55	1.53	.99
$\epsilon=0.80$	333	3.67	.202	1.55	1.51	1.00
	353	3.40	.194	1.52	1.48	1.00
	373	3.14	.185	1.53	1.46	1.01

TABLE 1. *Summary of the analysis of the dielectric data for pure liquids*[a]—Continued

Substance	T(°K)	ϵ	P_D/V	$G_{On.}$	$G^*_{On.}$	G_ϵ	Substance	T(°K)	ϵ	P_D/V	$G_{On.}$	$G^*_{On.}$	G_ϵ
OBLATE—Continued													
	193	34.5	.251	1.03	1.11	0.96		233	17.4	.260	1.06	1.11	1.03
	213	31.3	.245	1.07	1.14	.98		253	15.9	.254	1.09	1.12	1.04
$(CH_3)_2CO$	233	28.4	.239	1.10	1.15	1.00	i-$C_4H_9COCH_3$	273	14.5	.249	1.11	1.12	1.04
$\mu_D=2.88$	253	25.9	.233	1.13	1.17	1.02	$\mu_D=(2.88)$[d]	293	13.1	.243*	1.11	1.11	1.03
$R_D=16.2$	273	23.7	.227	1.16	1.18	1.02	$R_D=30.3$	313	11.8	.237	1.09	1.08	1.00
$\epsilon=0.55$	293	21.5	.220*	1.18	1.18	1.02	$\epsilon=0.40$	333	10.7	.231	1.09	1.06	0.98
	313	19.4	.214	1.18	1.17	1.01		353	9.75	.225	1.08	1.04	.97
								373	8.90	.220	1.08	1.02	.95
	213	27.2	.255	1.10	1.17	1.00							
	233	24.6	.249	1.13	1.18	1.01		253	15.1	.256	1.15	1.18	1.01
$C_2H_5COCH_3$	253	22.3	.243	1.15	1.19	1.02		273	13.8	.251	1.17	1.18	1.01
$\mu_D=(2.88)$[d]	273	20.3	.237	1.18	1.19	1.02	$(n$-$C_3H_7)_2CO$	293	12.6	.246*	1.18	1.18	1.01
$R_D=20.7$	293	18.5	.231*	1.19	1.19	1.02	$\mu_D=(2.88)$[d]	313	11.4	.240	1.17	1.15	1.00
$\epsilon=0.55$	303	16.8	.225	1.20	1.18	1.02	$R_D=34.1$	333	10.4	.235	1.16	1.13	0.99
	333	15.3	.219	1.20	1.17	1.01	$\epsilon=0.56$	353	9.48	.230	1.17	1.11	.97
	353	13.9	.213	1.20	1.15	1.00		373	8.65	.223	1.15	1.09	.95
								393	8.00	.217	1.15	1.08	.93
	273	18.9	.245	1.26	1.28	1.05							
$(C_2H_5)_2CO$	293	17.0	.239*	1.26	1.26	1.04		253	14.3	.263	1.06	1.09	1.01
$\mu_D=(2.88)$[d]	313	15.3	.233	1.25	1.23	1.02		273	13.1	.257	1.08	1.10	1.02
$R_D=25.3$	333	13.8	.227	1.24	1.21	1.00	n-$C_5H_{11}COCH_3$	293	12.0	.252*	1.06	1.09	1.01
$\epsilon=0.60$	353	12.5	.221	1.23	1.18	0.98	$\mu_D=(2.88)$[d]	313	10.9	.246	1.08	1.07	0.99
	373	11.5	.215	1.24	1.17	.98	$R_D=35.2$	333	9.93	.241	1.08	1.05	.98
							$\epsilon=0.40$	353	9.08	.235	1.08	1.04	.97
	213	22.0	.261	1.04	1.10	.97		373	8.27	.229	1.07	1.01	.95
	233	20.2	.255	1.08	1.13	1.00		393	7.61	.223	1.06	1.00	.93
	253	18.4	.249	1.10	1.13	1.01		413	7.10	.217	1.08	1.00	.93
n-$C_3H_7COCH_3$	273	16.5	.243	1.13	1.14	1.01							
$\mu_D=(2.88)$[d]	293	15.5	.238*	1.15	1.15	1.02		253	12.5	.269	1.01	1.04	1.04
$R_D=25.4$	313	14.1	.232	1.16	1.14	1.01		273	11.5	.263	1.02	1.04	1.04
$\epsilon=0.50$	333	12.9	.226	1.16	1.13	1.01		293	10.4	.258*	1.02	1.02	1.02
	353	11.7	.220	1.16	1.12	0.99	n-$C_6H_{13}COCH_3$	313	9.42	.252	1.01	1.00	1.00
	373	10.8	.212	1.19	1.12	1.00	$\mu_D=(2.88)$[d]	333	8.70	.247	1.02	0.99	0.99
							$R_D=40.3$	353	8.01	.241	1.02	.98	.98
							$\epsilon=0$	373	7.42	.236	1.02	.97	.97
								393	6.90	.230	1.03	.96	.96
								413	6.49	.224	1.04	.97	.97
								433	6.10	.218	1.06	.97	.97

[a] Sources of data: A. A. Maryott and E. R. Smith, Table of dielectric constants of pure liquids, NBS Circular 514 (1951); A. A. Maryott, and Floyd Buckley, Table of dielectric constants and electric dipole moments of substances in the gaseous state, NBS Circular 537 (1953).

[b] All values of dipole moment given in Debye units (1 Debye = 10^{-18} esu).

[c] Data at the lower temperatures have been omitted since the tabulated values of dielectric constant are inconsistent with the graphical representation (R. N. Cole, J. Chem. Phys. **9**, 251 (1951)).

[d] Value assumed to be the same as for acetone.

The factors designated as $G^*_{On.}$ and G_ϵ were obtained from eq (1) and (2), respectively, with the assumption of a fixed cavity volume. In these cases, the value of R_D/V noted by an asterisk, a value usually pertaining to room temperature or its vicinity, was rather arbitrarily used. Estimates of the parameter a/r are not critical, and values that differ reasonably from the selected values do not entail significant changes in the results of the calculations or the interpretation of the data. Compounds have been classified as prolate or oblate, depending upon whether $G^*_{On.}$ is less or greater than unity. Using the reaction and cavity field coefficients appropriate to this shape, values of eccentricity were found that fitted eq (2). As the corresponding deviation factors G_ϵ have been adjusted near unity, they are only indicative with respect to their constancy with temperature and with respect to any correlation between the required cavity shape and the molecular geometries of the simpler types of molecules considered.

Table 1 shows that the values of $G_{On.}$ frequently increase with rising temperature. Such behavior, if confined to cases where $G_{On.}$ is less than unity, might be rather simply explained in terms of molecular interactions. Thus for molecules simulating prolate spheroids, dipole interactions would be such as to favor antiparallel alinement [13] and thereby tend to reduce the dipolar polarization. Value of $G_{On.}$ should then be less than unity but approach unity at more elevated temperatures as a consequence of the diminishing effect of such interactions. In like manner, values of $G_{On.}$ greater than unity, if interpretable in terms of parallel association in conformity with the general oblate geometry of this group, should also approach unity with rising temperature. However, except for ethyl ether, no such trend is evident. Furthermore, the values of $G^*_{On.}$, calculated on the basis of a fixed cavity volume, generally show little or no variation with temperature for the prolate cases. Thus the evidence for association in these

substances would appear to depend upon Onsager's assumption of an expanding cavity volume.

With the exception of nitrobenzene and several of the ketones, the modifications for cavity shape and cavity volume lead to good agreement with the experimental data. The values of G_e usually vary from unity by no more than 1 or 2 percent over wide ranges of temperature, 180° in some instances, and are probably commensurate with the experimental uncertainties in the values of dielectric constant. The series CH_2Cl_2, $CHCl_3$, and $(C_2H_5)_2O$ is particularly indicative. Although the values of $G_{On.}$ are all greater than unity, they show a different type of dependence on temperature in each case. These differences are readily interpretable in terms of the modified relation. For CH_2Cl_2, which is typical of substances having relatively high values of dielectric constant and only moderate values of eccentricity, $G_{On.}$ shows a pronounced increase with rising temperature. It is evident from figures 1 and 2 that in this case the correction factors for the reaction and cavity fields, k_R and k_c, are insensitive to the changes in dielectric constant accompanying changes in temperature. As G_e is independent of temperature, the variation in $G_{On.}$ arises almost entirely from the assumption that the cavity volume expands with the thermal expansion of the liquids. The values of $G_{On.}$ are relatively independent of temperature for $CHCl_3$ and decrease with increasing temperature for $(C_2H_5)_2O$. As these substances have unusually low values of dielectric constant and require exceptionally high values of eccentricity, k_R and k_c now vary significantly with temperature.

Nitrobenzene fits the Onsager relation more closely than most substances, although there is a definite decrease in $G_{On.}$ with increasing temperature. The modified relation leads to a greater dependence of G on the temperature. On the presumption that this variation is attributable to association, the shape was chosen to fit the data at the highest temperature. The value of eccentricity required on this basis is in reasonable accord with that anticipated in comparison with chlorobenzene and other benzene derivatives of similar shape.

Of the eight ketones listed only acetone, methyl ethyl ketone, and methly *n*-propyl ketone conform reasonably well to eq (1). Diethyl ketone and higher members of the series show a definite downward trend in G_e with increasing temperature. This trend can hardly be attributed to association in view of the normal behavior of the lower members for which such association should be most pronounced. However, all of the ketones except acetone have flexible alkyl groups and it is not unreasonable to suppose that the effective shapes, especially of the higher members, may vary with the temperature. The observed trend in G_e then suggests a change to a less oblate or more prolate shape as the temperature increases. Although similar complications might conceivably arise because of sufficient molecular flexibility in several other cases, namely, ethyl ether and the *n*-butyl halides, only the higher ketones appear to exhibit any abnormal behavior.

Table 2 contains a number of additional liquids for which reliable data were not available over a sufficient temperature range to be included in table 1. The values of eccentricity required to fit eq (2) in the vicinity of room temperature are listed in the final column.

It is of interest to see how the shapes derived from the dielectric analyses correspond to estimates of the molecular shapes for those compounds where the dipole moment is directed along an axis of symmetry. In table 3 values of the axial ratio b/a corresponding to the listed eccentricities are compared with those obtained by scaling models constructed from the Fisher-Hirshfelder-Taylor atomic models. The dimension a refers to the dipole axis while b was taken as the largest dimension perpendicular to this axis. Some molecules containing flexible ethyl groups are included. For these cases, the values of b were obtained from the most extended configuration and, consequently, these axial ratios represent upper limits. In no case do the two procedures lead to a definite conflict in the assignment of oblate and prolate character. However, the molecular geometry of *t*-butyl chloride is virtually spherical, whereas eq (2) requires a decidely oblate shape. A similar discrepancy, but in the reverse sense, is noted for methylene bromide. On the other hand, the high eccentricities needed for ethyl ether and triethylamine are close to those estimated for the most extended configurations. In the prolate cases the agreement is consistently good, except for iodobenzene.

TABLE 2. *Summary of the analysis of the dielectric data for pure liquids for which data over an extended temperature interval are not available* [a]

Substance	μ_0 [b]	P_D	T	ϵ	P_D/V	G_{Oo}	ϕ
PROLATE							
CH_3CN	3.97	11.1	293	37.5	0.212	0.80	0.67
n-C_3H_7CN	4.07	20.4	293	20.3	.234	.69	.90
n-C_4H_9CN	4.12	25.0	293	17.4	.239	.58	.91$_5$
$C_2H_5NO_2$	3.62	17.0	303	28.1	.235	.96	.30
n-$C_3H_7NO_2$	3.66	21.4	303	23.2	.239	.95	.30
n-C_3H_7I	2.04	28.9	293	7.00	.297	.68	.80
n-C_3H_7Br	(2.10)	26.6	298	8.09	.259	.84	.60
n-$C_4H_{11}Br$	(2.10)	33.1	298	6.31	.265	.82	.65
n-$C_5H_{11}Br$	(2.10)	37.7	298	5.82	.266	.83	.65
n-$C_7H_{15}Br$	(2.10)	42.1	298	5.33	.267	.81	.67
n-$C_8H_{17}Br$	(2.10)	46.7	298	5.00	.268	.81	.68
n-$C_9H_{19}Br$	(2.10)	51.5	298	4.74	.270	.81	.68
n-$C_{10}H_{21}Br$	(2.10)	56.4	298	4.44	.271	.79	.71
n-$C_{12}H_{25}Br$	(2.10)	66.1	298	4.07	.272	.78	.72
n-$C_{14}H_{29}Br$	(2.10)	74.6	298	3.84	.272	.78	.72
C_6H_5F	1.59	26.0	293	5.47	.277	.83	.64
C_6H_5I	1.70	39.3	293	4.63	.353	.45	.95
CH_2Br_2	1.43	21.9	283	7.77	.320	.99	0
OBLATE							
CH_2CHCl_2	2.06	21.2	291	10.0	0.252	1.03	0.30
CH_3CCl_3	1.79	26.2	293	7.52	.263	1.12	.50
$(CH_3)_2CCl_2$	2.27	25.8	293	10.2	.248	1.09	.45
$CH_3COC_6H_5$	3.02	34.5	298	17.4	.294	1.12	.45
$(n$-$C_3H_7)_2O$	1.21	31.7	299	3.39	.230	1.16	.05
$(n$-$C_4H_9)_2O$	1.17	40.8	298	3.06	.239	1.15	.02
$(C_2H_5)_2S$	1.54	28.5	298	5.72	.263	1.17	.58
$(C_2H_5)_3N$	0.66	33.8	298	2.42	.242	1.31	.80

[a] Sources of data: A. A. Maryott and E. R. Smith, Table of dielectric constants of pure liquids, NBS Circular 514 (1951); A. A. Maryott and Floyd Buckley, Table of dielectric constants and electric dipole moments of substances in the gaseous state, NBS Circular 537 (1953).
[b] All values of dipole moment given in Debye units (1 Debye = 10^{-18} esu).

TABLE 3.—*Comparison of axial ratios determined from dielectric data and from molecular geometry*

Substance	b/a (dielectric)	b/a (geometry)	Substance	b/a (dielectric)	b/a (geometry)
PROLATE			**OBLATE**		
CH_3Cl	0.9	0.8	CH_2Cl_2	1.3	1.4
CH_3Br	.7	.7	CH_2Br_2	1.0	1.7
CH_3I	.5	.7	$CHCl_3$	1.7	1.4
CH_3CN	.7	.7	CH_3CCl_3	1.2	1.0
$C_6H_5NO_2$	.6	.8	$(CH_3)_2CCl_2$	1.1	1.2
C_6H_5Cl	.7	.8	$(CH_3)_3CCl$	1.4	1.0
C_6H_5Br	.6	.8	$(CH_3)_2O$	1.2	1.7
C_6H_5I	.3	.7	$(C_2H_5)_2O$	2.2	2.0
C_6H_5CN	.7	.7	$(CH_3)_2CO$	1.2	1.3
			$(C_2H_5)_2CO$	1.4	1.8
			$(C_2H_5)_2S$	1.2	1.8
			$(C_2H_5)_3N$	1.7	1.8
			CH_3NO_2	1.0	0.9

Variations in the values of eccentricity obtained from the dielectric analysis are usually in the direction anticipated for members of homologous series and other related compounds. For example, the prolate eccentricity increases with increasing size of the halogen atom, F<Cl<Br<I, for the alkyl and aryl halides. The prolate eccentricity also increases with increasing chain length in homologous series of alkyl halides and nitriles, excepting certain first members of the series.

4. Analyses of Data on Solutions and Mixtures

On the assumption that the Onsager-Kirkwood polarizations conform to the additive mixture law, eq (1) becomes for a two component mixture

$$P_{12}=\frac{(\epsilon_{12}-1)(2\epsilon_{12}+1)}{9\epsilon_{12}}V_{12}=f_1P_1+f_2P_2=\frac{4\pi N}{3}f_1\left[\frac{\alpha_1}{1-\frac{\alpha_1}{v_1}g_{12}}+\frac{\mu_1^2}{3kT\left(1-\frac{\alpha_1}{v_1}g_{12}\right)^2}\right]$$
$$+\frac{4\pi N}{3}f_2\left[\frac{\alpha_2}{1-\frac{\alpha_2}{v_2}g_{12}}+\frac{\mu_2^2}{3kT\left(1-\frac{\alpha_2}{v_2}g_{12}\right)^2}\right], \quad (3)$$

where f is the mole fraction, and P_1 and P_2 are the polarizations of the components in the mixture. The subscripts 1, 2, and 12 refer to the two components and the mixture, respectively. For dilute solutions of a polar solute in a nonpolar solvent, it is convenient to expand eq (3) in the Hedestrand [14] manner. The polarization of the solute at infinite dilution P_2^∞ is then given by

$$P_2^\infty=P_1\frac{M_2}{M_1}+P_1\left[\frac{2\epsilon_1^2+1}{\epsilon_1(2\epsilon_1+1)(\epsilon_1-1)}-\frac{8\pi\frac{\alpha_1}{v_1}}{\left(1-\frac{\alpha_1}{v_1}g_1\right)(2\epsilon_1+1)^2}\right]\left(\frac{\Delta\epsilon_{12}}{\Delta f_2}\right)_{f_2=0}-\frac{P_1}{d_1}\left(\frac{\Delta d_{12}}{\Delta f_1}\right)_{f_2=0}, \quad (4)$$

where M is the molecular weight, d the density, and

$$P_1=\frac{(\epsilon_1-1)(2\epsilon_1+1)}{9\epsilon_1}\frac{M_1}{d_1}.$$

If the Clausius-Mossotti relation is accepted for the pure nonpolar solvent so that

$$\alpha_1/v_1=\frac{3(\epsilon_1-1)}{4\pi(\epsilon_1+2)},$$

the second term in brackets simplifies to

$$\frac{8\pi\frac{\alpha_1}{v_1}}{\left(1-\frac{\alpha_1}{v_1}g_1\right)(2\epsilon_1+1)^2}=\frac{6P_1d_1}{M_1(2\epsilon_1+1)^2}.$$

For spheroidal molecular shapes,

$$P_2^\infty=\frac{4\pi N}{3}\frac{\alpha_2}{1-\frac{\alpha_2}{v_2}g_1k_R}+\frac{\mu_0^2k_c}{3kT\left(1-\frac{\alpha_2}{v_2}g_1k_R\right)^2} \quad (5)$$

where the coefficients k_R and k_c are functions of the eccentricity of the solute and the dielectric constant of the solvent.

Data on six polar solutes in a number of nonpolar solvents having dielectric constants in the range 1.9 to 2.8 are given in table 4. As in the case of the pure liquids, values of G_{On} fall below unity for C_2H_5Br, C_6H_5Br, CH_3CN, and C_6H_5CN, and above unity for $(CH_3)_3CCl$ and $CHCl_3$, indicating that these differences may be again correlated with molecular shape. When the data are interpreted in terms of the modified Onsager expression (eq 5), using values of k_R and k_c corresponding to the eccentricities derived from the pure liquids, the deviation factors G_c are usually much closer to unity. The correction for shape usually leads to a value of the dipole moment within several percent of the measured gas value. Exceptions are CH_3CN and $CHCl_3$, where the corrections are decidedly too small.

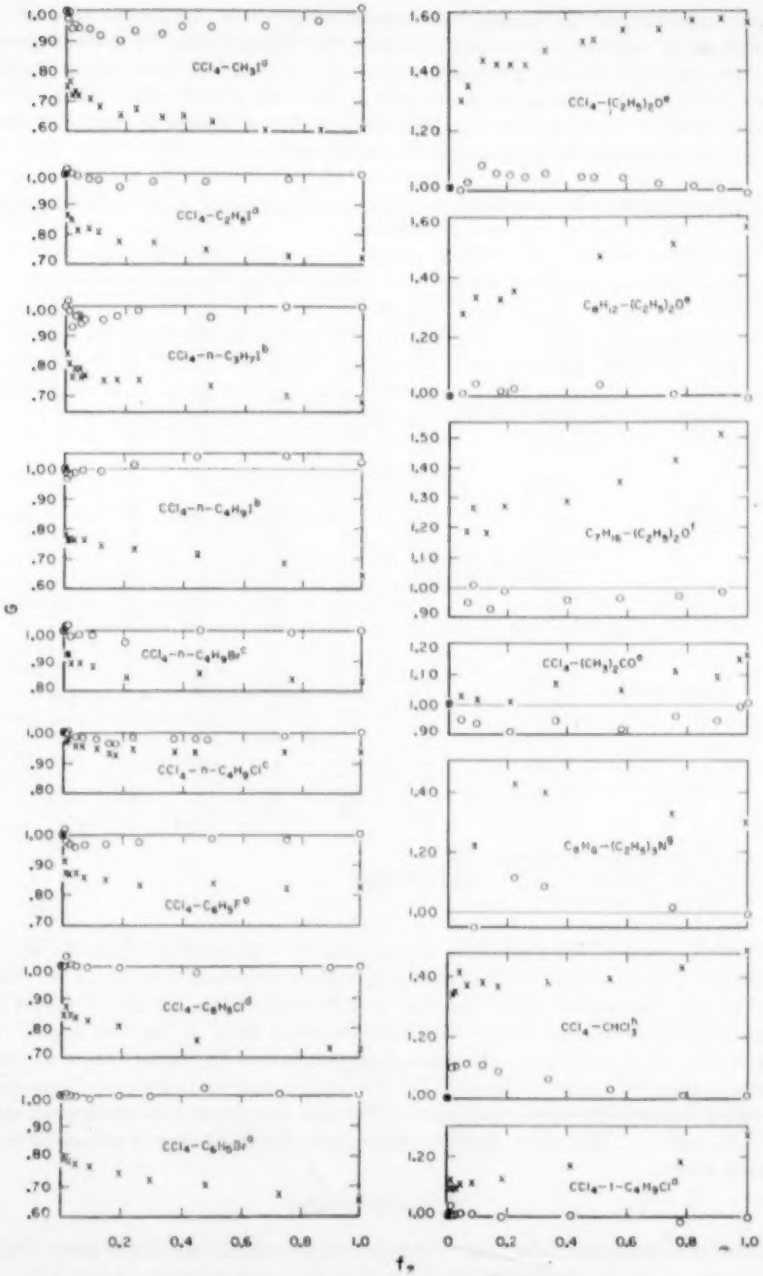

FIGURE 3. *G-factor versus mole-fraction plots of mixture at 20° C.*

×, $G_{observed}$. ○, G_2; f_2, mole fraction of polar constituent.

a, A. Audsley and F. R. Goss, J. Chem. Soc. **1941**, 864;. b, A. Audsley and F. R. Goss, J. Chem. Soc. **1942**, 358; c, A. Audsley and F. R. Goss, J. Chem. Soc. **1942**, 497; d, F. R. Goss, J. Chem. Soc. **1937**, 1918; e, D. P. Earp and S. Glasstone, J. Chem. Soc. **1935**, 1709; f, G. Briegleb, Z. physik.Chem. **B16**, 249 (1932); g, D. D. Hammick, A. Norris, and L. E. Sutton, J. Chem. Soc. **1938**, 1755; h, F. R. Goss, J. Chem. Soc. **1940**, 755

From a comparison of the deviation factors obtained from the Debye relation and listed in the last column of table 4, it is evident that both the Onsager relation and the present modification lead to a marked improvement with regard to the apparent variation in dipole moment from solvent to solvent. This is most evident in the four prolate cases for which values of G_{Debye} decrease from 20 to 35 percent in going from media of lowest to highest dielectric constant, whereas there is little or no trend in the values of G_e.

TABLE 4. *Hedestrand coefficients and G factors for dilute solutions of several polar solutes in various nonpolar solvents*

Solute	Solvent	$\epsilon_{solvent}$	$d\epsilon/df_2$	dd/df_2	$G_{On.}$	G_e	G_{Debye}
C_2H_5Br [a] (20° C)	n-C_6H_{14}	1.90	3.18	0.445	0.95	1.00	0.97
	C_6H_{12}	2.02	3.85	.453	.93	.98	.92
	CCl_4	2.24	4.62	−.088	.95	1.02	.94
	C_6H_6	2.28	5.03	.488	.94	1.01	.90
	CS_2	2.64	6.68	.225	.90	.97	.76
C_2H_5Br [a] (20° C)	n-C_6H_{14}	1.90	2.51	.692	.83	1.00	.90
	C_6H_{12}	2.02	2.90	.67	.81	.99	.90
	CCl_4	2.24	3.26	−.068	.80	1.00	.85
	C_6H_6	2.28	3.51	.722	.79	1.00	.81
	CS_2	2.64	4.34	.372	.68	.93	.67
CH_3CN [b] (25° C)	n-C_6H_{14}	1.88	8.75	.0112	.72	.77	.71
	Dioxane	2.20	17.5	−.1428	.88	.95	.80
	CCl_4	2.23	14.5	−.4308	.81	.89	.75
	C_6H_6	2.27	16.5	−.0406	.79	.87	.77
	CS_2	2.63	23.9	−.4711	.77	.86	.65
	Tetralin	2.75	10.3	−.0640	.75	.84	.60
C_6H_5CN [c] (20° C)	n-C_6H_{14}	1.90	14.16	.330	.82	.94	.88
	C_6H_{12}	2.02	17.25	.188	.80	.93	.79
	CCl_4	2.24	21.19	−.003	.83	.98	.86
	C_6H_6	2.28	22.97	.135	.82	.96	.82
	CS_2	2.64	33.51	−.483	.75	.91	.71
$(CH_3)_3CCl$ [b] (25° C)	n-C_6H_{14}	1.88	3.70	.143	1.04	.95	1.04
	n-C_7H_{16}	1.91	3.33	.110	1.02	.94	1.04
	Dioxane	2.20	6.51	−.227	1.15	1.03	1.08
	CCl_4	2.23	5.64	−.837	1.12	1.01	1.05
	C_6H_6	2.27	5.93	−.038	1.08	.97	1.01
	CS_2	2.63	8.29	−.792	1.03	.90	.90
	Tetralin	2.75	3.65	−.084	1.04	.90	.87
$CHCl_3$ [d] (20° C)	n-C_6H_{14}	1.90	1.30	.507	1.40	1.21	1.26
	C_6H_{12}	2.20	1.35	.397	1.41	1.18	1.40
	CCl_4	2.24	1.64	−.101	1.41	1.15	1.41
	C_6H_6	2.28	1.90	.849	1.47	1.21	1.43
	CS_2	2.64	2.18	.236	1.35	1.07	1.24

[a] E. G. Cowley and J. R. Partington, J. Chem. Soc. **1937,** 130.
[b] J. W. Smith and L. B. Whitten, Trans. Faraday Soc. **47,** 1304 (1951).
[c] E. G. Cowley and J. R. Partington, J. Chem. Soc. **1936,** 1184.
[d] T. G. Scholte, Rec. trav. chim. **70,** 50 (1951).

Values of $G_{On.}$ and G_e for the polar constituent in a number of mixtures with CCl_4 and other nonpolar solvents are plotted as a function of concentration in figure 3. Slight differences between the values of G shown for the pure liquid and those listed in tables 2 and 3 are due to slightly different values of the dielectric constant used in the two cases. In general, the values of $G_{On.}$ show a definite dependence on concentration, being closer to unity for the dilute solutions than for the pure liquid. On the other hand, the values of G_e are substantially independent of concentration in most cases. For the 10 systems containing an alkyl or aryl halide in CCl_4, only for CH_3I does G_e differs from unity by more than 4 percent over the entire concentration range.

5. Conclusion

The preceding analyses show that a decided improvement in the original Onsager treatment is obtained when the molecular cavity is altered to accommodate nonspherical molecular shapes, provided the volume of the cavity is kept independent of temperature. The behavior of pure polar liquids over an extended range of temperature and of dilute solutions and mixtures with a nonpolar solvent is, for the most part, satisfactorily correlated with a single set of molecular quantities involving size, shape, polarizability, and dipole moment. At the present time, however, limited knowledge concerning the appropriate values of polarizability,

size, and shape would appear to preclude the determination of dipole moments from data on liquids and mixtures with an accuracy comparable with direct measurements on the vapor. In view of the rather arbitrary assignment of cavity volume, inadequate allowance of atomic polarizability, neglect of optical anisotropy, and other factors that could lead to an overly complicated molecular model, the exact values derived for the eccentricities are not of particular significance and should be regarded only as useful molecular parameters.

Liquids subject to the influence of hydrogen bonding have not been considered. They usually depart drastically from Onsager's theory and obviously require more specialized treatment as provided by the theory of Kirkwood. This need is also supported by a variety of independent evidence. On the other hand, much of the evidence supporting the concept of close-range structure or association in the systems under consideration results from a rather restricted interpretation of the dielectric behavior. Usually inherent is the assumption that, in the absence of association, the dipole moment enhanced by its reaction field would be the same as obtained from Onsager's model. With the modifications proposed here, it does not appear necessary, in general, to take into account specific molecular interactions and the approximation of a continuum for the molecular environment appears adequate.

6. References

[1] L. Onsager, J. Am. Chem. Soc. **58,** 1486 (1936).
[2] J. N. Wilson, Chem. Rev. **25,** 377 (1939).
[3] J. A. Abbott and H. C. Bolton, Trans. Faraday Soc. **48,** 422 (1952).
[4] I. G. Ross and R. A. Sack, Proc. Phys. Soc. (London) [B] **63,** 893 (1950).
[5] A. D. Buckingham, Australian J. Chem. **6,** 93 (1953).
[6] T. G. Scholte, Physica **15,** 437 and 450 (1949); Rec. trav. chim. **70,** 50 (1951).
[7] J. G. Kirkwood, J. Chem. Phys. **7,** 911 (1939).
[8] H. Frohlich, Theory of dielectrics (Oxford University Press, London, 1949).
[9] W. F. Brown, Jr., J. Chem. Phys. **21,** 1327 (1953).
[10] F. E. Harris and B. J. Alder, J. Chem. Phys. **21,** 1031 (1953).
[11] G. Oster, J. Am. Chem. Soc. **68,** 2036 (1946).
[12] C. J. F. Böttcher, Theory of electric polarization, ch. VII. (Elsevier Publishing Co., New York, N. Y., 1952).
[13] R. M. Fuoss, J. Am. Chem. Soc. **56,** 1031 (1934).
[14] G. Hedestrand, Z. physik. Chem. **B2,** 428 (1929).

7. Appendix

It is required to find the reaction field, $\vec{R}_\mu$, of a point polarizable dipole located at the center of a cavity. The cavity is imbedded in an infinite homogeneous and continuous medium having a macroscopic dielectric constant of ϵ_0.

The potential inside the cavity can be written

$$\varphi_i^{(\mu)} = \varphi_i^{(0)} + \varphi_i^{(R)}, \tag{1}$$

where $\varphi_i^{(0)}$ reduces to the potential of a dipole for points in the neighborhood of the origin and $\varphi^{(R)}$ remains finite at all points within the cavity. Then

$$\vec{R}_\mu = -\nabla\varphi_i^{(R)}. \tag{2}$$

For the cases that follow it is convenient to consider the corresponding problem for a charge, Q, situated at a point on the axis of symmetry and then to calculate $\varphi_i^{(\mu)}$ and $\vec{R}_\mu$ by the relations

$$\varphi_i^{\mu} = \lim_{Q\delta x \to \mu} \delta x \frac{\partial \varphi_i^{(0)}}{\partial x}, \tag{3}$$

$$\vec{R}_\mu = -\nabla\varphi_i^{(R)}. \tag{4}$$

7.1. Sphere

If a charge Q is located at the point $(x_0,0,0)$ then the potentials inside and outside the sphere are

$$\varphi_i = Q\sum_{n=0}^{\infty}\frac{x_0^n}{r^{n+1}}P_n(\cos\theta)+\sum_{n=0}^{\infty}B_n r^n P_n(\cos\theta) \tag{5}$$

$$\varphi_0 = \frac{Q}{\epsilon_0}\sum_{n=0}^{\infty}C_n\frac{x_0^n}{r^{n+1}}P_n(\cos\theta), \tag{6}$$

where (r,θ,φ) are the spherical polar coordinates of a point P, and the P_n's are the Legendre polynomials.

The usual boundary conditions over the surface of the sphere of radius r suffice to determine the coefficients B_n and C_n. Only the B_n are of interest. Calculation gives

$$B_n = -Q(\epsilon_i-1)\frac{x_0^n}{r^{2n+1}}(n+1)\frac{1}{[\epsilon_0(n+1)+n]}, \tag{7}$$

so that

$$\varphi_i^{(R)} = \lim_{Q\delta x_0\to\mu}\delta x_0\left(\frac{\partial\varphi_i}{\partial x_0}\right) = \frac{-\mu}{r^3}\frac{2(\epsilon_0-1)}{(2\epsilon_0+1)}x \tag{8}$$

$$\vec{R}_\mu^{(x)} = -\nabla\varphi_i^{(R)} = \frac{\vec{\mu}}{r^3}\frac{2(\epsilon_0-1)}{(2\epsilon_0+1)} = \vec{\mu}g_i. \tag{9}$$

7.2 Prolate Spheroid

It is convenient to use prolate spheroidal coordinates (ξ,η,φ) for which

$$\left.\begin{aligned} x &= c\xi\eta \\ y &= c\sqrt{(\xi^2-1)(1-\eta^2)}\cos\varphi \qquad -1\leqq\eta\leqq 1 \\ z &= c\sqrt{(\xi^2-1)(1-\eta^2)}\sin\varphi \qquad 0\leqq\varphi\leqq 2\pi \end{aligned}\right\} \tag{10}$$

If D is the distance between a point P' on the axis of symmetry (between the foci) and the point P, Hobson's expansion for D^{-1} reduces to

$$\frac{1}{D} = \frac{1}{c}\sum_{n=0}^{\infty}(2n+1)P_n(\eta)Q_n(\xi)P_n(\eta'), \tag{11}$$

in which P_n, Q_n are the Legendre functions of the first and second kind.

The required potentials can be written in the form

$$\varphi_i = \frac{Q}{c}\sum_{k=0}^{\infty}(2k+1)P_k(\eta)Q_k(\xi)P_k(\eta')+\sum_{k=0}^{\infty}\alpha_k P_k(\eta)P_k(\xi), \tag{12}$$

$$\varphi_0 = \frac{1}{\epsilon_0}\sum_{k=0}^{\infty}\beta_k P_k(\eta)Q_k(\xi). \tag{13}$$

The boundary conditions on the spheroid

$$\left.\begin{aligned} \varphi_i &= \varphi_0 \qquad \xi=\xi_0 \\ \epsilon_i\frac{d\varphi_i}{d\xi} &= \epsilon_0\frac{d\varphi_0}{d\xi} \qquad \xi=\xi_0 \end{aligned}\right\}, \tag{14}$$

give

$$\alpha_k = \frac{Q}{c}(\epsilon_0-1)(2k+1)\frac{Q_k(\xi_0)Q_k'(\xi_0)P_k(\eta')}{Q_k(\xi_0)P_k'(\xi_0)-\epsilon_0 Q_k'(\xi_0)P_k(\xi_0)}, \tag{15}$$

in which the prime on the function denotes differentiation.

The first term in the potential of the reaction field of a dipole at the origin reduces to

$$\varphi_R^{(1)}=\frac{3\mu}{c^2}(\epsilon_0-1)\frac{Q_1(\xi_0)Q_1'(\xi_0)P_1(\xi)P_1(\eta)}{Q_1(\xi_0)P_1'(\xi_0)-\epsilon_0 Q_1'(\xi_0)P_1(\xi_0)} \tag{16}$$

and to the same approximation the reaction field of the dipole is

$$\vec{R}_\mu^{(1)}=\frac{3\vec{\mu}}{c^3}\frac{(\epsilon_0-1)}{\epsilon_0}\frac{\left[-1+\frac{1}{2e}\log\frac{1+e}{1-e}\right]\left[\frac{-e}{1-e^2}+\frac{1}{2}\log\frac{1+e}{1-e}\right]}{\left[\frac{-e^2}{1-e^2}+\frac{\epsilon_0-1}{\epsilon_0}\left(-1+\frac{1}{2e}\log\frac{1+e}{1-e}\right)\right]}=\mu g_{\|}, \tag{17}$$

where the eccentricity $e=\xi_0^{-1}=\sqrt{1-(b/a)^2}$ and b/a is the axial radio of the spheroid.

The reaction field coefficient previously defined becomes

$$k_R=\frac{R_\mu^{(1)}}{R_\mu^{(\varphi)}}=\frac{3}{2}\frac{r^3}{c^3}\frac{2\epsilon_0+1}{\epsilon_0}f(e). \tag{18}$$

The indefinite factor r^3/c^3 can be eliminated through the natural assumption that the volumes of the Onsager sphere and the spheroid are equal. This condition gives

$$\frac{r^3}{c^3}=\frac{1-e^2}{e^3}, \tag{19}$$

so that finally

$$k_R=\frac{3}{2}\frac{2\epsilon_0+1}{\epsilon_0}\frac{1-e^2}{e^3}f(e). \tag{20}$$

A family of curves representing k_R is shown in figure 1.

The modified Onsager equation can be written

$$\epsilon-1=4\pi\frac{N}{V}\frac{\left(\vec{m}\cdot\vec{E}_0\right)_{\text{ave}}}{E_0^2}=4\pi\frac{N}{VE_0^2}\frac{\int e^{-\mathcal{E}/kT}\left(\vec{m}\cdot\vec{E}_0\right)d\omega}{\int e^{-\mathcal{E}/kT}d\omega} \tag{21}$$

in which $\vec{E}_0$, $\vec{m}$, N, V are the applied field, molecular moment, Avagadro's number, and molar volume, respectively. An extension of Onsager's treatment of the sphere gives, to a high approximation

$$\mathcal{E}=-\left(\vec{\mu}\cdot\vec{E}_{\text{local}}\right) \tag{22}$$

$$\vec{E}_{\text{local}}=\vec{\mu}\frac{g_{\|}}{1-\alpha_{\|}g_{\|}}+\frac{\vec{E}_{c\|}}{1-\alpha_{\|}g_{\|}}+\frac{\vec{E}_{c\perp}}{1-\alpha_\perp g_\perp} \tag{23}$$

in which $\vec{E}_c$ is the cavity field, α is the polarizability, and $g=R/\mu$. The subscripts $\|$ and $\perp$ denote the directions parallel and perpendicular to the dipole axis. Hence, to a good approximation

$$\left(\frac{\vec{m}\cdot\vec{E}}{E_0^2}\right)_{\text{ave}}=L\left\{\frac{1}{1-\alpha_{\|}g_{\|}}\left[\frac{1}{3}\alpha_{\|}+\frac{2}{3}\frac{M}{L}\alpha_\perp\left(\frac{1-\alpha_{\|}g_{\|}}{1-\alpha_\perp g_\perp}\right)\right]+\frac{\mu^2}{3kT}\frac{1}{(1-\alpha_{\|}g_{\|})^2}\right\}, \tag{24}$$

in which

$$L=\frac{1}{1-\frac{ac^2}{2\epsilon_0}(\epsilon_0-1)A_z} \qquad A_z=\int_0^\infty\frac{ds}{(s+b^2)(s+a^2)^{3/2}}$$

$$M=\frac{1}{1-\frac{ac^2}{2\epsilon_0}(\epsilon_0-1)A_y} \qquad A_y=\int_0^\infty\frac{ds}{(s+b^2)^2(s+a^2)^{1/2}}.$$

If the anisotropy of polarizability and shape are such that $\alpha_{\parallel}g_{\parallel}=\alpha_{\perp}g_{\perp}$ then

$$\epsilon-1=\frac{4\pi N}{3V}\left\{\frac{\left(\frac{1}{3}\alpha_{\parallel}+\frac{2}{3}\frac{M}{L}\alpha_{\perp}\right)}{(1-\alpha_{\parallel}g_{\parallel})}+\frac{\mu^2}{3kT}\frac{1}{(1-\alpha_{\parallel}g_{\parallel})^2}\right\}L \tag{25}$$

and if the polarizability is isotropic then

$$\epsilon-1=\frac{4\pi N}{V}\left\{\frac{\alpha}{1-\alpha g_{\parallel}}\left(\frac{1}{3}+\frac{2}{3}\frac{M}{L}\frac{1-\alpha g_{\parallel}}{1-\alpha g_{\perp}}\right)+\frac{\mu^2}{3kT}\frac{1}{(1-\alpha g_{\parallel})^2}\right\}L. \tag{26}$$

The determination of $g_{\perp}$ follows the method used to find $g_{\parallel}$. In the present case, the complete expansion of D^{-1} is required. Hobson's expansion, for P' on the minor axis (z), is

$$\frac{1}{D}=\frac{1}{c}\left\{\sum_{n=0}^{\infty}(2n+1)P_n(\eta)Q_n(\xi)P_n(0)P_n(\xi')\right.$$
$$\left.+2\sum_{n=1}^{\infty}\sum_{m=1}^{n}(2n+1)(-1)^m\left\{\frac{(n-m)!}{(n+m)!}\right\}^2P_n^m(\eta)Q_n^m(\xi)P_n^m(0)P_n^m(\xi')\cos m(\varphi-\pi/2)\right\}, \tag{27}$$

in which $P_n^m(x)$, $Q_n^m(x)$ are the Associated Legendre functions. The potentials are

$$\varphi_i^{(Q)}=Q\frac{1}{D}+\sum_{n=0}^{\infty}\alpha_nP_n(\eta)P_n(\xi)+\sum_{n=1}^{\infty}\sum_{m=1}^{n}\bar{\alpha}_{nm}P_n^m(\eta)P_n^m(\xi)\cos m(\varphi-\pi/2) \tag{28}$$

$$\varphi_0^{(Q)}=\frac{Q}{\epsilon_0}\sum_{n=0}^{\infty}\beta_nP_n(\eta)Q_n(\xi)+\sum_{n=1}^{\infty}\sum_{m=1}^{n}\bar{\beta}_{nm}P_n^m(\eta)Q_n^m(\xi)\cos m(\varphi-\pi/2). \tag{29}$$

The boundary conditions over the spheroid $\xi=\xi_0$ yield two sets of equations to determine (α_n, β_n) and $(\bar{\alpha}_{nm}, \bar{\beta}_{nm})$. Only $(\alpha_n, \bar{\alpha}_{nm})$ are of interest and algebraic solution gives

$$\alpha_n=\frac{Q}{c}2(2n+1)(\epsilon_0-1)\frac{Q_n(\xi_0)Q_n'(\xi_0)P_n(0)P_n(\xi')}{Q_n(\xi_0)P_n'(\xi_0)-\epsilon_0Q_n'(\xi_0)P_n(\xi_0)}. \tag{30}$$

$$\bar{\alpha}_{nm}=\frac{Q}{c}2(2n+1)(-1)^m\left\{\frac{(n-m)!}{(n+m)!}\right\}^2(\epsilon_0-1)\frac{Q_n^m(\xi_0)Q_n^{m\prime}(\xi_0)P_n^{m\prime}(0)P_n^m(\xi')}{Q_n^m(\xi_0)P_n^{m\prime}(\xi_0)-\epsilon_0Q_n^{m\prime}(\xi_0)P_n^m(\xi_0)}. \tag{31}$$

The only terms contributing to the potential of the reaction field for a dipole at the origin are those containing the $\bar{\alpha}_{nm}$. Hence the leading term is

$$\varphi_{R_{11}}^{(R)}=\frac{3}{2}\frac{\mu}{c^2}(\epsilon_0-1)\frac{Q_1^1(\xi_0)Q_1^{1\prime}(\xi_0)P_1^1(\eta)P_1^1(\xi)\sin\varphi}{\epsilon_0Q_1^{1\prime}(\xi_0)P_1^1(\xi_0)-Q_1^1(\xi_0)P_1^{1\prime}(\xi_0)}, \tag{32}$$

so that

$$\vec{R}_{\mu}^{(1)}=\frac{3}{2}\frac{\vec{\mu}}{c^3}(\epsilon_0-1)\frac{Q_1^1(\xi_0)\,Q_1^{1\prime}(\xi_0)}{Q_1^1(\xi_0)\,P_1^{1\prime}(\xi_0)-\epsilon_0Q_1^{1\prime}(\xi_0)\,P_1^1(\xi_0)}. \tag{33}$$

After algebraic reduction, the required factor becomes

$$\frac{g_{\perp}}{g_{\parallel}}=\frac{1}{2}\frac{\left[1+\frac{2}{x-1}\right]\left[\frac{(\epsilon_0-1)}{\epsilon_0}-\frac{1}{x}\right]}{\left[\frac{\epsilon_0-1}{\epsilon_0}+\frac{2}{x-1}\right]}>1 \tag{34}$$

$$x=\left(\frac{1-e^2}{e^2}\right)\left(-1+\frac{1}{2e}\log\frac{1+e}{1-e}\right).$$

The cavity field coefficient previously defined is

$$k_c = E_c^{(\text{ell})}/E_c^{(\text{s})} = \frac{2\epsilon+1}{3\epsilon} L = \beta k_R \tag{35}$$

$$\beta = \frac{9}{2}\left(\frac{1-e^2}{e^2}\right)^2\left[-1+\frac{1}{2e}\log\frac{1+e}{1-e}\right]\left[\frac{1}{(1-e^2)}-\frac{1}{2e}\log\frac{1+e}{1-e}\right]. \tag{36}$$

A family of curves representing k_c is given in figure 2.

Calculation shows that for practical ranges of ϵ the quantity $1-\alpha g_{\parallel}/1-\alpha g_{\perp}$ is only slightly dependent upon ϵ (and therefore upon the temperature) and except for high eccentricities and exceptional values of α/r^3 differs from unity by less than 10 percent. Moreover, the quantity $(\frac{1}{3}+\frac{2}{3}M/L)k_c$ differs insignificantly from unity except for very large eccentricities, so that

$$\alpha k_a k_c = \alpha\left\{\left(\frac{1}{3}+\frac{2}{3}\frac{M}{L}\left[1+\frac{1-\alpha g_{\parallel}}{1-\alpha g_{\perp}}\right]\right\}k_c \simeq \alpha \tag{37}$$

can be taken as virtually constant.

The final equation used in the numerical computations reduces to

$$\epsilon - 1 = \frac{4\pi}{3}\frac{N}{V}\left\{\frac{\alpha}{1-\alpha g^{\parallel}}+\frac{\mu^2}{3kT}\frac{k_c}{(1-\alpha g_{\parallel})^2}\right\}\frac{3\epsilon}{2\epsilon+1}. \tag{38}$$

7.3. Oblate Spheroid

The appropriate coordinates are the oblate spheroidal coordinates for which

$$\left.\begin{aligned} x &= c\xi\eta\sin\varphi && \xi \geqq 1 \\ y &= c\sqrt{(\xi^2-1)(1-\eta^2)} && -1 \leqq \eta \leqq 1 \\ z &= c\xi\eta\cos\varphi && 0 \leqq \varphi \leqq 2\pi \end{aligned}\right\}. \tag{39}$$

Hobson's expansion for D^{-1}, in which the point P' is on the y-axis, reduces to

$$\frac{1}{D} = \frac{1}{c}\sum_{n=0}^{\infty}(2n+1)P_n(\bar{x})Q_n(i\bar{y})P_n(i\bar{y}'), \tag{40}$$

in which $\bar{x}=\sqrt{1-\eta^2}$ and $\bar{y}=\sqrt{\xi^2-1}$.

The required potentials are

$$\varphi_i^{(Q)} = \frac{Q}{c}\sum_{k=0}^{\infty}(2k+1)P_k(\bar{x})Q_k(i\bar{y})P_k(i\bar{y}')+\sum_{k=0}^{\infty}\alpha_k P_k(i\bar{y})P_k(\bar{x}) \tag{41}$$

$$\varphi_0^{(Q)} = \frac{1}{\epsilon_0}\sum_{k=0}^{\infty}\beta_k Q_k(i\bar{y})P_k(\bar{x}). \tag{42}$$

The boundary conditions over the spheroid $\xi=\xi_0$ determine the (α_k,β_k). Only terms containing α_k contribute to the potential $\varphi_i^{(R)}$. Algebraic solution gives

$$\alpha_k = \frac{-Q}{c}(\epsilon_0-1)(2k+1)\frac{Q_k(i\bar{y}_0)Q_k'(i\bar{y}_0)P_k(i\bar{y}')}{\epsilon_0 P_k(i\bar{y}_0)Q_k'(i\bar{y}_0)-P_k'(i\bar{y}_0)Q_k(i\bar{y}_0)} \tag{43}$$

so that the first term in the potential of the reaction field of the dipole at the origin is

$$\varphi_R^{(1)} = -\frac{3\mu}{c^2}(\epsilon_0-1)Q_1(i\bar{y}_0)Q_1'(i\bar{y}_0)P_1(i\bar{y})P_1(\bar{x}). \tag{44}$$

The reaction field of the dipole to the same approximation is

$$\vec{R}_{\mu}^{(1)}=\frac{3\vec{\mu}}{e^3}\frac{(\epsilon_0-1)}{\epsilon_0}\frac{\left[-1+\frac{\sqrt{1-e^2}}{e}\tan^{-1}\frac{e}{\sqrt{1-e^2}}\right]\left[e\sqrt{1-e^2}-\tan^{-1}\frac{e}{\sqrt{1-e^2}}\right]}{\left[e^2+\frac{\epsilon_0-1}{\epsilon_0}\left(-1+\frac{\sqrt{1-e^2}}{e}\tan^{-1}\frac{e}{\sqrt{1-e^2}}\right)\right]} \tag{45}$$

in which $e=\xi_0^{-1}$.

The reaction field coefficient, on the assumption that the volume of the spheroid and equivalent Onsager sphere are equal, reduces to

$$k_R=\frac{3}{2}\frac{2\epsilon_0+1}{\epsilon_0}\frac{\sqrt{1-e^2}}{e^3}\frac{\left[-1+\frac{\sqrt{1-e^2}}{e}\tan^{-1}\frac{e}{\sqrt{1-e^2}}\right]\left[e\sqrt{1-e^2}-\tan^{-1}\frac{e}{\sqrt{1-e^2}}\right]}{\left[e^2+\frac{\epsilon_0-1}{\epsilon_0}\left(-1+\frac{\sqrt{1-e^2}}{e}\tan^{-1}\frac{e}{\sqrt{1-e^2}}\right)\right]}. \tag{46}$$

The calculation of the quantity $(\vec{m}\cdot\vec{E}_0)_{ave}$ parallels that carried out for the prolate case. In view of the results obtained for this model, it will be assumed that to a good approximation

$$\frac{(\vec{m}\cdot\vec{E}_0)_{ave}}{E_0^2}=\left\{\frac{\alpha}{(1-\alpha g_{\parallel})}\left(\frac{1}{3}+\frac{2}{3}\frac{L}{M}\right)+\frac{\mu^2}{3kT}\frac{1}{(1-\alpha g_{\parallel})^2}\right\}M \tag{47}$$

in which

$$\frac{1}{L}=1-\frac{a^2b}{2\epsilon_0}(\epsilon_0-1)A_x \qquad A_x=\int_0^{\infty}\frac{ds}{(s+a^2)^2(s+b^2)^{1/2}}$$

$$\frac{1}{M}=1-\frac{a^2b}{2\epsilon_0}(\epsilon_0-1)A_y \qquad A_y=\int_0^{\infty}\frac{ds}{(s+a^2)\,(s+b^2)^{3/2}}.$$

The cavity field coefficient is

$$k_c=\beta k_R=\frac{2\epsilon_0+1}{\epsilon_0}M, \tag{48}$$

where

$$\frac{1}{\beta}=\frac{9}{2}\frac{1}{e^4}\left[-1+\frac{\sqrt{1-e^2}}{e}\tan^{-1}\frac{e}{\sqrt{1-e^2}}\right]\left[(1-e^2)-\frac{\sqrt{1-e^2}}{e}\tan^{-1}\frac{e}{\sqrt{1-e^2}}\right]. \tag{49}$$

A family of curves representing k_c is given in figure 2.

The complete equation now becomes

$$\epsilon_0-1=4\pi\frac{N}{V}\left\{\frac{\alpha(\frac{1}{3}+\frac{2}{3}L/M)}{(1-\alpha g_{\parallel})}+\frac{\mu^2}{3kT}\frac{1}{(1-\alpha g_{\parallel})^2}\right\}k_c\frac{3\epsilon_0}{2\epsilon_0+1}. \tag{50}$$

Calculation shows that $k_c(\frac{1}{3}+\frac{2}{3}L/M)$ is essentially unity for practical ranges of ϵ_0 and e, so that the working equation simplifies to

$$(\epsilon_0-1=4\pi\frac{N}{V}\left\{\frac{\alpha}{(1-\alpha g_{\parallel})}+\frac{\mu^2}{3kT}\frac{k_c}{(1-\alpha g_{\parallel})^2}\right\}\frac{3\epsilon_0}{2\epsilon_0+1}. \tag{51}$$

In the case of the prolate spheroid, for which the calculations have been made, it should be noted that the inclusion of the correction factor $1-\alpha g_{\parallel}/1-\alpha g_{\perp}$ in the optical term of the polarization in part nullifies the effect of the correction for shape and increases this term to a value more nearly that of the Onsager approximation for a sphere. Calculations for a number of specific examples indicates that if this correction is made, the values of G_e listed in the tables will be reduced by about 1 percent or less.

WASHINGTON, February 19, 1954.

Journal of Research of the National Bureau of Standards Vol. 53, No. 4, October 1954 Research Paper 2540

Temperature Dependence of Compression of Linear High Polymers at High Pressures[1]

Charles E. Weir

Pressure-volume-temperature data for polyethylene, polytetrafluoroethylene, polymonochlorotrifluoroethylene, polyvinyl fluoride, polyvinylidene fluoride, polyvinyl alcohol, a copolymer of ethylene-tetrafluoroethylene (1:1), and a polyester are reported over the range 20° to 80° C and 1 to 10,000 atmospheres. Empirical equations of state for some of the polymers are derived. Internal-energy changes were calculated for most of the polymers studied.

1. Introduction

Previous studies of the effects of high pressures on polymeric materials have resulted in reports on pressure-volume-temperature data on rubber-sulfur vulcanizates [1][2] and on transitions found in Teflon [2]. The behavior of Teflon was of considerable interest, and it was decided to study the available, chemically related polymers to ascertain the extent of the uniqueness of Teflon. This report contains the data obtained for pressures as high as 10,000 atm at temperatures from 20° to 80° C. Pressure-volume-temperature data are given, and, in most instances, equations of state and thermodynamic data of interest are presented. The polymers studied were polyethylene, polyvinyl alcohol, polytetrafluoroethylene (Teflon), polymonochlorotrifluoroethylene (Kel-F), polyvinyl fluoride, polyvinylidene fluoride, a copolymer of ethylene and tetrafluoroethylene in a 1:1 ratio and a polyester. No irregularities in behavior were observed in any of these materials except Teflon.

2. Experimental Method

2.1. Compression Measurements

The procedures used for measuring isothermal compression and for temperature control have been described previously in detail [3, 1]. The only departure from previous procedures was necessitated by the fact that certain of the polymers studied were available only in the form of powders. Such powders were measured in a steel container that was open at one end. The powders were packed into the container and impregnated with the confining liquid before measurement. In the case of the powders no irregularities were observed either in the experimental behavior or in the resulting data.

2.2. Volume Measurements

Volumes were measured as described previously [1] by weighing specimens in air before compression and in the confining liquid immediately following compression. These measurements were made at 21° C only. Volumes at other temperatures were determined from expansion data. Powdered specimens were treated in a similar manner, except that corrections for the weight and volume of the container were required.

Expansion data were obtained on all samples to permit calculation of volumes at elevated temperatures from the measured volume at 21° C. For Teflon the data of Quinn, Roberts, and Work [4] were utilized, since they studied a specimen cut from the same sample. For all other polymers, volumes were studied, using mercury-filled dilatometers. Temperatures were allowed to reach equilibrium before each volume measurement was made. Powdered polymers were molded into disks for such studies. The fluoride polymers are not readily molded and measurements were made on disks that were probably only sintered. Initial efforts to use such powders in water-filled dilatometers were unsuccessful due to instability of the water level. In one instance, however, reproducible data obtained, using a water-filled dilatometer agreed well with data obtained from a compressed disk in the mercury-filled dilatometer.

3. Specimens

Test specimens of polytetrafluoroethylene (Teflon), polyethylene, polymonochlorotrifluoroethylene (Kel-F), and a polyester (Selectron 5003) have been described previously [5].

Polyvinyl alcohol was used in the form of a fine powder with a faint yellow color.

Polyvinyl fluoride, polyvinylidene fluoride, and the copolymer of ethylene and tetrafluoroethylene were made available through the courtesy of a commercial manufacturer of high polymers. These materials were all white powders.

4. Results

4.1. Experimental Data

The experimental results consist of the measured compressions and the corresponding PVT data derived therefrom. The experimental compressions are shown in table 1.

Compressions at 1 atm and 1,000 atm appear as negative values since 2,000 atm is used as a reference point. This feature along with the method used to obtain values at 1 atm has been discussed previously [1]. Total compression based on 1 atm

[1] This work was sponsored by the Office of Naval Research, Department of the Navy.

[2] Figures in brackets indicate the literature references at the end of this paper.

TABLE 1. *Compression of polymers*

$-\Delta V/V_0$

Pressure	Polyethylene at—					Polymonochlorotrifluoroethylene (Kel-F) at—					A polyester (Selectron 5003) at		
	21.0° C	37.8° C	50.4° C	63.9° C	81.0° C	21.0° C	38.1° C	50.4° C	63.2° C	82.0° C	21.0° C	38.4° C	50.5° C
atm													
1	−0.0500	−0.0520	−0.0540	−0.0560	−0.0620	−0.0400	−0.0410	−0.0420	−0.0420	−0.0430	−0.0400	−0.0410	−0.0430
1,000	−.0205	−.0233	−.0255	−.0278	−.0306	−.0190	−.0189	−.0201	−.0207	−.0219	−.0189	−.0189	−.0208
2,000	.0000	.0000	.0000	.0000	.0000	.0000	.0000	.0000	.0000	.0000	.0000	.0000	.0000
3,000	+.0179	+.0189	+.0196	+.0209	+.0229	+.0154	+.0161	+.0158	+.0171	+.0172	+.0164	+.0167	+.0163
4,000	.0327	.0343	.0357	.0381	.0402	.0284	.0287	.0289	.0314	.0313	.0307	.0314	.0311
5,000	.0448	.0475	.0486	.0528	.0547	.0391	.0402	.0401	.0430	.0431	.0431	.0443	.0434
6,000	.0560	.0588	.0610	.0651	.0671	.0486	.0498	.0504	.0536	.0535	.0538	.0554	.0549
7,000	.0659	.0687	.0714	.0767	.0775	.0570	.0583	.0593	.0624	.0619	.0633	.0651	.0649
8,000	.0744	.0778	.0806	.0835	.0879	.0646	.0664	.0671	.0704	.0703	.0718	.0738	.0738
9,000	.0824	.0858	.0883	.0946	.0964	.0712	.0731	.0741	.0785	.0778	.0795	.0820	.0821
10,000	.0894	.0929	.0964	.1027	.1049	.0774	.0790	.0802	.0854	.0848	.0864	.0892	.0894

Pressure	Polyvinyl alcohol at—					Polytetrafluoroethylene (Teflon) at—					
	21.0° C	38.7° C	50.2° C	63.5° C	79.0° C	9.2° C	21.3° C	38.5° C	50.5° C	4.0° C	80.5° C
1	−0.0300	−0.0300	−0.0310	−0.0310	−0.0320	−0.0400	−0.0500	−0.0500	−0.0450	−0.0460	−0.0480
1,000	−.0123	−.0129	−.0136	−.0134	−.0173	−.0181	−.0178	−.0144	−.0201	−.0192	−.0200
2,000	.0000	.0000	.0000	.0000	.0000	.0000	.0000	.0000	.0000	.0000	.0000
3,000	+.0103	+.0119	+.0113	+.0130	+.0136	+.0140	+.0137	+.0148	+.0214	+.0153	+.0162
4,000	.0205	.0230	.0230	.0261	.0257	.0255	.0251	.0272	.0339	.0328	.0307
5,000	.0294	.0316	.0306	.0361	.0372	.0357	.0364	.0413	.0905	.0641	.0440
6,000	.0381	.0399	.0389	.0450	.0472	*.0647*	.0671	.0689	.0762	.0769	.0754
7,000	.0458	.0467	.0477	.0533	.0573	*.0735*	.0759	.0787	.0854	.0865	.0856
8,000	.0502	.0540	.0551	.0606	.0668	*.0830*	.0833	.0864	.0934	.0949	.0945
9,000	.0575	.0586	.0611	.0682	.0688	*.0889*	.0896	.0932	.0993	.1017	.1018
10,000	.0634	.0654	.0674	.0753	.0784	*.0933*	.0950	.0998	.1038	.1079	.1079

Pressure	Polyvinyl fluoride at—				Polyvinylidene fluoride at—				Copolymer of ethylene-tetrafluoroethylene (1:1) at—			
	21.0° C	38.3° C	50.2° C	63.5° C	21.0° C	38.7° C	50.3° C	63.5° C	21.0° C	38.2° C	50.6° C	63.2° C
1	−0.0400	−0.0430	−0.0460	−0.0480	−0.0450	−0.0460	−0.0470	−0.0480	−0.0400	−0.0420	−0.0440	−0.0460
1,000	−.0190	−.0197	−.0198	−.0205	−.0205	−.0193	−.0183	−.0223	−.0215	−.0221	−.0235	−.0235
2,000	.0000	.0000	.0000	.0000	.0000	.0000	.0000	.0000	.0000	.0000	.0000	.0000
3,000	+.0148	+.0167	+.0140	+.0184	+.0163	+.0161	+.0144	+.0168	+.0169	+.0187	+.0164	+.0178
4,000	.0291	.0305	.0278	.0339	.0293	.0302	.0273	.0333	.0317	.0329	.0319	.0326
5,000	.0420	.0432	.0396	.0477	.0422	.0414	.0369	.0472	.0439	.0459	.0433	.0432
6,000	.0519	.0530	.0496	.0594	.0511	.0512	.0484	.0570	.0553	.0559	.0557	.0560
7,000	.0613	.0631	.0585	.0699	.0598	.0623	.0567	.0669	.0647	.0658	.....	.0650
8,000	.0709	.0723	.0672	.0771	.0694	.0705	.0642	.0754	.0737	.0782	.0730	.0726
9,000	.0790	.0792	.0747	.0870	.0780	.0765	.0717	.0844	.0820	.0826	.0810	.0820
10,000	.0860	.0859	.0837	.0954	.0840	.0821	.0793	.0914	.0895	.0893	.0886	.0902

may be obtained by changing the sign of the value given at 1 atm and adding the resulting figure to each value in the corresponding column.

The data for Kel–F at 21.0° C, which represent the average of two measurements, are corrected data that have been reported erroneously in an earlier report [5] through the use of an incorrectly calculated specific volume.

Italicized results shown for Teflon at 9.2° C represent adjusted experimental data. As noted previously [2], the transition at this temperature was very sluggish, and the values measured at higher pressures were most probably not the equilibrium values. The measured data at these pressures were therefore adjusted on the assumption that the discontinuity in volume at 9.2° C was the same as that measured at 21.3° C. Evidence for the validity of this process will be shown later.

From the isothermal compression values obtained and the volume-temperature data at 1 atm, specific volume-temperature-pressure tables were constructed. The experimental specific volumes were plotted isobarically on a large scale and smooth curves were drawn which, except for Teflon and polyethylene, consisted essentially of straight lines. The transitions encountered in Teflon necessitated the use of broken line isobars while the isobars for polyethylene exhibited considerable curvature at the higher temperatures. From the smooth curves drawn, smoothed data were read from the graphs at 10-deg-C intervals. These data are shown in table 2 and represent the basis for all subsequent calculations and for the following observations.

The expansivity of the polyethylene specimen used here agreed well with the value reported by Hunter and Oakes [6], although the specific volume differed slightly.

The 1-atm volume-temperature data for Kel-F are in fair agreement with the results of Price [7], except that the volume of the specimen studied here

TABLE 2. *Smoothed specific volume-pressure-temperature data for polymers*

Pressure	Polyethelene at—							Copolymer of ethylene-tetrafluoroethylene (1:1) at—					
	20° C	30° C	40° C	50° C	60° C	70° C	80° C	20° C	30° C	40° C	50° C	60° C	70° C
atm	*cm³/g*	*cm³/g*	*cm³/g*	*cm³/g*	*cm³/g*	*cm³/g*	*cm³/g*	*cm³/g*	*cm³/g*	*cm³/g/*	*cm³/g*	*cm³/g*	*cm³/g*
1	1. 0893	1. 0956	1. 0123	1. 1094	1. 1124	1. 1269	1. 1409	0. 6916	0. 6950	0. 6984	0. 7018	0. 7053	0. 7087
1,000	1. 0573	1. 0645	1. 0717	1. 0789	1. 0861	1. 0940	1. 1091	. 6787	. 6817	. 6844	. 6872	. 6900	. 6928
2,000	1. 0354	1. 0404	1. 0454	1. 0504	1. 0555	1. 0608	1. 0690	. 6640	. 6663	. 6687	. 6711	. 6734	. 6757
3,000	1. 0152	1. 0916	1. 0240	1. 0284	1. 0329	1. 0380	1. 0441	. 6524	. 6543	. 6563	. 6583	. 6603	. 6623
4,000	0. 9992	1. 0030	1. 0067	1. 0107	1. 0145	1. 0182	1. 0240	. 6422	. 6442	. 6461	. 6480	. 6500	. 6519
5,000	. 9864	0. 9897	0. 9929	0. 9962	0. 9995	1. 0029	1. 0075	. 6336	. 6358	. 6380	. 6401	. 6423	. 6445
6,000	. 9735	. 9765	. 9795	. 9825	. 9855	0. 9884	0. 9932	. 6259	. 6278	. 6298	. 6317	. 6337	. 6356
7,000	. 9638	. 9663	. 9688	. 9714	. 9739	. 9765	. 9810	. 6193	. 6216	. 6235	. 6257	. 6277	. 6299
8,000	. 9540	. 9561	. 9585	. 9608	. 9630	. 9655	. 9694	. 6131	. 6153	. 6176	. 6198	. 6220	. 6242
9,000	. 9455	. 9475	. 9494	. 9514	. 9533	. 9554	. 9593	. 6073	. 6094	. 6114	. 6135	. 6156	. 6177
10,000	. 9376	. 9396	. 9414	. 9430	. 9449	. 9468	. 9498	. 6021	. 6041	. 6060	. 6080	. 6099	. 6119

Pressure	Polymonochlorotrifluoroethylene (Kel-F) at—							Polyvinylidene fluoride at—					
	20° C	30° C	40° C	50° C	60° C	70° C	80° C	20° C	30° C	40° C	50° C	60° C	70° C
	cm³/g	*cm³/g*	*cm³/g*	*cm³/g*	*cm³/g*	*cm³/g*	*cm³/g*	*cm³/g*	*cm³/g*	*cm³/g*	*cm³/g*	*cm³/g*	*cm³/g*
1	0. 4662	0. 4675	0. 4689	0. 4702	0. 4717	0. 4731	0. 4745	0. 6439	0. 6468	0. 6497	0. 6525	0. 6554	0. 6582
1,000	. 4575	. 4581	. 4598	. 4609	. 4621	. 4633	. 4644	. 6280	. 6304	. 6326	. 6349	. 6372	. 6395
2,000	. 4478	. 4490	. 4500	. 4510	. 4520	. 4530	. 4541	. 6149	. 6172	. 6194	. 6207	. 6240	. 6262
3,000	. 4408	. 4415	. 4424	. 4431	. 4349	. 4448	. 4556	. 6044	. 6062	. 6080	. 6112	. 6135	. 6158
4,000	. 4345	. 4352	. 4360	. 4368	. 4375	. 4383	. 4392	. 5961	. 5982	. 6002	. 6023	. 6044	. 6065
5,000	. 4296	. 4301	. 4307	. 4312	. 4318	. 4324	. 4329	. 5878	. 5896	. 5916	. 5935	. 5954	. 5973
6,000	. 4250	. 4255	. 4260	. 4265	. 4271	. 4276	. 4282	. 5817	. 5838	. 5856	. 5877	. 5897	. 5917
7,000	. 4214	. 4216	. 4220	. 4224	. 4226	. 4230	. 4234	. 5763	. 5782	. 5800	. 5818	. 5836	. 5853
8,000	. 4175	. 4179	. 4182	. 4186	. 4190	. 4194	. 4197	. 5703	. 5719	. 5735	. 5752	. 5768	. 5785
9,000	. 4146	. 4150	. 4152	. 4155	. 4158	. 4162	. 4165	. 5648	. 5663	. 5681	. 5698	. 5716	. 5731
10,000	. 4120	. 4121	. 4123	. 4124	. 4126	. 4128	. 4130	. 5609	. 5623	. 5638	. 5654	. 5669	. 5683

Pressure	Polyvinyl alcohol at—							Polyvinyl fluoride at—					
	20° C	30° C	40° C	50° C	60° C	70° C	80° C	20° C	30° C	40° C	50° C	60° C	70° C
	cm³/g	*cm³/g*	*cm³/g*	*cm³/g*	*cm³/g*	*cm³/g*	*cm³/g*	*cm³/g*	*cm³/g*	*cm³/g*	*cm³/g*	*cm³/g*	*cm³/g*
1	0. 7720	0. 7744	0. 7767	0. 7790	0. 7814	0. 7836	0. 7861	0. 7956	0. 7992	0. 8028	0. 8064	0. 8099	0. 8135
1,000	. 7585	. 7606	. 7626	. 7648	. 7669	. 7690	. 7712	. 7791	. 7814	. 7837	. 7860	. 7883	. 7906
2,000	. 7491	. 7510	. 7528	. 7546	. 7565	. 7582	. 7600	. 7638	. 7658	. 7677	. 7696	. 7715	. 7735
3,000	. 7413	. 7426	. 7440	. 7456	. 7470	. 7486	. 7500	. 7512	. 7535	. 7548	. 7569	. 7572	. 7585
4,000	. 7332	. 7345	. 7358	. 7370	. 7383	. 7395	. 7409	. 7408	. 7421	. 7434	. 7447	. 7459	. 7472
5,000	. 7265	. 7274	. 7282	. 7290	. 7298	. 7307	. 7316	. 7306	. 7318	. 7331	. 7345	. 7358	. 7371
6,000	. 7203	. 7210	. 7217	. 7224	. 7232	. 7239	. 7246	. 7225	. 7241	. 7255	. 7269	. 7283	. 7297
7,000	. 7151	. 7158	. 7165	. 7171	. 7179	. 7186	. 7194	. 7152	. 7167	. 7182	. 7197	. 7211	. 7226
8,000	. 7100	. 7105	. 7111	. 7119	. 7125	. 7130	. 7136	. 7075	. 7090	. 7104	. 7119	. 7133	. 7148
9,000	. 7048	. 7053	. 7059	. 7065	. 7070	. 7075	. 7082	. 7012	. 7024	. 7036	. 7047	. 7059	. 7071
10,000	. 7003	. 7008	. 7012	. 7016	. 7021	. 7025	. 7030	. 6955	. 6962	. 6968	. 6975	. 6982	. 6989

Pressure	A polyester (Selectron 5003) at—				Polytetrafluoroethylene (Teflon) at—							
	20° C	30° C	40° C	50° C	10° C	20° C	30° C	40° C	50° C	60° C	70° C	80° C
	cm³/g	*cm³/g*	*cm³/g*	*cm³/g*	*cm³/g*	*cm³/g*	*cm³/g*	*cm³/g*	*cm³/g*	*cm³/g*	*cm³/g*	*cm³/g*
1	0. 8377	0. 8402	0. 8427	0. 8452	0. 4442	--------	0. 4522	0. 4537	0. 4550	. 04565	0. 4578	0. 4592
1,000	. 8199	. 8221	. 8243	. 8264	. 4345	. 4356	. 4367	--------	. 4436	. 4446	. 4456	. 4465
2,000	. 8042	. 8059	. 8075	. 8091	. 4267	. 4278	. 4289	. 4318	. 4347	. 4357	. 4364	. 4372
3,000	. 7906	. 7921	. 7936	. 7951	. 4208	. 4218	. 4228	. 4238	. 4249	. 4280	. 4287	. 4292
4,000	. 7787	. 7800	. 7813	. 7826	. 4155	. 4165	. 4174	. 4184	. 4193	. 4204	. 4228	. 4232
5,000	. 7682	. 7695	. 7708	. 7721	. 4106	. 4113	. 4120	. 4128	. 4064	. 4073	. 4082	--------
6,000	. 7591	. 7603	. 7614	. 7625	. 3973	. 3979	. 3985	. 3992	. 3998	. 4005	. 4012	. 4018
7,000	. 7511	. 7521	. 7530	. 7540	. 3931	. 3937	. 3942	. 3948	. 3954	. 3959	. 3965	. 3971
8,000	. 7442	. 7450	. 7459	. 7467	. 3896	. 3902	. 3907	. 3912	. 3918	. 3924	. 3929	. 3935
9,000	. 7377	. 7383	. 7389	. 7395	. 3870	. 3875	. 3879	. 3884	. 3889	. 3894	. 3899	. 3904
10,000	. 7315	. 7321	. 7327	. 7333	. 3849	. 3852	. 3856	. 3859	. 3863	. 3867	. 3871	. 3876

increases more rapidly at the higher temperatures. This increased expansivity probably arises from melting of crystalline material near 80° C [8].

Expansivities at 1 atm for the rarer polyfluorides and polyvinyl alcohol do not appear to be available. The expansivities found here were fitted to an equation of the type

$$1/V_0(dV/dt)=a+b(t-20),$$

where t is the temperature in degrees Celsius, and V_0 is the volume of 20° C. Appropriate values for

TABLE 3. *Coefficients of expansivity equation*

$(1/V_0)\ (dV/dt) = a + b\ \ (t > 30)$

Polymer	a	b
Polyvinyl alcohol	0.000208	0.0000017
Polyvinyl fluoride	.000153	.0000021
Polyvinylidene fluoride	.000352	.0000024
Copolymer of ethylene and tetrafluoroethylene (1:1).	.000195	.0000022

a and b are given in table 3 for values of t between 20° and 90° C.

The slightly different densities and expansivities of the 1:1 copolymer of ethylene and tetrafluoroethylene and its isomer, polyvinylidene fluoride, indicated the advisability of a check on the composition of the copolymer. A mass spectrographic analysis indicated that the ratio of ethylene and tetrafluoroethylene present in the polymer was 1:1. The lower initial density of the copolymer as well as its somewhat different expansivity is undoubtedly due to a lower degree of order along the polymer chains with a resulting lower packing efficiency.

The specific volumes given at 70° C for the rarer polyfluorides are extrapolated data since the highest temperature at which measurements were made was approximately 63° C. However, the isobars appeared to be linear and the data are believed to be reliable.

Measurements on "Selectron 5003" were limited to a maximum of 50° C. These data may be of interest as indicative of the behavior of a polyester and are included for that purpose. The expansivity of this material was determined dilatometrically at 1 atm, but no equation representing the expansivity was derived.

Several blanks are noted in the specific volume data for Teflon. These are caused by uncertainties in the specific volumes at the points in question due to proximity of a transition line. The isobars for this material show an interesting behavior (fig. 1). In order to understand the behavior of the isobars the phase diagram [2] is superimposed on the isobars. The peculiar behavior of the 5,000-atm isobar arises from the fact that this isobar enters and emerges from the Teflon III region in the ranges covered.

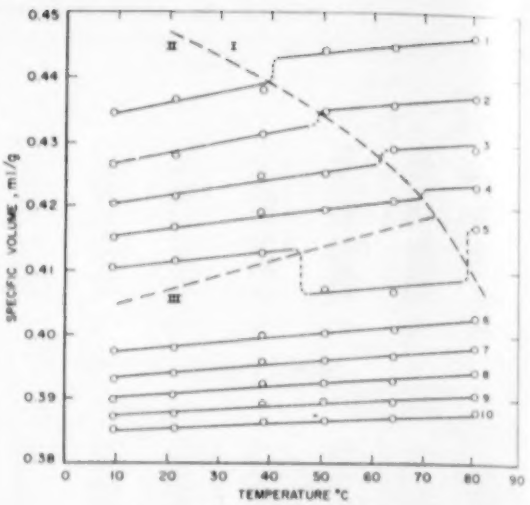

FIGURE 1. *Isobars for Teflon.*

The phase diagram is superimposed on the isobars to show their relationship to the forms of Teflon. The number at the right of each isobar represents the pressure in thousands of atmospheres.

4.2. Calculated Data

The preceding specific volume-pressure-temperature data have been utilized for calculations of equations of state, and work, heat, and internal energy changes.

Following in detail the procedure described for rubbers [1], empirical PVT equations of state were derived for the materials of primary interest. These equations are of the form

$$V_{sp} = V_0[1 + a_1P + a_2P^2 + a_3P^3 + t(b_0 + b_1P + b_2P^2 + b_3P^3) + t^2(c_0 + c_1P + c_2P^2 + c_3P^3)],$$

and the derived coefficients are given in table 4. Values of P and t are taken to be in atmospheres and degrees Celsius, respectively. In most instances the coefficients will reproduce the experimental data to within a few tenths of 1 percent, although for

TABLE 4. *Coefficients of empirical PVT equation*

$V_{sp} = V_0[1 + a_1P + a_2P^2 + a_3P^3 + t(b_0 + b_1P + b_2P^2 + b_3P^3) + t^2(c_0 + c_1P + c_2P^2 + c_3P^3)]$

Coefficient	Polymer					
	Teflon			Polyethylene	Kel-F	Polyvinyl alcohol
	I	II	III			
V_0	0.4481	0.4421	0.4351	1.0881	0.4636	0.7674
a_0	-7.03×10^{-4}	-1.37×10^{-3}	-1.994×10^{-3}	-3.354×10^{-3}	-2.127×10^{-3}	-1.584×10^{-3}
a_1	-1.53×10^{-6}	-3.96×10^{-6}	8.540×10^{-10}	3.511×10^{-6}	1.363×10^{-6}	1.178×10^{-6}
a_2	3.32×10^{-12}	7.37×10^{-12}	-3.050×10^{-15}	-1.575×10^{-12}	-3.537×10^{-13}	-4.863×10^{-13}
b_0	3.08×10^{-4}	4.75×10^{-4}	1.95×10^{-4}	-2.86×10^{-5}	2.76×10^{-4}	3.61×10^{-4}
b_1	-2.77×10^{-7}	-1.30×10^{-7}	-3.53×10^{-9}	2.66×10^{-7}	-3.90×10^{-8}	-3.92×10^{-7}
b_2	2.63×10^{-10}	4.35×10^{-12}	-7.14×10^{-12}	-5.92×10^{-11}	3.73×10^{-12}	-1.09×10^{-14}
b_3	-5.31×10^{-14}	2.12×10^{-13}	8.72×10^{-16}	3.44×10^{-13}	-2.44×10^{-16}	1.68×10^{-15}
c_0	1.96×10^{-6}	0	0	7.73×10^{-6}	2.35×10^{-7}	3.18×10^{-6}
c_1	1.00×10^{-8}	1.10×10^{-11}	0	-3.85×10^{-9}	-9.21×10^{-11}	1.67×10^{-11}
c_2	-1.56×10^{-13}	5.29×10^{-16}	0	6.70×10^{-13}	-5.84×10^{-13}	-1.41×10^{-13}
c_3	3.37×10^{-18}	-1.53×10^{-17}	0	-3.58×10^{-17}	9.94×10^{-19}	-5.38×10^{-18}

eflon I and Teflon II the discrepancy is somewhat rger. The larger deviations for these two materials e probably due to the smaller amount of data ailable for fitting the equations.

It must be emphasized that these equations are esigned to reproduce only V_{sp} within the range in hich measurements were made. Extrapolation in ny sense may lead to serious errors, as shown by the ign of b_0 for polyethylene. The equations likewise have not been examined analytically. The first partial derivatives appear to yield reasonable values, which do not always agree with the experimental expansivities and compressibilities within the experimental error. Therefore, deductions based on first and higher derivatives of these equations must be made with caution.

In most instances the values of the c terms will be found to be negligible except at high pressures and temperatures. Inasmuch as these values are of importance in some instances, they are recorded. In the case of Teflon III, the term involving t^2 was identically zero.

Similar equations were not derived for the rarer fluorine polymers because the amount of data available were limited, and these materials are of more academic interest at present. However, such equations can be derived from the data if required.

From the tabulated specific volume-pressure-temperature data, values for work of compression ($w = \int P(\partial V/\partial P)_T dP$), heat of compression ($q = -T\int(\partial V/\partial T)_P dP$), and internal-energy change ($\Delta E = q - w$) were calculated [9]. Work and heat values were computed by mechanical integration [10] under appropriate curves constructed from the PVT data. The internal-energy changes were then calculated from the corresponding work and heat data. Complete data for work and heat values are not reported, but the calculated internal energy changes are shown graphically in figures 2 to 8. The changes in internal energy represent the energy in joules per gram (j/g) evolved or absorbed on an isothermal compression from 1 atm to the pressure given by the abscissa.

It is to be noted that graphical integrations for all materials except Teflon are straightforward. For Teflon the integration for heat values is complicated by the latent heats of the two transitions encountered. The value of latent heat reported by Furukawa [11] was taken to apply at all pressures in transforming I to II. This assumption is most probably in error at the higher pressures, since the shape of the I–II line is curved and ΔV_{I-II} changes markedly. However, a more reliable estimate of the latent heat cannot be made from the present data. This heat is evolved on compression. Latent heats absorbed in forming III from II were calculated from the Clapeyron equation and are tabulated in a following section. Sufficient data are not available for a reliable calculation of the latent heat involved in the I–III transition. Values of heat of compression involving this quantity and the corresponding internal-energy changes could not be calculated.

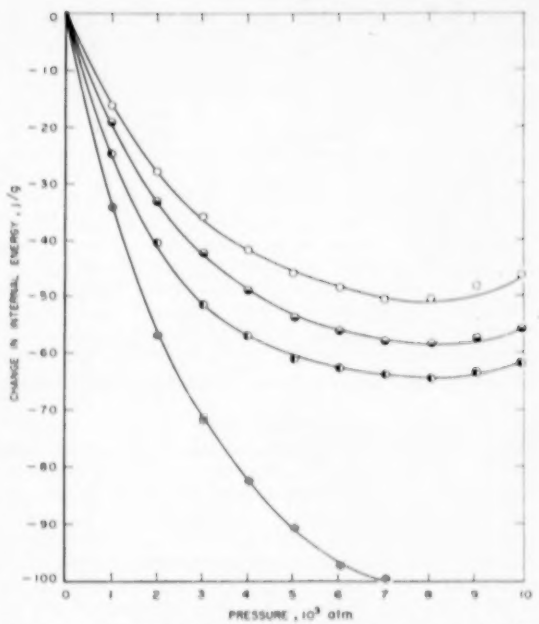

FIGURE 2. *Change in internal energy on compression of polyethylene.*

○, 20° C; ◒, 40° C; ◐, 60° C; ⊕, 80° C.

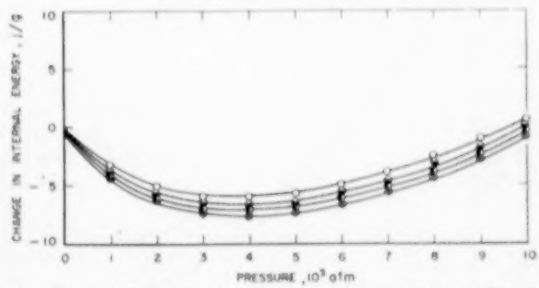

FIGURE 3. *Change in internal energy on compression of Kel-F.*

○, 20° C; ◒, 40° C; ◐, 60° C; ⊕, 80° C.

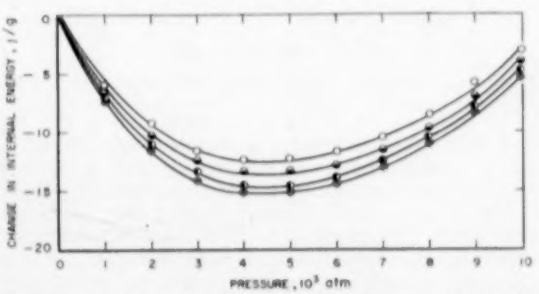

FIGURE 4. *Change in internal energy on compression of polyvinyl alcohol.*

○, 20° C; ◒, 40° C; ◐, 60° C; ⊕, 80° C.

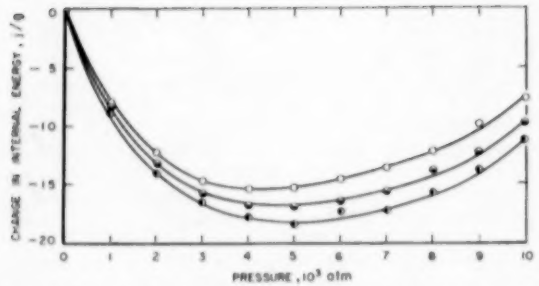

FIGURE 5. *Change in internal energy on compression of polyvinyl fluoride.*
○, 20° C; ◒, 40° C; ◐, 60° C.

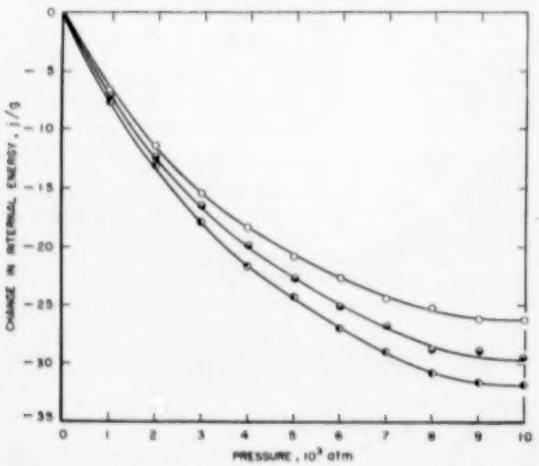

FIGURE 6. *Change in internal energy on compression of polyvinylidene fluoride.*
○, 20° C; ◒, 40° C; ◐, 60° C.

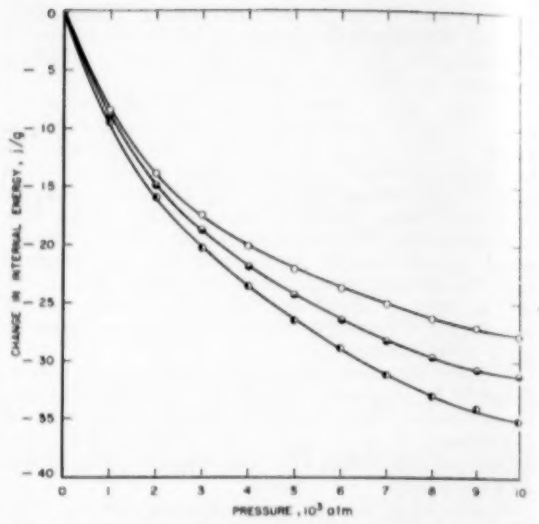

FIGURE 7. *Change in internal energy on compression of copolymer.*
○, 20° C; ◒, 40° C; ◐, 60° C.

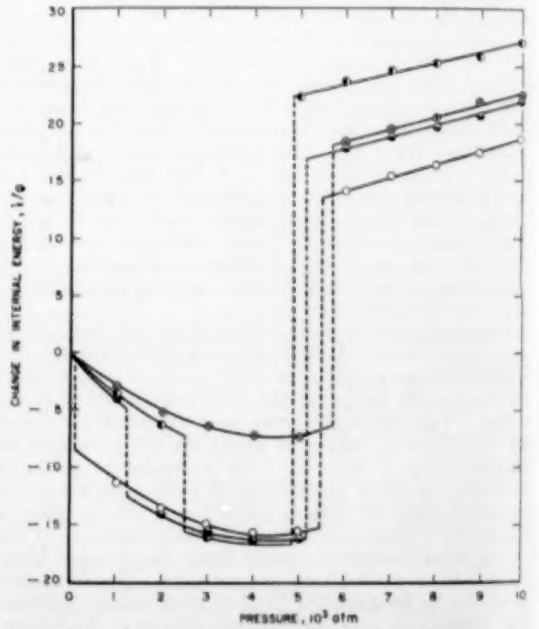

FIGURE 8. *Change in internal energy on compression of Teflon*
⊕, 10° C; ○, 20° C; ◒, 40° C; ◐, 60° C.

5. Discussion

Considering first the numerical magnitude of the compressions shown in table 1, it is noted that these values are, in general, of the same order as those previously obtained for rubbers [10]. The comparative compression is directly proportional to the density, as has been noted by Bridgman, except for Teflon, which shows the highest compression. This anomaly arises from the transitions encountered, the Teflon being relatively incompressible. It may be noted that at still higher pressures polyethylene shows a greater compression than Teflon, despite the transitions in the latter [12].

Certain deductions may be drawn from the behavior of the internal energy. Bridgman [9] has proposed that the observed change in internal energy as the pressure is varied isothermally may be explained on the basis that the intermolecular forces are normally predominantly attractive. On compression the potential energy decreases, and the internal energy, therefore, decreases. However, at some compressed volume the process must reverse because the intermolecular forces utlimately become repulsive. Hence, on increasing the pressure, the internal-energy change decreases, then reverses direction and increases, ultimately becoming increasingly positive. The comparative behavior of the internal-energy change may be used for a qualitative comparison of the intermolecular forces.

In polyethylene (see fig. 2) the internal-energy change reverses direction within the pressure range investigated at the lower temperatures but does not become positive. This is similar to the behavior in rubbers [10]. The marked differences in behavior at the elevated temperatures is probably connected with the melting of crystalline material in this region or may be due to attack of the polyethylene by the confining liquid at these temperatures. Although inert at lower temperatures, the confining liquid severely attacked the surface of the polyethylene at 80° C. Kel-F, Teflon, polyvinyl alcohol, and polyvinyl fluoride all exhibit reversal in direction of ΔE at moderate pressures, an indication of strong repulsive forces. In Kel-F alone ΔE becomes zero or positive in this pressure range but only at temperatures below about 40° C. The behavior is not clearly shown by Teflon because of the complications of the transitions. Polyvinyl alcohol differs appreciably from polyethylene, a result that is probably due, in part at least, to the effects of hydrogen bonds. Polyvinyl fluoride differs markedly from the behavior exhibited by the polyvinlidene fluoride and copolymer in which the pressure of reversal appears to be just outside the pressure range used here.

In Teflon (see fig. 8), the II–III transition appears to occur at pressures slightly higher than that required to cause the internal-energy change to reverse direction. The forces at these and higher pressures will be essentially repulsive. Under these circumstances the formation of III from II requires a further decrease of volume against increasingly strong repulsive forces and must result in a greatly increased potential energy. The absorption of heat that attends this decrease in volume may be understood if the work performed on contraction is insufficient to supply the increased potential and possibly kinetic energies demanded. From the same viewpoint the liberation of energy in the transition I–II occurring in the region of attractive forces is to be expected. The previously reported anomalies in energies at the triple point [2] are indicated by the incongruous temperature dependence of the internal energy at the higher pressures. The inconsistencies are probably more apparent than real, however, since the latent heat of the I–II transition has been taken as independent of pressure, an assumption that is probably far from true. No alternative exists at present because the ΔV values are not reliably known except at 1 atm.

The transition II–III was studied in some detail and, following Bridgman [9], differences between the properties of these forms may be evaluated. From the temperature dependence of the transition pressure and the measured volume discontinuities the latent heat can be calculated from the Clapeyron equation. Pertinent data calculated from the experimental results are given in table 5. Inasmuch as the transition II–III is not very sharp except at higher temperatures [2], the data of the table, as well as subsequently calculated values, cannot be considered as more than approximate.

From Bridgman's relationships [9] $d(\Delta V)/dP = \Delta\alpha dT/dP - \Delta\beta$ and $d(\Delta H)/dP = \Delta C_p dT/dP - T\Delta\beta$, where α and β are expansivity and compressibility, respectively, and the other terms have the usual significance. Values for $\Delta\alpha$ and ΔC_p can be calculated from the data of the table. These are $\Delta\alpha = \alpha_{II} - \alpha_{III} \approx 40\text{x}10^{-6}/°$ C and $\Delta C_p = C_{p_{II}} - C_{p_{III}} \approx 0.18$ j/g per °C. $\Delta V/V_0 = (V_{II} - V_{III})/V_0$ was taken to be 0.025.

TABLE 5. *Transitional data for Teflon II–III*

Temperature	Volume discontinuity	Latent heat	Compressibility	
			II	III
°K	cm^3/g	j/g	atm^{-1}	atm^{-1}
295	0.0467	−24.5	1.18×10^{-4}	0.75×10^{-4}
312	.0518	−28.6	1.19	.72
323	.0542	−31.1	1.20	.72
337	.0570	−34.0	1.24	.76

Similar calculations are precluded for the I–II transition because of the small ΔV values at the higher pressures at which accurate measurements are possible. Compression curves show that II is less compressible than I [2]; Furukawa [11] has shown that C_{p_I} is greater than $C_{p_{II}}$; whereas Quinn, Roberts, and Work [4] showed that α_I is greater than α_{II}. The differences in compressibilities cannot be estimated reliably, and reference should be made to the data cited for information on C_p and α at 1 atm.

In a general discussion of the data presented here the following remarks may be made:

No comparable data appear to exist for high polymers to permit comparisons of results. Parks and Richards [13] have reported PVT data for polyethylene that cover a wider temperature range but are limited to a maximum pressure of 2,000 atm. Their results are clearly of the same order of magnitude.

It will be noted that specific heat data are available for three of the polymers studied. Raine, Richards, and Ryder [14] and Dole, Hettinger, Larson, and Wethington [15] have reported data for polyethylene, and Hoffman [16] has reported on Kel-F. These data were all determined at relatively high temperatures, approximately −20° C being the lowest temperature studied. Furukawa [11] has reported data on Teflon that extends to very low temperatures. These data can be utilized with the results of this report to calculate all the thermodynamic quantities of interest for these three materials in the pressure-temperature range studied here.

It is also noted that some uncertainty exists in values reported here between 1 and 1,000 atm [3, 5] because the measurements did not cover this pressure interval. Such uncertainty in no way affects the validity of the changes reported between 1,000 and 10,000 atm. In addition, the compression between 1 and 1,000 atm, which was arrived at by successive approximations, is not expected to be seriously in error.

The finding that Teflon alone of the polymers studied was found to exhibit polymorphism is not surprising. From Bridgman's [9] studies it is known that polymorphism at high pressures is not a rare occurrence. In polymers, however, it is most likely to be very rare. This probability follows from the consideration that a high degree of crystallinity is most likely a requirement for polymorphism. This requirement cannot be met by more than a few known polymers. It must be pointed out, however, that the pressure-temperature range investigated here is limited and the possibility exists that the effects sought may exist outside this range.

The question arises as to the effect of molecular weight on these data. In this pressure range, two processes appear to be involved [9], first removal of "holes" and second, distortion of the molecules or atoms. The second process is probably relatively inactive at the lower pressures, whereas the first will probably occur over this whole pressure range but diminishing in effect with increasing pressure. The number of "holes" is expected to vary with the molecular weight (i. e., with the number of chain ends). However, it is expected that this variation will be most marked in extremely low molecular weights and become of decreasing importance as the molecular weight increases. For high molecular weights, therefore, it is believed that the molecular weight will have a rather small influence on compressibility. Bridgman [12] has reported data on polyethylene that verify this expectation. The materials studied here are for the most part insoluble at room temperature, and hence molecular weight data were not obtained. The results, however, are believed to be representative of such materials of high molecular weight. Furthermore, as all polymers studied possess a C—C chain structure, which will behave similarly to a first approximation at least, the differences noted most probably are due to differences in interchain forces and free volumes.

6. References

[1] C. E. Weir, J. Research NBS **50,** 153 (1953) RP2403.
[2] C. E. Weir, J. Research NBS **50,** 95 (1953) RP2395.
[3] C. E. Weir, J. Research NBS **45,** 468 (1950) RP2160.
[4] F. A. Quinn, D. E. Roberts, and R. N. Work, J. Appl. Phys. **22,** 1085 (1951).
[5] C. E. Weir, J. Research NBS **46,** 207 (1951) RP2192.
[6] E. Hunter and W. G. Oakes, Trans. Faraday Soc. **41,** 49 (1945).
[7] F. P. Price, J. Am. Chem. Soc. **74,** 311 (1952).
[8] C. E. Weir (unpublished data).
[9] P. W. Bridgman, The physics of high pressure (G. Bell & Sons, Ltd., London, England, 1949).
[10] C. E. Weir, J. Research NBS **50,** 321 (1953) RP2421.
[11] G. T. Furukawa, R. E. McCoskey, and G. J. King, J. Research NBS **49,** 273 (1953) RP2364.
[12] P. W. Bridgman, Proc. Am. Acad. Arts and Sci. **76,** 71 (1948).
[13] W. Parks and R. B. Richards, Trans. Faraday Soc. **45,** 203 (1949).
[14] H. C. Raine, R. B. Richards, and H. Ryder, Trans. Faraday Soc. **41,** 56 (1945).
[15] M. Dole, W. Hettinger, N. Larson, and J. Wethington, J. Chem. Phys. **20,** 781 (1952).
[16] J. Hoffman, J. Am. Chem. Soc. **74,** 1696 (1952).

WASHINGTON, May 18, 1954

Journal of Research of the National Bureau of Standards Vol. 53, No. 4, October 1954 Research Paper 2541

Turbulent Flow in Shock Tubes of Varying Cross Section*

Robert F. Dressler

The unsteady escape flow of a compressible gas is investigated subject to the influences of varying duct cross section and mechanical retardation due to turbulence and frictional dissipation. This study is applicabe to shock tubes, intermittent wind tunnels, and general pneumatic-control systems, such as airbrakes. Wave-front velocities and trajectories are obtained by direct integration along the bounding Mach lines. In the general case, calculation of first-order approximations is reduced to a set of independent ordinary differential equations for easy stepwise integration. For the special cases of constant resistance or exponentially converging-diverging ducts, first-order solutions are obtained analytically. An error estimate is derived. Local Mach number variations are presented throughout the flow.

1. Introduction

One type of wind tunnel in present use employs the principle of intermittent discharge of atmospheric air into a vacuum chamber, or intermittent high-pressure discharge into an atmospheric chamber. In the latter case, a rapidly advancing shock discontinuity will also be generated in the forward wave. The familiar Riemann shock tube furnishes such an example; for this type of duct Riemann [1][†] studied the basic theory of one-dimensional unsteady gas flows. In the present paper the emphasis will be upon the flow immediately after the diaphragm is broken, not upon the flow developing after a sufficiently long time when an almost steady-state regime is approached. The intermittent-vacuum-type system gives a more constant stagnation temperature and requires less power than the intermittent-pressure type, but gives lower densities in the test section. In the first stages of operation, these flows in shock tubes or vacuum-type wind tunnels can be approximately described by the known centered simple-wave solution [2, ch. III], defining a subsonic-supersonic pattern about the diaphragm position. It is the purpose of this paper to investigate quantitatively the possible improvement in density, velocity, or Mach number that might be created if such an unsteady flow is made to pass through a test section of varying cross section; at the same time the retarding effect due to wall resistance and ensuing turbulence will also be considered.

Any forward shock discontinuity that would be created in an actual flow if it propagates into a region containing some gas will be ignored in the present treatment. Even if a relatively strong shock exists, the results to be derived here will still be approximately applicable to the backward moving rarefaction wave region. This will furnish quantitative information, for example, concerning frictional effects in the rarefaction waves propagating through pneumatic-control circuits, such as airbrake lines.

The case of steady flows in variable ducts has recently been studied by Meyer [3], emphasizing the propagation of advancing and receding wave fronts due to a finite disturbance superimposed upon a basic steady flow, with consideration given to the varying cross-section effect, but not the resistance effect.

Dimensional quantities (barred) will first be introduced to define the dimensionless ones (unbarred), which will then be used throughout this paper. In the standard notation as given in [2], $\bar{x}$ is taken in the direction of flow; time is denoted by $\bar{t}$, with the valve or diaphragm at $\bar{x}=0$ opened at $\bar{t}=0$. Let $\bar{p}$ denote pressure, $\bar{\rho}$ the mass density, and $\bar{u}$ the velocity component in the downstream direction. We consider the nonlinear flow of a polytropic gas having the equation of state

$$\bar{p}=\bar{A}\bar{\rho}^{\gamma}, \tag{1}$$

*The preparation of this paper was sponsored by the Office of Naval Research, USN.
† Figures in brackets indicate the literature references at the end of this paper.

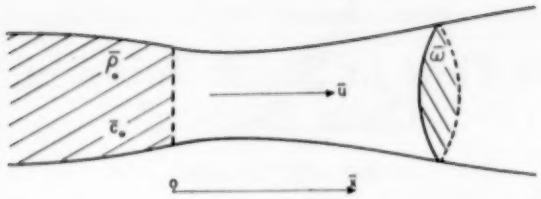

FIGURE 1.

with known constant $\bar{A}$ and adiabatic exponent γ. We introduce in the usual manner the local sound speed $\bar{c}$ into the differentiated equation of state,

$$\bar{c}^2=\gamma\bar{A}\bar{\rho}^{\gamma-1}. \tag{2}$$

For $\bar{t}<0$, the gas is at rest to the left of the valve, $\bar{x}<0$, and has properties $\bar{\rho}_0$, $\bar{c}_0$, and $\bar{u}_0=0$. For $\bar{t}<0$, there is no gas in $\bar{x}>0$ (see fig. 1). We assume the flow to occur in a duct with cross section varying gradually enough to keep the flow essentially one-dimensional with uniform velocity over any cross section, and subject to the retarding force from the wall friction and turbulence, depending empirically upon the square of the velocity and the roughness coefficient for the wall surface. The dynamic equation is then

$$\frac{\partial\bar{u}}{\partial\bar{t}}+\bar{u}\frac{\partial\bar{u}}{\partial\bar{x}}+\frac{2}{\gamma-1}\bar{c}\frac{\partial\bar{c}}{\partial\bar{x}}+\epsilon\overline{R}(\bar{x})\bar{u}^2=0, \tag{3}$$

where ϵ is a small dimensionless expansion parameter, and the given function $\overline{R}(\bar{x})>0$ varies if the roughness of the wall surface changes from region to region, or if the cross section varies, thus varying the hydraulic radius [2] of the duct in a known manner. Letting $\bar{\omega}(\bar{x})$ denote the area of the cross section of the duct, the modified equation of continuity will be

$$2\frac{\partial\bar{c}}{\partial\bar{t}}+2\bar{u}\frac{\partial\bar{c}}{\partial\bar{x}}+(\gamma-1)\bar{c}\frac{\partial\bar{u}}{\partial\bar{x}}+(\gamma-1)\epsilon\bar{a}(\bar{x})\bar{u}\bar{c}=0, \tag{4}$$

in which $\bar{a}(\bar{x})=[d\bar{\omega}/d\bar{x}]/\bar{\omega}$, with $\epsilon\bar{a}=0$ corresponding to a uniform duct.

In eq (1), (3), and (4) we have tacitly assumed constant entropy for the flow. This is a simplification tantamount to neglecting the heat change (and hence its extra resulting effects upon the mechanics of the gas flow) which will always be produced by the operation of the resistance term in converting kinetic energy into thermal energy. The present discussion will consider the mechanics of the flow including only the retarding force, not the full thermodynamical aspects of the problem. To do so would require also the inclusion of the energy equation, creating a system of three equations in the three unknowns: particle velocity, sound velocity, and specific entropy. Such a system has an associated set of six characteristic equations; these have been used by Hall [4] and others for purposes of quite arduous numerical integrations performed over characteristic meshes in the (x,t) plane. The simplified model used in our present paper can be described also in the following manner. We consider a one-dimensional flow through a tube with the mass traveling in thin slices perpendicular to the walls. Each slice is subjected to a retarding shear force distributed over its peripheral area. This force $F(\rho,u)=-\lambda\rho u^2$ varies with the changing density and velocity of the moving slice. Results obtained for this model will thus extract the purely mechanical effect of the friction from the full nonisentropic thermodynamical effects.

[2] If $\bar{\epsilon}(\bar{x})$ measures the roughness of the wall material, then $\overline{R}=\bar{\epsilon}(\bar{x})/\overline{P}(\bar{x})$, where the hydraulic radius $\overline{P}$ is defined as $\bar{\omega}/\overline{P}$. $\overline{P}$ is the perimeter of the cross section having area $\bar{\omega}$.

Now introduce the unbarred dimensionless quantities defined by $x=(g/\bar{c}_0^2)\bar{x}$, $\bar{t}=(g/\bar{c}_0)\bar{t}$, $u=(1/\bar{c}_0)\bar{u}$, $c=(1/\bar{c}_0)\bar{c}$, $\rho=(1/\bar{\rho}_0)\bar{\rho}$, $R=(\bar{c}_0^2/g)\bar{R}$, $a=(\bar{c}_0^2/g)\bar{a}$, and abbreviate $2/(\gamma-1)=l$, the unmodified escape speed. Equations (3) and (4) then become

$$\frac{\partial u}{\partial t}+u\frac{\partial u}{\partial x}+lc\frac{\partial c}{\partial x}+\epsilon R(x)u^2=0 \tag{5}$$

$$l\frac{\partial c}{\partial t}+lu\frac{\partial c}{\partial x}+c\frac{\partial u}{\partial x}+\epsilon a(x)uc=0. \tag{6}$$

The escape flow solution for $\epsilon=0$ (uniform duct and resistance neglected) is

$$u^0=\frac{2}{\gamma+1}(1+m) \tag{7}$$

$$c^0=\frac{\gamma-1}{\gamma+1}(l-m), \tag{8}$$

where $m=x/t$. This is supersonic in the forward region $0<x\leq lt$; subsonic in the backwave $-t\leq x<0$; and $u^0=c^0=2/(\gamma+1)$ at the fixed sonic point $x=0$.

The equations for the Mach lines of the system (5), (6) are

$$I_+:\frac{dx}{dt}=u-c$$

$$I_-:\frac{dx}{dt}=u+c$$

$$II_+:d(u-lc)=-\epsilon(Ru-ac)udt \tag{9}$$

$$II_-:d(u+lc)=-\epsilon(Ru+ac)udt,$$

where the I_+ and II_+ relations hold along the b_+ family of receding Mach lines in the (x,t) plane, and the other pair along the b_- advancing lines. The Mach lines OB and OF in figure 2 define the moving limits of the flow zone. As the quantities $R(x)$ and $a(x)$ do not appear in the first equation of (9), it follows that the curve OB must remain a straight line with direction $m=-1$ in all cases.

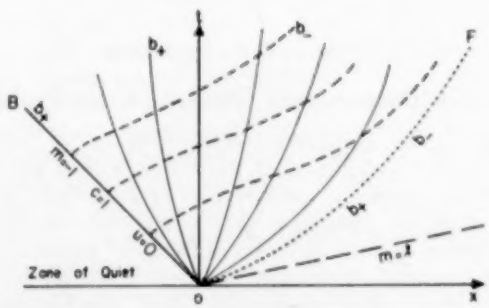

FIGURE 2.

2. Locus of the Wavefront

It is seen at once from the last two equations in (9) that, within the accuracy of the basic relations (5) and (6), the duct shape has no effect upon the wavefront trajectory where $c=0$ because the terms containing $a(x)$ will vanish along this wave front. Its locus is a function of ϵR, however, and will remain a double Mach line as the plus and minus relations coincide for $c=0$ in (9). The *I* and *II* pair of equations can then be integrated explicitly to obtain the exact wavefront locus, which is

$$t_F(x)=\frac{\gamma-1}{2}\int_0^x e^{\int_\zeta^x \Re(\xi)d\xi}\,d\zeta, \tag{10}$$

in which ϵ is included in the notation $\epsilon R=\Re$. The velocity of the wavefront is given by

$$u_F(x)=\frac{2}{\gamma-1}\,e^{-\int_0^x \Re(\xi)d\xi}. \tag{11}$$

In particular, if $\Re=$ constant, e. g., in a duct having homogeneous wall surface and uniform cross section, the position and velocity will be

$$\begin{aligned} x_F&=\frac{1}{\Re}\ln\left(\frac{2\Re}{\gamma-1}\,t+1\right)\\ u_F&=\left(\Re t+\frac{\gamma-1}{2}\right)^{-1}. \end{aligned} \tag{12}$$

These exact results will be used later to furnish an error estimate for the approximations to be derived for the interior wave zone. The forward wave velocity will not approach asymptotically any nonzero value, but will continually slow down, approaching, but never attaining, a state of rest. This is true more generally for any variable $R(x)$ with $a(x)$ arbitrary, as can be seen from (11), because $R(x)$ is always nonnegative.

The Mach lines inside the flow will be locally distorted by the influence of R and a from their positions for the basic solution (7) and (8), which are

$$b_+:\ x=mt,\ -1\le m\le 2/(\gamma-1), \tag{13}$$

$$b_-:\left(\frac{x}{p}\right)=\frac{2}{\gamma-1}\left(\frac{t}{p}\right)-\frac{\gamma+1}{\gamma-1}\left(\frac{t}{p}\right)^{\frac{2-\gamma}{1+\gamma}},\quad 0<a<\infty, \tag{14}$$

where each b_- curve emanates from the point $(-p,p)$ on OB.

3. Comparison with Hydrodynamic Problem

If $\epsilon=0$ in (3) and (4), the equations become identical for $\gamma=2$ with the approximate Saint-Venant equations for two-dimensional water flow with a free surface, where c^2 is the water height, and u is the horizontal velocity of a cross section. If this analogy extended also to the equations when the resistance term is included, then the present aerodynamic problem would be analogous to the hydraulic "dam-break" problem previously considered by the author in [5]. The hydraulic-resistance function, however, is more complicated in an essential way, taking the form $-Ru^2/c^2$ rather than $-Ru^2$. The hydraulic dam-break wavefront contains a second-order pole singularity, and its locus is thereby not a characteristic curve itself, but only an envelope of such curves. Explicit integration for its trajectory is apparently not possible in that case. The simpler nature of the present problem permits carrying the different mathematical results somewhat farther and with less approximation involved for the basic model used.

4. Functions for First-Order Effects

Using (7) and (8), we substitute

$$u(x,t,\epsilon)=u^0(x,t)+U(x,t)\epsilon+O(\epsilon^2)$$
$$c(x,t,\epsilon)=c^0(x,t)+C(x,t)\epsilon+O(\epsilon^2) \tag{15}$$

into (5) and (6). The terms in ϵ define the system

$$(\gamma+1)\frac{\partial U}{\partial t}+2\left(\frac{x}{t}+1\right)\frac{\partial U}{\partial x}+2\left(l-\frac{x}{t}\right)\frac{\partial C}{\partial x}+\frac{2}{t}U-\frac{2}{t}C+\frac{4}{\gamma+1}\left(\frac{x}{t}+1\right)^2R(x)=0$$
$$(\gamma-1)\left(l-\frac{x}{t}\right)\frac{\partial U}{\partial x}+l(\gamma+1)\frac{\partial C}{\partial t}+2l\left(\frac{x}{t}+1\right)\frac{\partial C}{\partial x}-\frac{2}{t}U+\frac{2}{t}C+2\left(\frac{\gamma-1}{\gamma+1}\right)\left(l-\frac{x}{t}\right)\left(\frac{x}{t}+1\right)a(x)=0. \tag{16}$$

This system for U and C has the same known Mach lines in the (x,t) plane as defined in (13) and (14), along which the following Riemann relations will hold:

$$b_+\colon d(U-lC)=\left[\frac{4}{(\gamma+1)t}(C-U)-(Ru^0-ac^0)u^0\right]dt$$
$$b_-\colon d(U+lC)=-(Ru^0+ac^0)u^0\,dt. \tag{17}$$

This second equation is independent of U and C on the right side; therefore, it is possible for given $R(x)$ and $a(x)$ to integrate the line integral explicitly along each known b_- curve, using (14). The result will be a known expression of form

$$U+lC=\Phi(t,p).$$

This will then permit a very easy separate step-wise numerical integration along each b_+ curve to solve for U and C. Thus the problem is reduced to a set of independent "one-dimensional" numerical calculations for a single ordinary differential equation along each b_+ curve. This is a calculation of much greater simplicity than the two-dimensional numerical procedure that would be necessary for the full problem in (5), (6), and (9).

5. Integration in Special Cases

Instead of using the numerical approach for arbitrary R and a, we return to solve the basic eq (16) explicitly for the special case when R and a are both constants. In particular, $a=0$, $R=\text{constant}>0$ will describe the resistive effects on the flow in a duct with any fixed cross section and homogeneous wall roughness. The combination $a=\text{constant}\neq 0$, $R=0$ will describe the effect of a converging or diverging duct, neglecting resistance effects. For example, $a>0$ can describe a duct with circular cross section, exponentially diverging, or with rectangular cross section, constant width, also exponentially diverging; $a<0$ corresponds to exponentially converging ducts of either type. The combination R and a, both nonzero constants, is less meaningful physically, because in such a varying duct the wall roughness would have to be varied in conformity with the changing hydraulic radius in order to maintain R constant. Therefore, the contributions of R and a will be considered separately, although the solution will be made for both simultaneously.

First, we put $\gamma=1.4$ for air to shorten the expressions; the escape velocity is then $l=5$.

System (16) has for its general solution

$$U(x,t)=-\frac{5}{t}K\left(\frac{x}{t}\right)-\frac{25}{144}\left[84-36\left(5-\frac{x}{t}\right)+5\left(5-\frac{x}{t}\right)^2\right]Rt-\frac{5}{48}\left[2\left(5-\frac{x}{t}\right)-\left(5-\frac{x}{t}\right)^2\right]at+F(\alpha),$$

$$C(x,t)=\frac{1}{t}K\left(\frac{x}{t}\right)-\frac{5}{144}\left[60-36\left(5-\frac{x}{t}\right)+7\left(5-\frac{x}{t}\right)^2\right]Rt-\frac{1}{48}\left[10\left(5-\frac{x}{t}\right)-3\left(5-\frac{x}{t}\right)^2\right]at+\frac{\delta}{\alpha}+ \tag{18}$$

$$\frac{1}{5}F(\alpha)+\frac{4}{5\alpha}\int^{\alpha}F(\xi)d\xi,$$

where $\alpha=(5-x/t)t^{1/3}$, K and F are arbitrary functions, and δ is an arbitrary constant. The form of this solution indicates that U and C must be either infinite or zero at $t=0$; hence we must choose $K=0$ and $\delta=0$ to keep the functions zero. The boundary conditions $U=C=0$ along line OB then determine the function $F=(1/1296)\,(50R-15a)(5-x/t)^3t$. With $x/t=m$, the main results reduce to

$$\begin{aligned}U&=-\frac{25}{1{,}296}\,(2m^3+15m^2+24m+11)Rt+\frac{5}{432}\,(m^3-6m^2+3m+10)at,\\ C&=-\frac{5}{1{,}296}\,(4m^3+3m^2-6m-5)Rt+\frac{1}{432}\,(2m^3-3m^2-30m-25)at.\end{aligned} \tag{19}$$

Denoting $aRt=\sigma$ and $aat=\tau$, the flow velocity and local sound speed correct to first order can be written from (19), using (7) and (8), in the form

$$\begin{aligned}u&=u^0+h_1(m)\sigma+h_2(m)\tau\\ c&=c^0+k_1(m)\sigma+k_2(m)\tau.\end{aligned} \tag{20}$$

Once u and c have been calculated by (19) and (20), the pressure and density are immediately known through relations (1) and (2).

5.1. Effects on Velocity and Density

To provide immediate perception of the various effects, the h, k polynomials are graphed in figure 3, in which h_1 is plotted to a separate vertical scale given on the right. We note that an

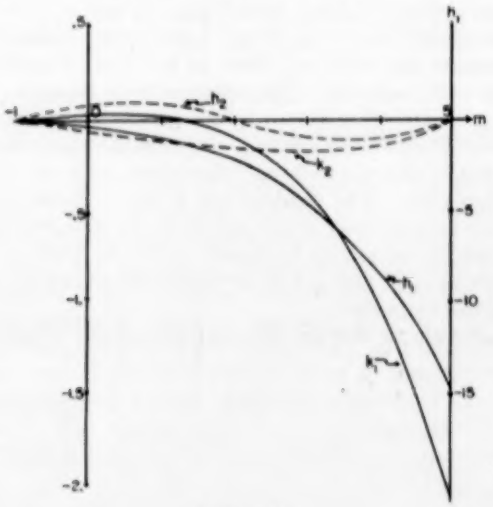

FIGURE 3.

exponential duct causes an antisymmetrical effect on the velocity about the moving midpoint of the flow zone ($m=2$), whereas the effect on sound speed and density is almost symmetrical about $m=2.8$. On the other hand, in a uniform duct, the resistance effect is a monotonic decrease in the velocity as it approaches the wavefront; it creates a very slight increase in sound speed at the rear of the flow, then a larger decrease in the forward region.

As a numerical example to illustrate the various separate effects, u, c, and the local Mach number $M=u/c$ are evaluated in figure 4, A, for $\sigma=1/10$; and for $\tau=+1$ in 4, B, and $\tau=-1$ in 4, C. The dotted lines represent the quantities u^0, c^0, and M^0 when $\sigma=\tau=0$.

5.2. An Error Estimate

As shown by the c curve in figure 4, A, the abscissa of the point where the solid curve intersects the m axis defines the position of the wavefront to the first order approximation. Likewise the corresponding value of u on the curve directly below furnishes an approximation for the velocity of the wavefront. We have, however, already obtained the exact expressions for the position and velocity of the wavefront in (12). The approximations and the full solution agree exactly along line OB; the resistive effect is a cumulative one with increasing velocity in the forward part of the wave; hence it is to be expected that the maximum of the approximation error will occur at the wavefront. Thus the error bound obtainable in this way should also be valid for all portions of the wave. Such a calculation for the position of the wavefront indicates that the approximate result will be about 10 percent too large when σ grows as large as 0.2. The other case of variable cross section does not permit this simple method for an error estimate.

5.3. The Sonic Path

If $x=s(t,\epsilon)$ is the path along which $u=c$, with $s=0+S\epsilon+0(\epsilon^2)$, the resulting double series expansion correct to first order gives the relation $S(t)=[C(0,t)-U(0,t)]t$. For the case $R=$

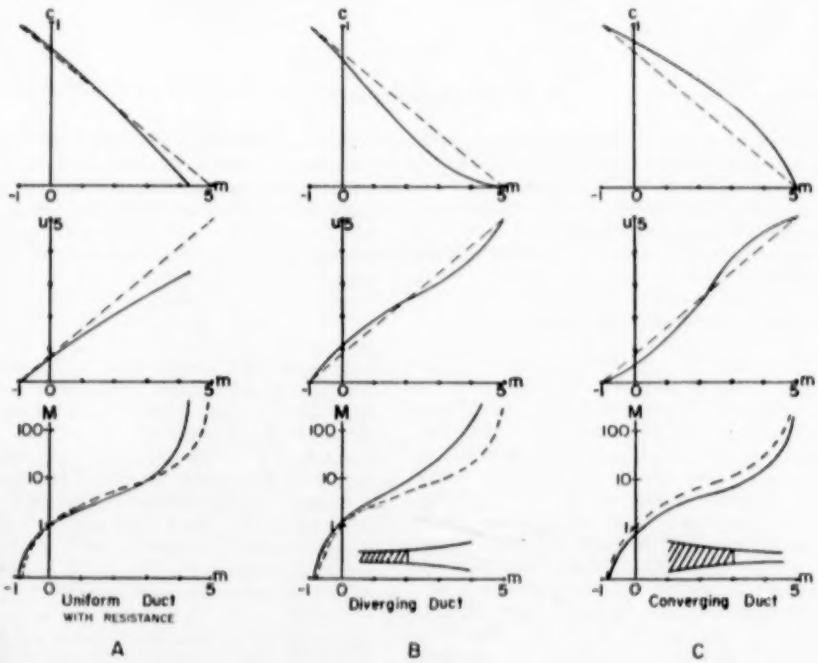

FIGURE 4.

constant, $a=0$, this defines the sonic path correct to first order to be the downstream parabola

$$x \doteq 0.23\epsilon R t^2.$$

For the other case $a=$constant, $R=0$, we get the parabola

$$x \doteq -0.18\epsilon a t^2,$$

going upstream or downstream as the duct is diverging or converging, respectively.

5.4. Flow Past a Fixed Point

The Mach number distribution across the entire flow at a fixed time has been presented in figure 4. Of more practical interest, however, from the standpoint of applications in shock tubes or wind tunnels is the time variation of local Mach number at a fixed point downstream in the duct, at a point where a fixed model might be placed. This can be derived in an obvious manner from the expressions already presented. As an illustrative example, the Mach number is shown in figure 5 at the fixed point $x=100$ for $\epsilon R=0.005$, $\tau=0$ in 5, A; for $\epsilon a=+0.01$, $\sigma=0$ in 5, B; and for $\epsilon a=-0.01$, $\sigma=0$ in 5, C. The dotted curve in each figure again represents the M^0 corresponding to the undisturbed solution.

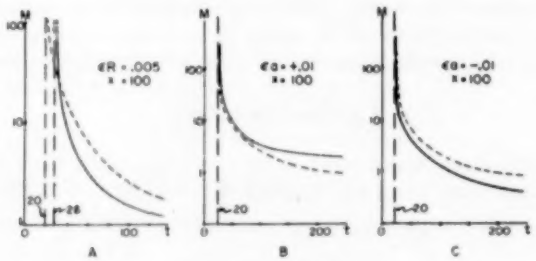

FIGURE 5.

6. References

[1] B. Riemann, Abhandlungen der Gesellschaft der Wissenschaften zu Göttingen, 8 (1860).

[2] R. Courant and K. O. Friedrichs, Supersonic flow and shock waves, Interscience (New York, N. Y., 1948).

[3] R. E. Meyer, On waves of finite amplitude in ducts, Quart. J. Mech. and Appl. Math., vol. V, pt. 3 (1952).

[4] N. A. Hall, The action of friction in nonsteady flow of fluids (First Midwestern Conf. on Fluid Dynamics, Edwards, Ann Arbor, Mich., 1951).

[5] R. F. Dressler, Hydraulic resistance effect upon the dam-break functions, J. Research NBS **23**, 217 (1952) RP2356.

WASHINGTON, February 25, 1954.

Journal of Research of the National Bureau of Standards Vol. 53, No. 4, October 1954 Research Paper 2542

Separation of Titanium, Tungsten, Molybdenum, and Niobium by Anion Exchange

John L. Hague, Eric D. Brown, and Harry A. Bright

The results of a systematic study of the elution behavior of titanium, tungsten, molybdenum, and niobium in various hydrochloric-hydroflouric acid media are given. These data demonstrate the behavior of the anion complexes of these elements on an anion-exchange resin column. The possibility of several interesting quantitative separations is evident, and experiments are described that demonstrate that these elements can be separated from each other.

1. Introduction

One of the more difficult problems of analytical chemistry is the separation of titanium, niobium, and tantalum. Existing methods [1, 2, 3, 5, 6] [1] for the separation of niobium and tantalum are not entirely satisfactory in the presence of titanium, and such methods are further complicated by additional separations when molybdenum and tungsten are present.

Kraus and Moore [4] have shown that niobium and tantalum can be separated as mixed chloro-fluoro anion complexes by use of an anion exchange resin in a hydrochloric-hydrofluoric acid medium. The results of a systematic study of the elution behavior of titanium, tungsten, molybdenum, and niobium in some hydrochloric-hydrofluoric acid media are presented here, as well as a demonstration of the separation of these elements from each other.

2. Experimental Method

2.1. Preparation of Column

The column used in these experiments was prepared from a 12-in. length of polystyrene tubing with a ⅞-in. inside diameter. The bottom of the tube is closed by a waxed No. 5 rubber stopper with a 3/16-in. hole. A 6-in. length of polystyrene tubing with a 5/16-in. outside diameter (1/16-in. bore) is inserted into the hole, flush with the upper surface of the stopper. Another 6-in. length of this tubing is attached to the smaller tube with a 2-in. length of Tygon R tubing, and the flow controlled by a pinch-cock on the Tygon tubing. The bottom of the large tube is covered with a ¼- to ⅜-in. layer of acid-resistant vinyl chloride plastic "wool". The column is filled with prepared [2] 200- to 400-mesh Dowex-1 resin, of 8- to 10-percent crosslinkage, to obtain a settled column of the resin 8 in. high. A measure of the liquid capacity of the column of resin is determined by washing with neutral ammonium chloride (150 g/liter, pH 6) until the resin darkens, and then determining the volume of diluted hydrochloric acid (1+3) required to lighten the color of the resin. The volume so determined was approximately 35 ml.

2.2. Elution Procedure

Acid mixtures to cover the range of 5 to 20 percent by volume of concentrated hydrofluoric acid (48%) and 10 to 60 percent by volume of concentrated hydrochloric acid (36%) were used. To expedite the work, the elements were run in pairs, molybdenum and titanium constituting one pair, and tungsten and niobium the other.

As an example of the procedure used, approximately 20 mg of high-purity molybdic oxide and 20 mg of high-purity titanium dioxide were transferred to a platinum crucible and fused with 0.5 g of potassium bisulfate. The fusion was dissolved in 50 ml of a mixture of 1 volume of hydrofluoric acid, 2 volumes of hydrochloric acid, and 17 volumes of water (designated 5-percent hydrofluoric–10-percent hydrochloric acid). The prepared column was washed with 50 ml of the same hydrofluoric-hydrochloric acid mixture, and the eluate discarded. The solution of the fusion was transferred to the resin, the first 25 ml of eluate being discarded. Elution of the resin was then continued with the hydrofluoric-hydrochloric acid solution, 50-ml fractions being collected in polystyrene graduates for analysis. Suitable portions (usually 10 ml) taken from each 50-ml fraction as the elution procedure was continued, were examined for titanium and molybdenum. Fluoride was eliminated from these portions by evaporation (usually three times) with sulfuric acid and hydrogen peroxide. Molybdenum was determined by the thiocyanate photometric method and titanium by the peroxide photometric method [2].

Elution was continued until examination of the fractions showed that the titanium and molybdenum were removed from the column. The amount of each element in each fraction examined was then calculated to a percentage of the total amount of each element eluted, and the accumulated percentages were plotted against volume of eluate. The procedure was then repeated with a solution of a fusion of tungsten and niobium oxides, the tungsten being determined by the hydroquinone photometric procedure and niobium by the peroxide photometric procedure.

[1] Figures in brackets indicate the literature references at the end of this paper.

[2] The finest and coarsest materials are removed from the main portion of the resin by settling in diluted hydrochloric acid (1+19), and several cycles of successively decanting the fine and main portions of the resin from the coarse fraction.

314715—54——5

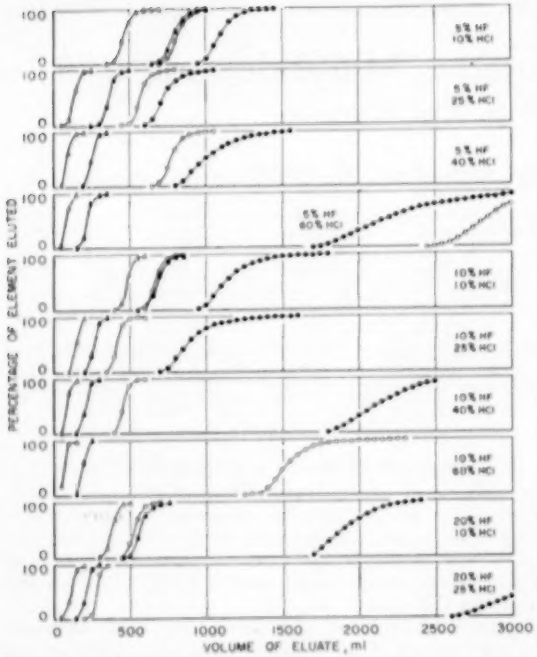

FIGURE 1. *Elution behavior of titanium, tungsten, molybdenum, and niobium.*

△, Titanium; ▲, tungsten; ○, molybdenum; ●, niobium.

3. Results and Discussion

The results of a series of experiments conducted as described above in various acid mixtures are presented in figure 1, except for niobium in 60-percent hydrochloric–10-percent hydrofluoric acid medium, in which niobium did not appear until more than 4 liters of eluate had been collected.

These curves demonstrate the possibility of several interesting quantitative separations. Titanium and niobium are easily separable under a wide variety of acid conditions, and as titanium is the first of the pair removed, even major quantities of titanium should offer few difficulties. Molybdenum and tungsten are also easily separable under several conditions; in fact, titanium and tungsten are the only pair of the group of elements considered here for which some latitude in separation does not exist.

To demonstrate that the separations can be made without the usual "loss of individuality" [5], several possible separation schemes were tried, and three of these are presented in figure 2. Figures 2a, and 2b, show the results of experiments involving 10 to 20 mg of each element. A trial of procedure 2,b, indicated it does not work well in handling decigram quantities of these elements. The extra solutions at the beginning of experiment 2,b, were designed to remove iron and cobalt, which are absorbed even in fluoride solution in the presence of high chloride-ion concentration, and to provide for the elimination of the alkali bisulfate used for fusion of the oxides.

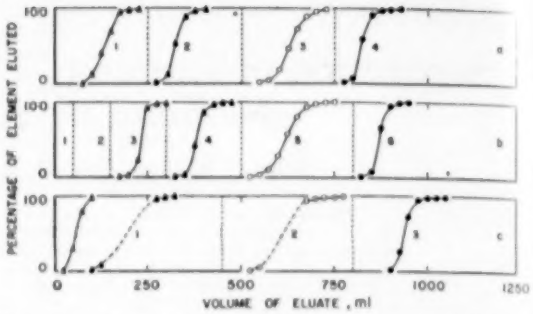

FIGURE 2. Separation of titanium, tungsten, molybdenum, and niobium.

a. Fraction 1: 250 ml of 25% HCl–5% HF; fraction 2: 250 ml of 40% HCl–5% HF; fraction 3: 250 ml of 40% HCl–10% HF; fraction 4: 250 ml of 14% NH_4Cl–4% HF.

b. Fraction 1: 50 ml of 10% HCl–20% HF; fraction 2: 100 ml of 10% HCl–5% HF; fraction 3: 150 ml of 25% HCl–5% HF; fraction 4: 200 ml of 40% HCl–5% HF; fraction 5: 300 ml of 40% HCl–10% HF; fraction 6: 250 ml of 14% NH_4Cl–4% HF.

c. Fraction 1: 450 ml of 50% HCl–10% HF; fraction 2: 350 ml of 25% HCl–20% HF; fraction 3: 350 ml of 14% NH_4Cl–4% HF.

△, Titanium; ▲, tungsten; ○, molybdenum; ●, niobium.

Figure 2,c, presents the separation of an oxide mixture obtained by suitable concentration from a 5-g sample of a high-temperature alloy and involves approximately 200-mg amounts each of molybdenum, tungsten, and niobium, with residual amounts of titanium and tantalum. It may be seen that the separations are good even with these larger quantities. Details of the niobium-tantalum separation have been omitted, as such data are already available [4].

Quantitative experiments are well advanced, and detailed procedures for the separation and determination of the components of several mixtures of commercial interest are being investigated.

4. Summary

The elution characteristics of titanium, tungsten, molybdenum, and niobium in hydrochloric-hydrofluoric acid mixtures on a Dowex–1 resin column differ sufficiently to indicate the possible separation of these elements from each other. Experiments are described that demonstrate the quantitative separation of these elements without the usual loss of individuality.

5. References

[1] F. H. Burstall and A. F. Williams, Analyst **77,** 983 (1952).
[2] W. F. Hillebrand, G. E. F. Lundell, H. A. Bright, and J. I. Hoffman, Applied inorganic analysis, 2d ed. (John Wiley & Sons, Inc., New York, N. Y., 1953).
[3] C. F. Hiskey, L. Newman, and R. H. Atkinson, Anal. Chem. **24,** 1988 (1952).
[4] K. A. Kraus and G. E. Moore, J. Am. Chem. Soc. **73,** 2900 (1951).
[5] W. R. Schoeller, The analytical chemistry of tantalum and niobium (Chapman & Hall, Ltd., London, 1937).
[6] A. F. Williams, J. Chem. Soc., p. 3155 (London, 1952).

WASHINGTON, July 19, 1954.

Journal of Research of the National Bureau of Standards Vol. 53, No. 4, October 1954 Research Paper 2543

Vapor Pressure of Nitrogen [1]

George T. Armstrong

The vapor pressure of nitrogen has been measured in the liquid range below the normal boiling point and can be represented by $\log P$ (mm) $= 6.49594 - 255.821/(T - 6.600)$. The normal boiling point calculated from this equation is 77.364° K. Nitrogen vapor densities along the saturation line are represented by $\log \rho T = 3.39858 - 282.953/(T - 3.83)$. The fugacity function $\ln f/p$ for the saturated vapor is tabulated.

1. Introduction

In the course of a study of the vapor-liquid phase behavior of mixtures of oxygen and nitrogen a series of measurements has been made on the vapor pressure of pure liquid nitrogen. These measurements cover the liquid range below the normal boiling point.

2. Description of Cryostat

The cryostat was designed for liquid-vapor equilibrium studies of mixtures and thus contains several features not essential to the vapor-pressure studies. The following description of the apparatus covers only those portions of the apparatus essential to the measurements.

The equilibrium vessel, in which the liquid nitrogen was contained is a cylinder having walls of ⅛-in. copper and an inner diameter of 1 in. The thermometer is in a well suspended from the upper lid. In these experiments the quantity of liquid nitrogen was insufficient to touch the thermometer well, so that reliance was placed on the uniform-temperature environment and the high thermal conductivity of the copper walls of the equilibrium vessel to insure that the thermometer and liquid were at the same temperature. The equilibrium vessel is suspended by thin-walled tubes within a copper can, which may be evacuated or filled with helium gas for heat transfer. This can forms a constant-temperature enclosure for the equilibrium vessel. It is completely immersed in a constant-temperature nitrogen bath. The temperature of this bath is maintained at the desired operating temperature by regulating the pressure under which it boils with the aid of a cartesian-diver manostat.

To reduce losses of liquid nitrogen from the constant-temperature nitrogen bath, and thus permit longer operation before refilling is required, the constant-temperature bath is immersed in a secondary liquid-nitrogen bath, which is allowed to boil freely at the prevailing atmospheric pressure.

The manometer tube passes through each of the liquid baths. The thermometer leads are brought through a tube into the helium-filled space surrounding the equilibrium vessel. To insure that they are at the bath temperature the leads are wound several times around the pumping tube, which projects into the helium-filled space, and are cemented to the tube.

3. Temperature Measurement

Temperatures were measured with a capsule-type platinum resistance thermometer immersed in a well in the lid of the equilibrium vessel. This thermometer was calibrated against the National Bureau of Standards provisional temperature scale below the the oxygen point [1], [2] and was checked at the oxygen point during the course of the measurements.

4. Pressure Measurement

The manometer used is a version of one described by Swindells, Coe, and Godfrey [2] modified in such a way as to make an absolute pressure-reading instrument. In this manometer the mercury surfaces are located by touching them with stainless-steel rods of calibrated lengths. The contacts are detected electrically, in this instance, by observing the extinction of a lighted neon bulb when a contact is made. The manometer has one fixed contact in the arm connected to the vapor-pressure apparatus. The other arm is closed and evacuated. The detecting rods are introduced into the closed arm through a mounting that can be moved vertically to bring the rod into contact with the mercury. After a contact is made, the position of the upper end of the movable rod is determined with the aid of a micrometer depth gage reading in millimeters. The manometer reads directly to 0.01 mm, and it is possible to interpolate to about 0.002 mm. The manometer as used in these measurements did not provide readings of this accuracy, because the temperature control of the mercury column was not sufficiently good. Errors as large as 0.015 mm or perhaps somewhat larger may have been introduced at times because of uncertainty in the mean temperature of the mercury column.

The measuring rods were calibrated by the Gage Section of the National Bureau of Standards. Thirty-seven quarter-inch stainless steel rods differing in length by increments of 1 in. permitted complete coverage of the pressure range. The rods have a conical lower end with a rounded tip of approximately 1/32-in. radius. The upper end of each is capped by a ¾-in. sphere of bearing bronze, against which the micrometer contact is made. The under surface of the sphere forms a vacuum tight but easily demountable seal against a conical opening through the movable mounting at the top of the closed arm of the manometer.

[1] This research was supported by the Air Research and Development Command, Department of the Air Force.

[2] Figures in brackets indicate the literature references at the end of this paper.

Mercury heights determined in this manometer were corrected to 0° C for thermal expansion of the rods and of mercury, and to a standard gravity of 980.665 cm sec^{-2}. The tube bore is 1 in., and so the necessity for capillary corrections was eliminated. This diameter also insures that the mercury surface is flat enough that the centering of the longer rods does not have to be closer than about 2 mm.

A small correction to the pressure was applied to compensate for the pressure difference between the mercury surface and the liquid-nitrogen surface caused by the greater density of the cold gas in the cryostat. This correction at most amounted to 0.08 mm and was very nearly proportional to the pressure in the system.

5. Material Investigated

The nitrogen used in the experiments was Linde Air Products Company standard high-purity dry nitrogen. This was stated by the supplier to contain less than 0.005 percent of argon. A calorimetric study of the melting point of a similar sample as a function of the fraction melted indicated that liquid-soluble solid-insoluble impurities amounted to much less than 0.01 percent. The material used in the last series of vapor-pressure measurements was analyzed by mass spectrometer after the measurements had been completed and was found to contain approximately 0.01 percent of oxygen. This sample had been in the vapor-pressure apparatus for approximately 2 weeks under reduced pressure, so it is probable that the oxygen entered from the walls or by seepage through stopcock grease, and it may have entered after the measurements were completed. In any case, the maximum effect produced by this amount of oxygen would be 0.06 mm at 760-mm total pressure.

6. Experimental Procedure and Results

In order to insure purity of the nitrogen introduced into the system, the connecting lines to the high-pressure cylinder were evacuated and filled several times and left full of nitrogen at a pressure slightly greater than atmospheric. The remainder of the apparatus was then evacuated overnight at a pressure below 10^{-4} mm. It was then filled with nitrogen, and the cryostat was cooled. Approximately 2 liters of gas was then condensed into the sample holder. The amount condensed was varied in some of the early measurements, and no effect on the measured pressures was observed. After filling the apparatus, all parts except the manometer were closed off by means of stopcocks.

It was impossible to keep the temperature absolutely steady. Drifts observed were of the order of 0.01 deg in 5 min at the lower temperatures and one-half to one-third this rate near the normal boiling point. A series of alternate temperature and pressure measurements was made over a period of 10 min to ½ hr. These were plotted as a function of time, and for each pressure reading a corresponding temperature was found by interpolation. Each value thus determined has been treated as a separate point, though in a sense the measurements of a series are not independent.

Because there was no stirring in the nitrogen constant-temperature bath, a period of 1 or 2 hr was needed to fix the temperature of the bath at a new value and to allow equilibrium to be reestablished. It was thought to be advantageous to start the measurements at a low temperature and to allow the temperature to rise between measurements. This procedure insured that the sample vessel, which always lagged the bath in temperature, would never be at a higher temperature than any part of the bath through which the manometer tube passed.

The measurements made on several different days, and using several different fillings of nitrogen, showed no consistent differences from one another. All measurements made in runs 1, 2, and 3 are shown in table 1. The only measurements not shown are some earlier ones in which the bath level was not properly controlled and in which the manostat regulating the bath pressure was not functioning properly. They showed large and erratic fluctuations, which did not appear again when these two factors were corrected.

TABLE 1. *Vapor pressure of liquid nitrogen*

Log P (mm)	T° K (observed)	$\triangle T \times 10^3$ (observed minus calculated)	Log P (mm)	T° K (observed)	$\triangle T \times 10^3$ (observed minus calculated)
Series 1			Series 3		
2.89075	77.5578	−1.1	2.89479	77.6398	+1.4
2.89040	77.5535	+1.5	2.89486	77.6405	+0.8
2.89037	77.5521	+0.7	2.89487	77.6412	+1.2
2.89025	77.5495	+.4	2.89504	77.6607	−0.4
2.89119	77.5683	+1.7	2.89611	77.6654	+.9
2.89111	77.5665	+0.5	2.11060	64.9360	+0.7
2.89114	77.5678	+1.2	2.11127	64.9452	+1.0
2.89188	77.5830	+0.9	2.11159	64.9495	+1.0
Series 2			2.21273	66.3274	+1.1
			2.21284	66.3291	+1.2
			2.24894	66.8354	−0.2
			2.24905	66.8501	+.2
2.83444	76.4986	+1.0	2.25058	66.8576	−1.2
2.83450	76.4997	+0.9	2.89618	77.6538	−2.1
2.83453	76.4704	+1.1	2.89619	77.6642	−1.9
2.79033	75.6344	−1.6	2.89618	77.6644	−1.5
2.79029	75.6267	+0.8	2.21036	66.2920	−1.3
2.78929	75.6181	+1.5	2.21138	66.3088	+1.3
2.78910	75.6130	−0.0	2.21457	66.3560	−2.0
2.78944	75.6186	−.8	2.27698	67.1998	−3.1
2.56364	71.6574	+.8	2.27418	67.1959	+0.2
2.56370	71.6580	+.8	2.27402	67.1915	−1.9
2.35740	68.4412	*+27.0	2.35583	68.3915	−0.7
2.35715	68.4386	*+28.2	2.35691	68.3916	−.3
2.35713	68.4370	*+26.9	2.35609	68.3939	−.7
2.27544	67.2135	+0.6	2.42898	69.5017	−.4
2.27547	67.2137	−.8	2.42905	69.5036	+.4
2.27556	67.2137	−2.3	2.42917	69.5054	+.3
2.21875	66.4091	−0.5	2.50438	70.6901	−.2
2.21881	66.4102	−1.7	2.50457	70.6933	−.1
2.21894	66.4121	−2.5	2.50473	70.6956	+.7
2.11814	65.0373	+1.5	2.58980	72.0041	+2.2
2.11837	65.0390	+0.1	2.58991	72.0052	+1.5
2.11864	65.0419	−.6	2.59002	72.0068	+1.3
2.05277	64.1776	+1.5	2.69836	73.9097	−1.3
2.05289	64.1777	0.0	2.69871	73.9709	+0.7
2.05296	64.1778	−.8	2.69917	73.9797	+1.3
			2.85437	76.8532	+3.2
			2.85470	76.8594	+3.0
			2.85472	76.8603	+2.5
			2.85465	76.8579	+2.5

* Discarded by Chauvenet's criterion.

The data have been fitted by the Antoine-type equation (1)

$$\log P(\text{mm}) = 6.49594 - 255.821/(T - 6.600). \quad (1)$$

Aside from three points at 68.4°, the measurements lie within a narrow band about eq (1). For these three points the observed and calculated pressures differ by very nearly 1 mm, so it is possible that an error was made in reading the micrometer depth gage. These three points were discarded on the basis of Chauvenet's criterion. The mean deviation from eq (1) of all measurements except those specified above is ±0.0012 deg K, or ±0.063 mm. It is possible that a slightly better fit could be obtained by the use of an additional constant or a different functional form of an equation because there appears to be a slight cyclic trend of the deviations. An estimation of the best fit in the form of a smooth curve drawn through the deviations suggests that the mean deviation could not be reduced below 0.0010 deg K by any other simple equation.

The normal boiling point calculated from eq (1) is 77.364 deg K. Some other experimental values are shown in table 2 [3 to 8]. The standard deviation in this temperature, which was found to be ±0.0013 deg for the present work, indicates only the internal precision of the data and does not give any indication of the reliability of the temperature scale. The values obtained by Henning and Otto [6] and by Keesom and Bijl [7] are very close to the present value. The value of 77.34 deg reported by Friedman and White [8] is obtained from their equation. Their value is subject to an uncertainty of 0.05 to 0.07 deg because of the deviation of their equation from their experimental values in the immediate vicinity of the boiling point.

A comparison of the experimental data from several laboratories with eq (1) is shown in figure 1. The deviations shown in table 1 have been omitted from figure 1 in order to avoid a confusion of points near the reference line. The present data are in good agreement with the data of Keesom and Bijl, showing only small systematic deviations. The rather large deviations of the data of Henning and Otto are not easy to account for because they are erratic; on the other hand, the deviations of the data of Giauque and Clayton are very systematic. The systematic deviations in the work from various laboratories are probably due to differences in the temperature scales. It is unlikely that any further improvement in the consistency of the vapor-pressure data of nitrogen will be made until the temperature scales used in various laboratories are brought into agreement in this region.

TABLE 2. *Normal boiling point of nitrogen*

Investigators	Date	T_B
		°K
Dodge and Davis [3]	1927	77.36
Heuse and Otto [4]	1932	77.346
Giauque and Clayton [5]	1933	77.32
Henning and Otto [6]	1936	77.352
Keesom and Bijl [7]	1937	77.373
Friedman and White [8]	1950	77.34
This research	1954	77.364

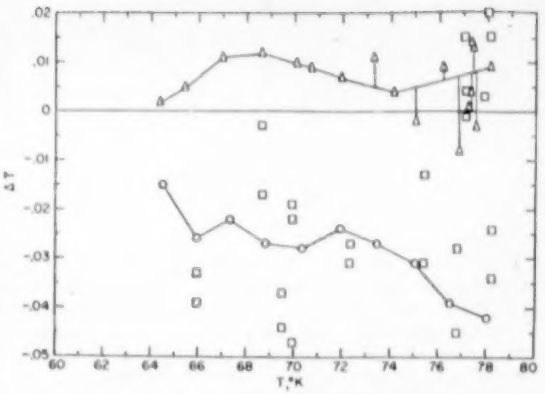

FIGURE 1. *Deviations (observed minus calculated) of other experimental values from equation 1.*

△, Keesom and Bijl; ○, Giauque and Clayton; □, Henning and Otto.

7. Calculation of Saturated Vapor Volume and Fugacity

Vapor-pressure data have at times been used for calculating the latent heat of vaporization, using the formula $\Delta H = T(V_g - V_l)dP/dT$. The vapor volume of nitrogen is, however, probably not as well known as the other quantities required in this formula. The only direct experimental measurements of this quantity were those of Mathias, Onnes, and Crommelin [9]. These were revised by Crommelin for inclusion in the International Critical Tables [10], using a reduced equation of state, but it is questionable whether any improvement resulted.

Because the heat of vaporization has been accurately measured by Furukawa and McCoskey [11], their data have been combined with the present vapor-pressure data to calculate the saturated vapor density at several temperatures. The liquid volumes used were those of Mathias, Onnes, and Crommelin. The saturated vapor density derived from the vapor-pressure data may be represented by eq (2), where ρ is the vapor density in grams per cubic centimeter,

$$\log \rho T = 3.39858 - 282.953/(T - 3.83). \qquad (2)$$

TABLE 3. *Saturated vapor density of nitrogen*

T	ΔH(vapor)[11]	$\rho \times 10^3$ (g/cm³)			
		1	2	3	4
°K	*abs j mole⁻¹*				
64.80	.....	0.883	.....	0.89	0.868
67.71	.....	1.376	.....	1.36	.....
68.00	6775.0	1.434	1.434	.....	.....
73.10	5735.2	2.818	2.818	.....	.....
73.13	.....	2.828	.....	2.78	.....
77.364	5563.0	4.593	4.593	.....	.....
78.00	5571.8	4.915	4.916	.....	.....
78.07	.....	4.952	.....	4.90	4.98

TABLE 4. *Fugacity function of nitrogen*

T	$\ln f/p$
°K	
64	−0.0096
66	−.0127
68	−.0163
70	−.0205
72	−.0250
74	−.0297
76	−.0348
78	−.0409

In column 1 of table 3 are shown values of vapor density calculated from eq (2). The values from which this equation was derived are shown in column 2; those given by Mathias, Onnes, and Crommelin are listed in column 3, and the revised values presented by Crommelin are shown in column 4.

The densities calculated from the vapor-pressure data are seen to be intermediate between the observed and revised values of Mathias, Onnes, and Crommelin. It should be noted that the revised value for the vapor density given by Crommelin at 64.80° K is incompatible with the behavior of a real gas near its saturation line, as it is less than ideal gas density at this temperature and pressure.

Using eq (2) for calculating vapor volumes, the fugacity of nitrogen along the saturation line has been calculated and is shown in the form $\ln f/p$ in table . There are no experimental data for this quant derived from PVT measurements below 80°. Ho ever, extrapolations of higher-temperature data fr various sources give values that are in some ca larger and in other cases smaller than those list in table 4.

8. References

[1] H. J. Hoge and F. G. Brickwedde, J. Research NBS **22,** 351 (1939) RP1188.
[2] J. F. Swindells, J. R. Coe, and T. B. Godfrey, J. Research NBS **42,** 1 (1952) RP2279.
[3] B. F. Dodge and H. N. Davis, J. Am. Chem. Soc. **49,** 610 (1927).
[4] W. Heuse and J. Otto, Ann. Phys. [5] **14,** 185 (1932).
[5] W. F. Giauque and J. O. Clayton, J. Am. Chem. Soc. **55,** 4875 (1933).
[6] F. Henning and J. Otto, Phys. Z. **37,** 633 (1936).
[7] W. H. Keeson and A. Bijl, Physica **4,** 305 (1937).
[8] A. S. Friedman and D. White, J. Am. Chem. Soc. **72,** 3931 (1950).
[9] E. Mathias, H. K. Onnes, and C. A. Crommelin, Koninkl. Akad. Wetenschap. Amsterdam **17,** 953 (1915); Commun. Leiden, 145C.
[10] C. A. Crommelin, International Critical Tables III, 204 (McGraw-Hill Book Co., Inc., New York, N. Y., 1930).
[11] G. T. Furukawa and R. E. McCoskey (informal communication).

WASHINGTON, May 18, 1954.

U. S. GOVERNMENT PRINTING OFFICE: 1954